Catalysis of Propane Oxidation and Premixed Propane–Air Flames

by

James T. Wiswall

A dissertation submitted in partial fulfillment
of the requirements for the degree of
Doctor of Philosophy
(Mechanical Engineering)
in The University of Michigan
2009

Doctoral Committee:
Professor Hong G. Im, Co-Chair
Professor Margaret S. Wooldridge, Co-Chair
Professor Arvind Atreya
Professor Matthias Ihme

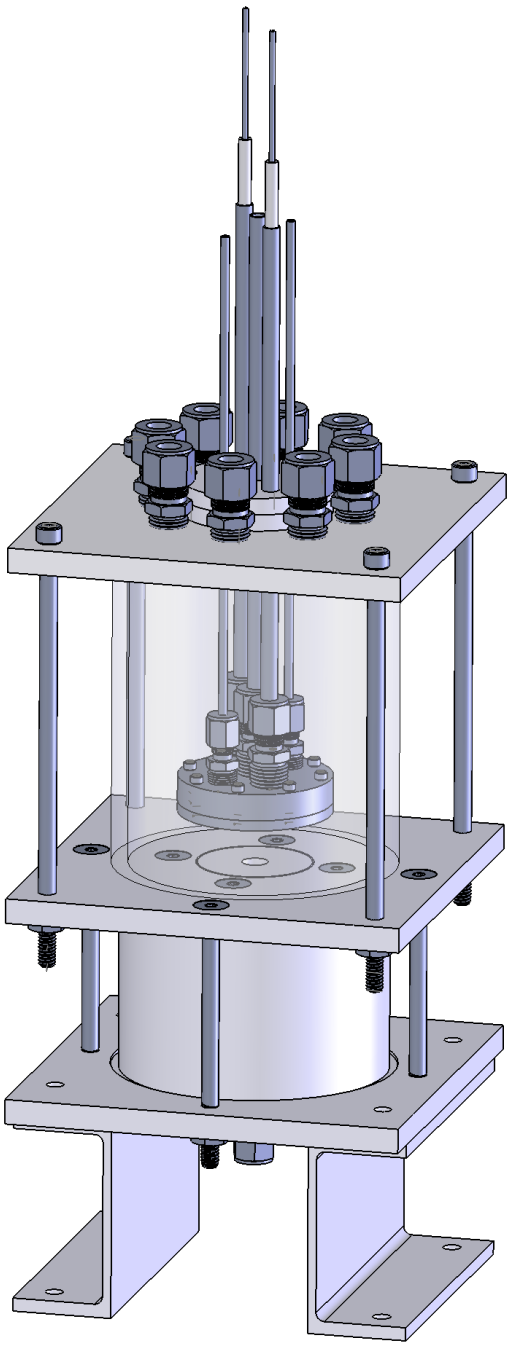

Acknowledgments

First, I would like to express my gratitude to my co-advisers, Margaret Wooldridge and Hong Im. Dr. Wooldridge helped me improve immensely on many aspects of research, especially on details which are not emphasized in published work. She also provided an environment where I felt able to develop my own personality as a researcher. I appreciate her support throughout this work. Dr. Im has also had a huge input to this research project. I worked with him, Dr. Jingjing Li, and Dr. Wooldridge to provide experimental data for a numerical model of the experimental system. I am also grateful to Arvind Atreya and Matthias Ihme for their insightful comments, and for serving on my committee.

I appreciate the efforts of the machine shop staff in the mechanical engineering department with whom I worked closely to machine the parts for apparatus used in this work. The Lurie Nanofabrication facility staff were also very helpful in the manufacture of some of the catalysts used in this work.

The input from my colleagues during this work has been indispensable. In particular, Smitesh Bakrania, Melissa Chernovsky, Darshan Karwat, Paul Teini, Stephen Walton, and Brad Zigler have had a huge influence throughout the research process. I also appreciate the conversations I have had with Jarod Kelly, Sarah Lillie, and Gregory Padowski, and their input on how my research is interpreted by people outside of my field.

Finally, I would like to thank my family for their continuous support throughout my life.

Preface

This work was developed over five years. The initial stages provided invaluable experience to draw from when designing, building, and obtaining data from the final experimental apparatus. I first started on a project to develop tunable wavelength diode lasers for use in spectroscopic measurements. I also helped assemble the single cylinder research engine with optical access in the laboratory.

I chose to work on catalytic oxidation and combustion from the suggestion of Dr. Wooldridge and Dr. Im. I built an experimental apparatus for my master's thesis work, and obtained data for a publication in the ASME journal of heat transfer. I designed and built the final apparatus for my dissertation work using the experience and knowledge gained from the first apparatus I used for my master's thesis.

As a researcher, I have found the research process to be circular. Results to test the initial hypothesis open new avenues to research which inevitably modify the initial hypothesis; this cycle continually develops the understanding of the research. The focus of this dissertation is on the final results, but many preliminary results were required to get the results to their final form. In addition to the catalytic performance of the materials in this study, I hope readers of this dissertation will understand the important details in the experimental apparatus used to obtain the results, and keep in mind the iterations required to obtain the final results.

Table of Contents

List of Tables

Table

List of Figures

Figure

List of Appendices

Appendix

List of Symbols

Roman symbols	
A_n	cross-sectional area at the nozzle exit
d	nozzle diameter
E_a	activation energy
$e(t)$	difference between the set-point and actual temperature
g	acceleration of gravity
h	nozzle-exit to stagnation-plane distance
I	heater current
k	thermal conductivity
K_p	proportional gain
K_i	integral gain
K_d	derivative gain
Le	Lewis number
$m(t)$	controller output as a function of time
n	number of moles
P	heater power
p	pressure
$\dot{Q}$	volumetric flow rate
R	electrical resistance of the heater
R_g	universal ideal-gas constant
R_T	thermal resistance
r	nozzle radius
s	stretch
T	temperature
T_{CO}	CO-inception temperature
T_h	heater temperature
$T_{i\ CO_2}$	CO_2-inflection temperature
$T_{P\ max}$	local-maximum-power temperature
$T_{P\ min}$	local-minimum-power temperature
T_s	stagnation-plane temperature
T_{sa}	catalyst-activation temperature
v	velocity
v_{ave}	average nozzle-exit velocity at room temperature

Roman symbols (continued)	
v_B	buoyancy velocity
V	voltage
V_h	voltage input to heater
U(var.)	uncertainty (of a variable)
v_{ave}	average nozzle-exit-velocity
x_{sep}	disk-flame to stagnation-plane distance

Greek symbols	
χ(Species)	mole-fraction of a gas species
χ_{rc} CO_2	carbon dioxide to reacted carbon fraction
χ_c (CO_2+CO)	reacted-carbon fraction
δ_m	mass diffusivity
δ_t	thermal diffusivity
ϕ	equivalence ratio
Φ	normalized equivalence ratio
ϕ_{min}	lean-extinction limit
ϕ_r	disk to ring flame transition
ρ	density
ρ_∞	ambient density

Acronyms	
PID	particle imaging velocimetry
PVD	particle vapor deposition

Abstract

Improvements in deriving energy from hydrocarbon fuels will have a large impact on our efforts to transition to sustainable and renewable energy resources. The hypothesis for this work is that catalysis can extend the useful operating conditions for hydrocarbon oxidation and combustion, improve device efficiencies, and reduce pollutants. Catalysis of propane oxidation and premixed propane-air flames are examined experimentally, using a stagnation-flow reactor to identify the important physical and chemical mechanisms over a range of flow, catalyst, and temperature conditions.

The propane oxidation studies consider five catalyst materials: platinum, palladium, SnO_2, 90% SnO_2 – 10% Pt (by mass), and quartz. The volume fractions of CO_2, O_2, C_3H_8, CO, NO and the electric power required to control the catalyst temperature quantify the activity of each catalyst for the equivalence ratios of $\phi = 0.67$, 1.00, and 1.50, and over the catalyst temperature range 23-800 °C. Quartz is used as a baseline and confirmed to be non-reactive at all conditions. 100% SnO_2 has minimal reactivity. Platinum, palladium, and 90% SnO_2 – 10% Pt show similar trends and have the highest catalytic activity at $\phi = 1.50$. Palladium and 90% SnO_2 – 10% Pt show an increasing catalyst-activation temperature (T_{sa}) for decreasing ϕ, and platinum shows an approximately constant catalyst-activation temperature for decreasing ϕ ($T_{sa} = 310$ °C). Of these, the 90% SnO_2 – 10% Pt catalyst shows the lowest T_{sa}, occurring for the $\phi = 1.5$ mixture ($T_{sa} = 250$ °C).

The studies of premixed propane-air flames consider platinum and quartz stagnation surfaces for fuel-mixture velocities from 0.6-1.6 m/s. Five flame structures

are observed: cool core envelope, cone, envelope, disk and ring flames. The lean-extinction limit, disk-to-ring flame transition ϕ, and the disk-flame to stagnation-plane distance are reported. Platinum inhibits the ring flame structure. The lean-extinction limit and disk-flame to stagnation-plane separation distance are insensitive to the stagnation-plane material.

The results set directions for development of improved catalyst systems, including the development of lean NO_x catalysts with low light-off temperatures, methods to quantify catalyst aging and poisoning properties, and fundamental data to develop models of the catalyst chemistry for the design of novel energy generation techniques.

Chapter 1

Introduction

For the past three decades, hydrocarbon fuels have supplied over 85% of the global energy demand. In that time, the global energy use has more than doubled: from about 215.39 quad (227 EJ) in 1970 to over 443.1 quad (467 EJ) in 2004 [1]. Hydrocarbon fuels provide the energy source in both mobile and stationary applications, and do so almost exclusively by combustion. Considering such large and widespread use, knowledge to improve combustion efficiencies and reduce pollutant emissions will have a dramatic impact on extending existing fuel resources, transitioning to sustainable energy resources, and reducing environmental impact.

For both economic and environmental reasons, it is imperative that our energy sources become sustainable and carbon neutral. Hydrocarbon fuels derived from biological sources can be both sustainable and carbon neutral and can be used in our existing energy infrastructure, which makes them a possible fuel source to aid a smooth transition away from our heavy reliance on net CO_2-emitting energy resources. Raw biomass is difficult to use for some applications, such as vehicle fuels. Catalysts play a role in the manipulation of raw biomass into easier to use fuels such as alcohols, bio-diesel, and methane.

There are many benefits to continued use of hydrocarbon fuels. Hydrocarbon fuels are energy dense in both volume and mass, which makes their transportation and

storage practical. They can supply the energy required for both mobile and stationary applications, and they can be derived from many different raw sources, allowing for diversified energy sources.

There are also significant technical challenges in using hydrocarbon fuels. The energy derived from hydrocarbon fuels is almost exclusively achieved by combustion. Some of the greater challenges in combustion systems are the environmental problems associated with their emissions, created by the narrow range of temperatures and fuel mixtures that yield efficient energy release. Gas-phase combustion is a high temperature process that can release pollutants into the environment, such as CO_2, CO, nitrogen oxides (NO_x), unburned hydrocarbons, particulate matter and sulfur oxides (SO_x). Nitrogen oxides and especially sulfur oxides can cause acid rain along with other atmospheric and environmental problems such as smog formation.

Catalysts can address many of the challenges associated with energy derived from hydrocarbon fuels. They are currently used for exhaust gas after treatment in vehicles to remove some pollutants from the exhaust, and are also used to refine and manipulate raw fuels into easier to use forms.

Catalysts can also take part in energy release by enabling oxidation reactions at lower temperatures and extending efficient reaction operating conditions. Unlike gas-phase combustion, catalytic oxidation can be sustained at low temperature. Low temperature oxidation inhibits the formation of some pollutants, such as nitrogen oxides, and can allow for a more efficient heat release. Low temperature reactions can also enable the development of devices that require lower temperatures to operate.

Catalytically stabilized combustion has been researched and reviewed by Pfefferle and Pfefferle [30, 31], Prasad et al. [32], and Trimm [33]; however, there are technical challenges to implimenting catalysts in combustion-system design, and catalysts are rarely used in current combustion applications. The research in this dissertation investigates catalytic fuel oxidation and the influence catalysts can have on premixed

flames.

1.1 Scientific Background

The surface chemistry of hydrocarbons and hydrogen with oxygen has been studied in depth since the early 20^{th} century [17, 18], and continues to be an active area of research. A brief summary, of studies closely related to the current work, is presented here.

1.1.1 Properties of catalytic reaction

Heterogeneous catalytic reaction requires that reactants be transported to the catalyst, react, and that combustion products be transported away from the catalyst. Therefore, surface reaction kinetics or transport of gas-phase species can limit the heterogeneous reaction rate. Pfefferle and Pfefferle [30], among many other sources, discuss the relative contributions of these processes. At low catalyst temperatures, surface kinetics are slow and limit the heterogeneous reaction. As the catalyst temperature increases, the rate of surface kinetics increase, until reactant transport to the catalyst limits the heterogeneous reaction. The transition from surface-kinetics-limited to diffusion-limited operation of a catalyst sometimes yields a step change in behavior. The step change occurs from the rapid increase in surface kinetic rate with increasing temperature. For example, the fuel conversion fraction in a catalytic-monolith reactor may increase abruptly when the inlet flow temperature is increased above a threshold temperature. In the example, as is the case with most systems, the threshold temperature represents a point of instability where an increase in temperature causes both increasing heat release and temperature until either the fuel is entirely consumed, or the transport of reactants to the catalyst limits the reaction rate. Consistent with other studies (e.g. McDaniel et al. [27]), this threshold is called *light-off* or *heterogeneous ignition* in the

current work.

Catalyst performance metrics are intertwined with the parameters of the specific apparatus used to study the catalyst. The flow geometry, the form of the catalyst (e.g. foil, washcoat, etc.), and the heat transfer properties of the catalyst support, are all characteristics which greatly influence catalyst performance. Thus, it is often difficult to compare results between different experimental facilities, and it is critical to establish clear baselines for conditions lacking catalytic effects. Simple flow geometry, catalyst temperature control, and wide operating ranges in flow and reactant mixture are important features for fundamental catalyst studies. The stagnation-flow reactor is an excellent example of an experimental approach that meets these criteria.

1.1.2 Research using the stagnation-flow reactor

The stagnation-flow configuration has served as a standard and simple geometry to investigate catalyst phenomena for many years. There are several important features making the stagnation-flow configuration suitable for fundamental experimental studies of catalyst performance. The species, temperature and velocity profiles vary by the distance from the stagnation surface only, and can therefore be analyzed using a one-dimensional approach. In addition to the simple flow geometry, the stagnation-flow reactor also allows independent control of the characteristic time scales for chemical reaction and flow.

Researchers using the stagnation-flow geometry have developed and validated heterogeneous reaction mechanisms [3, 24, 27], investigated light-off and the effects of catalysts on homogeneous flammability limits and ignition phenomena [27, 34, 36], and quantified fuel conversion efficiencies [7], to only name a few areas of research. Among the most relevant papers to this study are the works by Veser and Schmidt [34] and Williams et al. [36], who experimentally studied heterogeneous and gas-phase ignition in a stagnation-flow; Law et al. [19], who examined the lean extinction limits

of propane-air flames in stagnation flow subject to different boundary conditions on the stagnation surface, including a platinum catalyst; and Ljungstrom et al. [24], who measured H_2O production while using H_2 and O_2 as reactants on platinum foil.

As described earlier, heat release thresholds can be used to define heterogeneous reaction ignition and extinction points; however, they are strongly connected with the heat transfer aspects of the particular apparatus used, and may therefore require more analysis to give a result dependent solely on the chemistry. In addition, hysteresis has been observed in heterogeneous ignition and extinction points in stagnation point flow reactors [14, 34, 36], which may be associated with properties of the systems used.

The ignition criteria vary from study to study. Dupont et al. [7, 8] sampled the exhaust gases exiting the reactor to determine the CH_4 % conversion and CO selectivity, and defined *homogeneous ignition* as the advent of CO in the exhaust gases. Homogeneous ignition in their case was not ignition of a gas phase flame, because the highest temperature in their reactor was at the surface and was less than 1800 K. Williams et al. [36] and Veser and Schmidt [34] defined the *heterogeneous ignition temperature* as the catalyst temperature at which a large increase in heat release occurred. They also defined the *autothermal temperature* as the catalyst temperature at which the foil could sustain high temperatures without electric heating, and the *extinction temperature* as the catalyst temperature at which a large decrease in heat release occurred. Ikeda et al. [14] defined the *heterogeneous ignition temperature* as the catalyst temperature at which there is a temperature increase without electric heating of the catalyst, and the *extinction temperature* as the catalyst temperature at which there is a temperature decrease without cooling of the catalyst.

Some researchers have supplemented their studies of catalytic ignition and combustion with in-situ species measurements. Ikeda et al. [14] exploited the one-dimensionality of the stagnation-flow configuration and sampled gases in the stagnation-flow stream using quartz capillary probes to measure O_2, N_2, H_2O and

H_2 mole-fractions as a function of distance from the stagnation plane. Similarly, Ljungstrom et al. [24] measured OH desorption from a platinum foil by laser-induced fluorescence (LIF). These data provide additional insight into the reaction pathways important in the systems studied.

1.1.3 The coupling between heterogeneous and gas-phase reaction

In general, both gas-phase and heterogeneous reactions contribute to fuel conversion in a catalytic system. Ignition characteristics can show dominance of either heterogeneous or gas-phase reactions. Veser and Schmidt [34] experimentally studied both heterogeneous and gas-phase ignition over heated platinum foil of methane, ethane, propane and iso-butane, and Williams et al. [36] studied methane and propane. Heterogeneous ignition occurred at a temperature several hundred degrees cooler than gas-phase ignition. Each fuel was found to have different ignition characteristics when catalyst ignition temperature as a function of fuel-air ratio was plotted. Of the fuels studied, ethane had the lowest gas-phase ignition at 950 °C, and methane had the highest at 1200 °C.

In order for heterogeneous catalysis to affect a gas phase flame, the flame must be brought sufficiently close to the catalytic surface so that diffusion to and from the surface affects species concentrations and temperatures in the flame reaction zone. Free radicals that desorb from the the surface or adsorb on the surface can strengthen or weaken the flame reaction. Assuming that the stagnation plane is at a lower temperature than the flame temperature, a quenching effect occurs when the flame is brought close to the solid surface. There is a competition between thermal diffusion and mass diffusion effects on the flame. Law and Sivashinsky [20] determined theoretically in stagnation flow reactors that for Lewis numbers (definded as $Le = \delta_t/\delta_m$ where δ_t is the thermal diffusivity and δ_m is the mass diffusivity) less than 1, the flame strengthens

due to an increased flame temperature as it approaches the surface, and for Lewis numbers greater than 1, the flame extinguishes due to a decreased flame temperature as it approaches the surface. Their primary conclusion is that there is a much greater likelihood that a flame will exhibit effects from heterogeneous catalysts if the Lewis number is less than 1.

There have been attempts to extend the lean extinction limits of catalytically-assisted gas-phase flames in the stagnation flow configuration [15, 19]; however, it is experimentally challenging to observe this phenomenon. Li and Im [21] numerically studied regimes where self-sustaining homogeneous flames interact with catalysts in a stagnation flow. Their results showed that the lean extinction limit was largely extended, while gas phase reactions were suppressed at lower strain rates. More recent studies by Li and Im [21, 22] specifically focused on the catalytic extension of lean extinction limits. Their numerical studies of a methane/platinum stagnation-point-flow reactor revealed that the lean extinction limit can be extended, provided that the characteristic time scales of the surface reactions are faster than those of the gas-phase reactions, as would be the case if the catalytic surface retains a high temperature with lower heat loss, or if the gas-phase mixture is diluted. It remains to be seen, however, whether the observed catalytic benefit of flammability extension can be realized experimentally.

While much has been learned regarding specific catalytic performance, catalytic combustion remains a highly empirical subject due to the large number of fuel-catalyst combinations. Advances in material characterization have also identified the importance of micro-structural features of the catalyst. As a consequence, the development of new materials and new methods to applying catalysts requires broader experimental studies that provide more variety of experimental measurements for more material-fuel systems. Based on these data, novel applications and insights into the fundamental chemistry can be pursued in future experiments.

1.1.4 Surface reaction mechanisms

Most elementary surface reactions can be described by two fundamental categories: decomposition reactions and bimolecular reactions. Decomposition reactions occur when a single species reacts into multiple product species. Bimolecular surface reactions are further divided into two categories that are named the Langmuir-Hinshelwood mechanism, and the Eley-Rideal mechanism. For the Langmuir-Hinshelwood mechanism, both reactants adsorb on the catalyst, react, and desorb from the catalyst. For the Eley-Rideal mechanism, only one reactant adsorbs on the catalyst, and the other reactant reacts with the adsorbed reactant from the gas phase. Figure 1.1 shows graphical representations of the three mechanisms. The subscript, s, denotes species adsorbed on the surface in the figure.

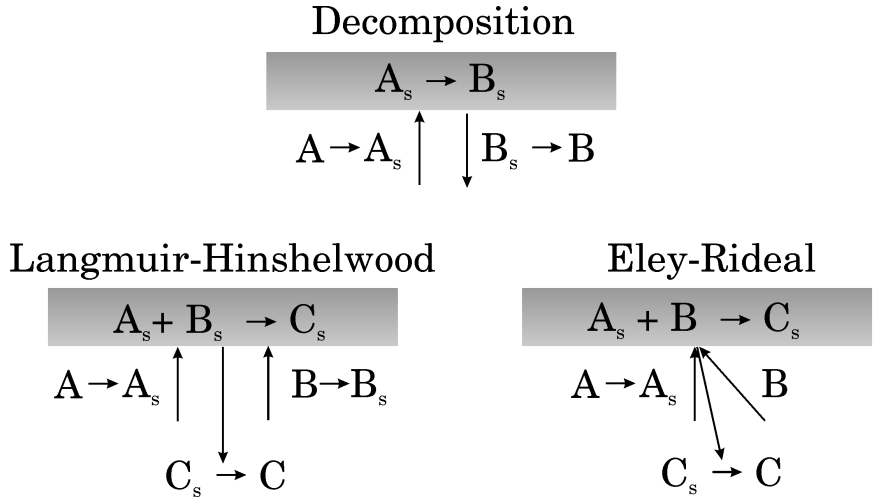

Figure 1.1 Schematics of the three categories of surface reaction mechanisms

Detailed reaction mechanisms of methane and ethane oxidation on a platinum surface have been developed largely due to the efforts of Deutschmann et al. [3, 4, 5, 6] and the experimental work of Williams, Vlachos, Veser, and Schmidt et al. [34, 35, 36]. Experimental research of the elementary reactions of hydrogen on platinum have been studied by Ljungstrom et al. [24] and Fridell et al. [11, 12, 13], and carbon monoxide on platinum has been studied by Campbell et al. [2]. These works are also important

contributions to the development of the methane and ethane oxidation on platinum mechanisms. Researchers have used the methane oxidation on platinum mechanism in conjunction with gas-phase methane oxidation mechanisms to study the interaction between heterogeneous and homogeneous chemical reactions [10, 26, 29].

The experimental research, used to develop heterogeneous mechanisms, predominantly uses bulk platinum as the catalyst in the form of a foil or wire. Analysis of the results suffers from the intertwined effects of reactant transport to the catalyst and heat transfer properties of the catalyst. Quantifying heterogeneous reactivity for different catalyst materials can be used to develop a larger database of surface reaction chemistry, and catalyst temperature control can isolate the reactant transport and surface reaction effects.

1.2 Objective, hypothesis and dissertation outline

The objective of this work is to broaden our fundamental understanding of the interactions between gas and surface phase chemistry in a well-defined system, to facilitate the application of catalysts for the improvement combustion and ignition systems. Several catalysts, including both traditional and novel materials, are investigated. The consideration of different catalytic surfaces allows comprehensive comparison of conditions at which gas-phase and heterogeneous reactions interact at varying degrees of relative dominance. The gas-phase reactant mixture impinges onto the solid surface, which can be non-reacting (quartz) or catalytic. The hypothesis is that catalysis can extend the useful operating conditions for hydrocarbon oxidation and combustion.

In this work, a stagnation-flow reactor is used to study catalytic interaction, which allows systematic control of the characteristic flow time scales by varying the nozzle inflow velocity independently of the chemical time scales. The apparatus has been developed from previous research by Wiswall et al. [37, 38] performed at the Combustion

and Environmental Research Laboratory at the University of Michigan. Wiswall et al. [38] is included in Appendix A for reference. In the present study, the stagnation plane is chosen to be either nonreactive or catalytic, so that the effects of surface reactions can be assessed in reference to the baseline results from using an inert surface.

Chapter 2 describes the experimental apparatus and procedure in detail. It describes the stagnation-flow-reactor design, the reactant flow delivery system, the catalyst materials studied, the exhaust gas sampling system, the measurement uncertainties, and the experimental procedures used. Chapter 3 presents the results for the propane oxidation catalysis studies, and Chapter 4 presents the results for the flame-catalyst interaction studies. Finally, Chapter 5 presents the conclusions of the study and suggestions for the future direction of the heterogeneous combustion research program.

Chapter 2

Experimental approach

This chapter has two parts. Section 2.1 describes the experimental apparatus: the stagnation-flow reactor, the reactant flow delivery, the catalyst materials, the exhaust gas sampling, and the measurement uncertainty. Section 2.2 describes the experimental procedure for the studies of catalytic propane oxidation and catalysis of premixed propane-air flames.

The stagnation-flow reactor has several features which make it suitable for experimental investigation of catalyst performance. Uniform stagnation flow implies the species concentration, temperature, and velocity profiles vary by the distance from the stagnation surface only; in other words, the flow geometry results in planes, parallel to the stagnation plane, that have constant species concentration, temperature, and velocity. Thus, given a uniform flow, a one-dimensional analysis can be used. The stagnation-plane temperature and flow velocity are independently controlled in the experiment. This allows independent control of the characteristic time scale for chemical reaction and the reactant residence time.

The stagnation-flow reactor design is developed from previous research, by Wiswall et al. [37, 38], conducted in *The Combustion and Environmental Research Laboratory*. Wiswall et al. [38] is included for reference in Appendix A, and describes the previous experimental efforts which led to this work.

2.1 Experimental apparatus

2.1.1 Stagnation-flow reactor

Figure 2.1 shows a photograph of the stagnation flow reactor. The flow direction in the photograph is from bottom to top. The reactant mixture enters the mixing chamber of the reactor, impinges on the flat stagnation plane where the catalyst is mounted, and continues out the exhaust vents into a chimney (not shown in the photograph). A portion of the flow is drawn into the sampling lines that are connected to gas sampling equipment. A glass cylinder (shown in the photograph) or aluminum cylinder seals the reactant flow from the atmosphere.

The electrically-heated catalyst mount is made from type 316 stainless steel. Type 316 stainless steel is chosen for its stability in both oxidizing and reducing environments at the temperatures in the experiment. All hardware, tubing, and fittings connected to the catalyst mount are also made from type 316 stainless steel. The remaining parts of the stagnation flow reactor are made from type 6061 aluminum. The heat transfer properties of aluminum help dissipate the heat transferred from the catalyst mount. Also, the aluminum is non-reactive with respect to the reactant and product gases at the temperatures the structure reaches.

Figure 2.2 shows a cross-sectional view of the stagnation-flow reactor with important dimensions included. There is another mixing chamber upstream from the stagnation-flow reactor, with volume 100 mL, to ensure complete mixing of the reactants (not shown in the photograph). The flow inlet is a tube with a diameter of 5 mm, and the mixing chamber has an inner diameter of 95.25 mm. After the mixing chamber, the flow continues through the contraction nozzle that has an area contraction ratio of 18.26:1. The flow then impinges on the stagnation plane. The nozzle exit diameter is 10 mm, and the separation distance between the stagnation plane and nozzle exit is adjustable in the setup and is denoted by the "nozzle-exit to

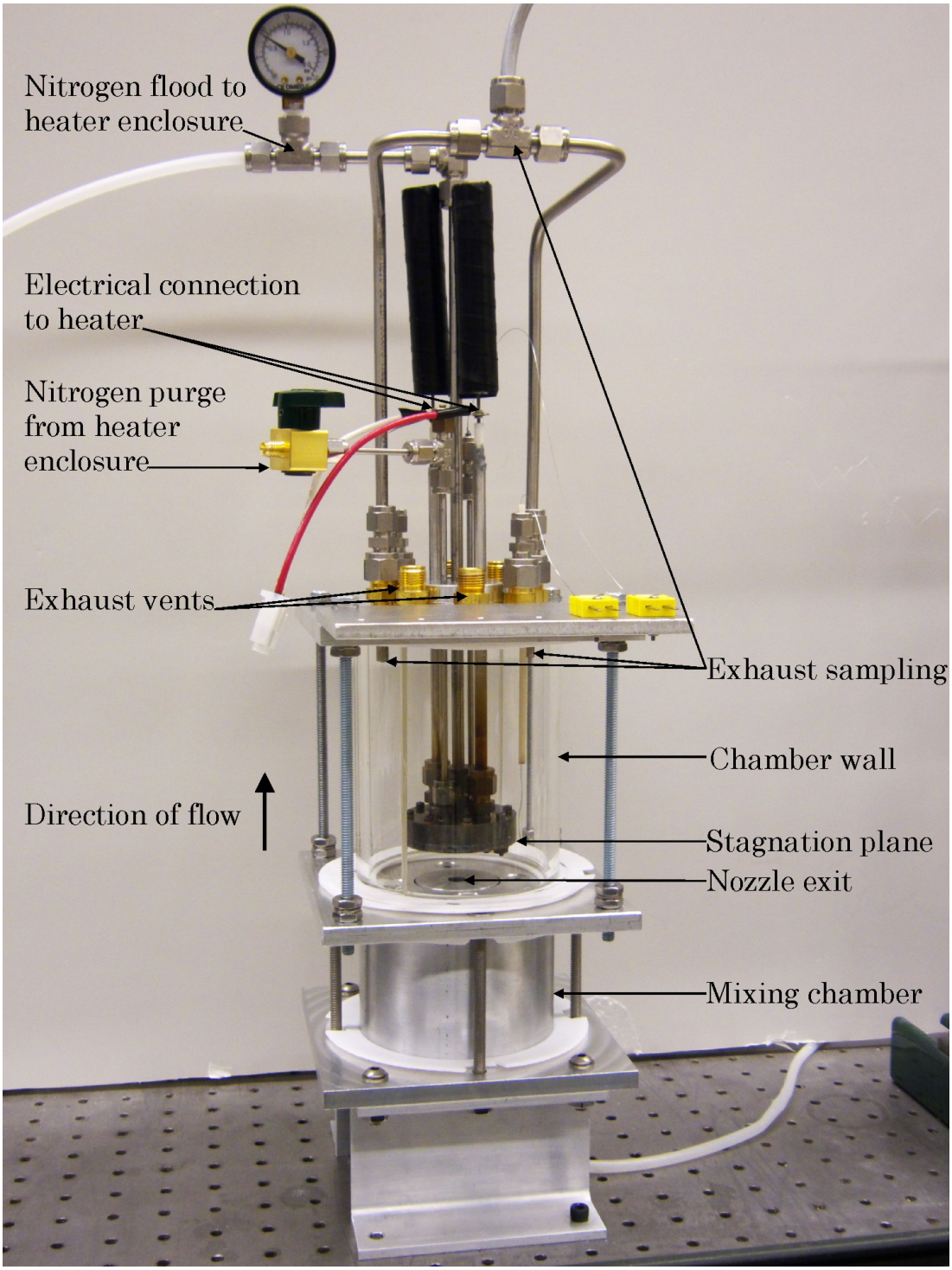

Figure 2.1 Photograph of the stagnation flow reactor. A glass cylinder is shown in this photograph as the chamber wall. An aluminum wall, not shown in the photograph, could also be used in the experiments.

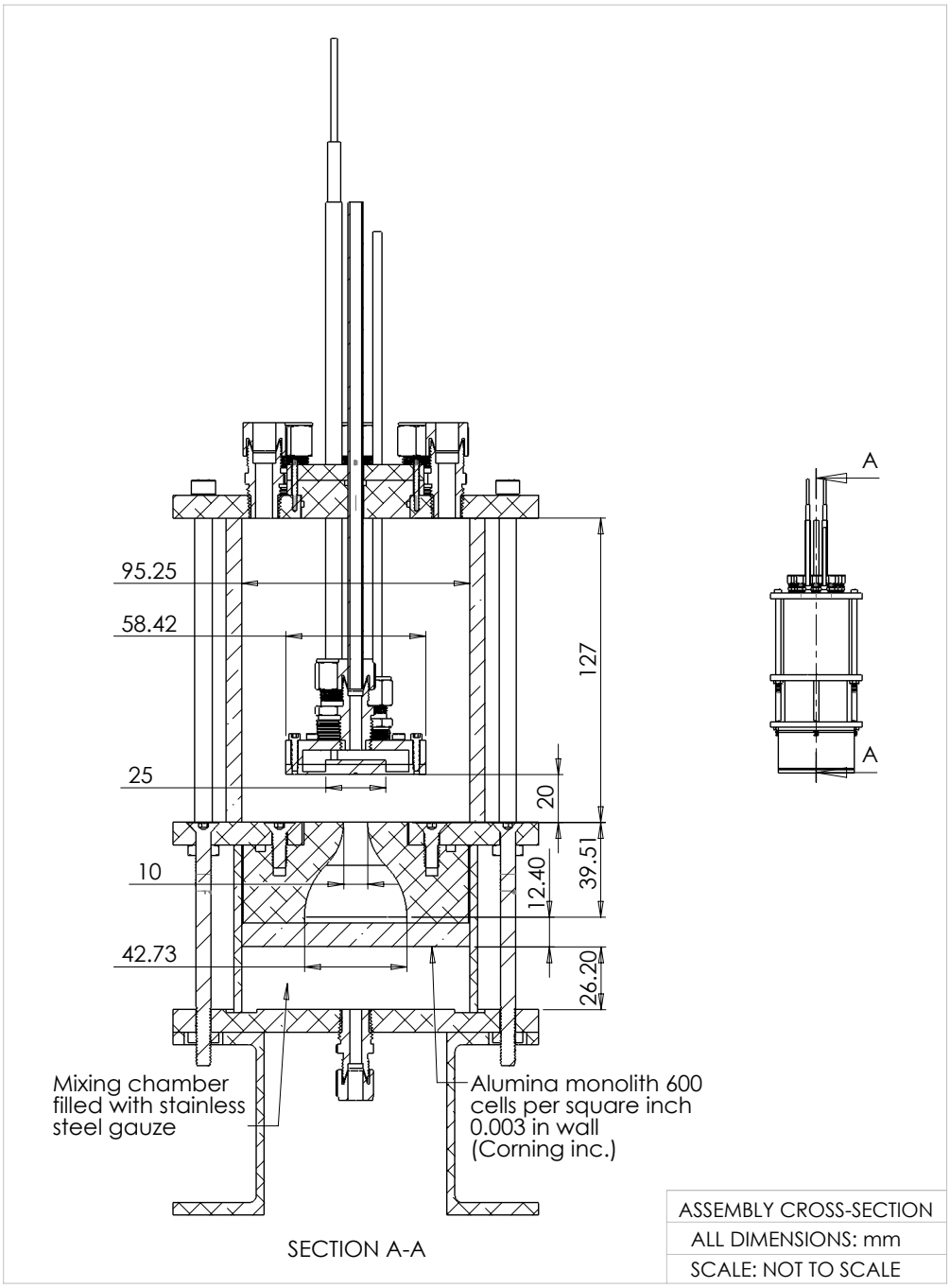

Figure 2.2 Cross-sectional view of the stagnation flow reactor with important dimensions.

stagnation-plane distance" (h). For the experiments in this work, the nozzle-exit to stagnation-plane distance is set to two nozzle diameters ($h = 20$ mm). The catalyst is mounted on a surface that has a heated portion 25 mm in diameter and an outer

diameter of 58.42 mm. The inner diameter of the reaction chamber is 95.25 mm, and its overall height is 127 mm. There are eight exhaust vents that have an inner diameter of 7 mm. Two exhaust vents are used to sample the flow, two exhaust vents are used for thermocouple access to the stagnation plane, and four exhaust vents are open. Appendix D includes detailed technical drawings of the parts comprising the stagnation flow reactor.

The cross-sectional view shows the flow-conditioning design. The design is developed from the work by Mi et al. [28] and the previous experimental setup, Wiswall et al. [37, 38]. The mixing chamber and nozzle are designed to condition the reactant flow to have a uniform velocity in the axial direction at the nozzle exit. Recall, this allows for a one-dimensional analysis of the flow. The flow first passes through stainless steel gauze in the mixing chamber; then the flow passes through a ceramic monolith that has 600 square cells per square inch (Corning Inc.); finally, the flow passes through the contraction nozzle (18.26:1 area contraction ratio) and impinges on the stagnation plane. The stainless-steel gauze makes the flow pathlines within the mixing chamber random and removes the flow-velocity profile due to the inlet flow tube. The ceramic monolith is incorporated in the design to orient the flow in the axial direction before it passes through the nozzle. The contraction nozzle accelerates the flow to its impinging velocity.

For experiments involving flames, the aluminum or glass cylinder is removed, and the flow impinging on the stagnation-plane is exposed to the atmosphere. Leaving the reactant flow open to the atmosphere reduces vibrations that occur when the flame is ignited in the cylinder. Figure 2.3 shows an image of a typical stagnation-flow disk flame. The flame is ignited using small a propane-air torch.

The flame image is a visualization of the flow velocity profile. The flame image in Fig. 2.3 shows the flow impinging on the stagnation plane is uniform; in other words, the flow velocity has a constant axial velocity component over the radius of

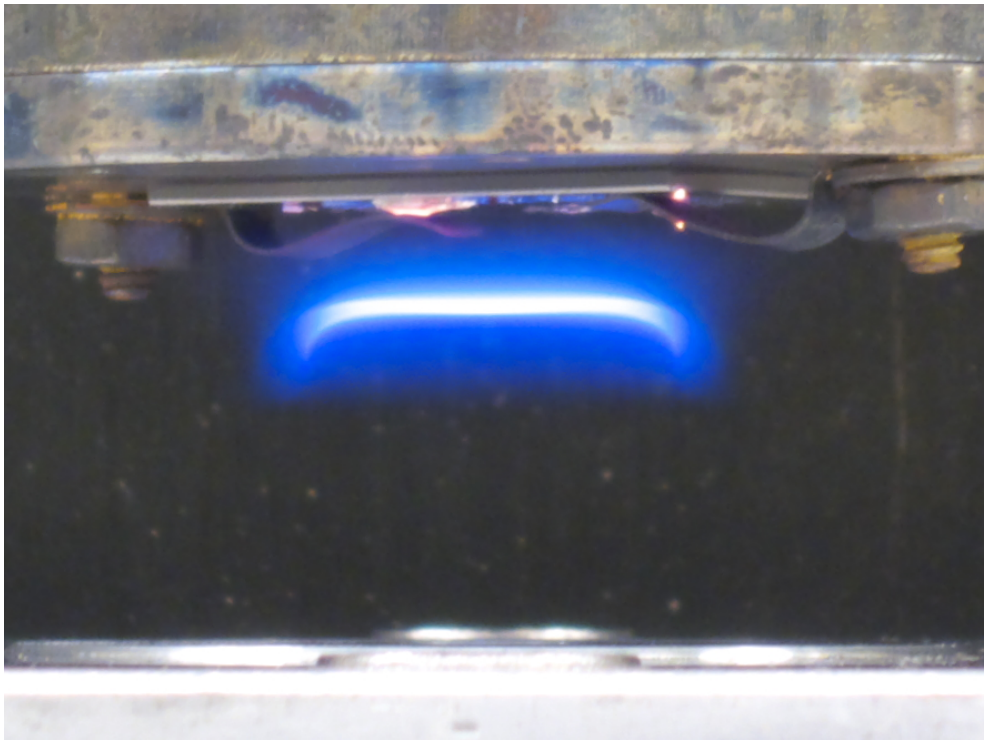

Figure 2.3 A stagnation-flow disk flame image. The flame shows the flow properties of the system. The average nozzle exit velocity is 1.3 m/s and $\phi = 0.82$ ($\Phi = 0.45$).

the nozzle. The previous experimental apparatus, used in Wiswall et al. [37, 38], has a Poiseuille flow impinging on a flat stagnation plane. Particle imaging velocimetry (PIV) experiments in Wiswall et al. [37] showed the relationship of the flame shape to the flow velocity gradient in the radial direction of the nozzle. It was found that the flame shape followed the velocity profile closely and that the flame shape can be used to visualize the flow gradients in the stagnation-flow reactor.

2.1.2 Inlet reactant flow

The reactants used in the experiments are compressed propane (Matheson Tri-Gas, Inc.) and synthetic dry air (Purity Plus Specialty Gases). The compressed propane has a purity of 99%. The synthetic dry air is a mixture of oxygen and nitrogen with an oxygen fraction in the range 20.995% to 21.005%. Cryogenic Gases Corp. provided a certification of the mixture. The volumetric flow rates of the propane and synthetic

air are measured using variable area flow meters (rotameters). The equivalence ratio, ϕ, and average nozzle-exit velocity, v_{ave}, are calculated from the volumetric flow rates of propane and air (equations 2.1 and 2.2). In equations 2.1 and 2.2, the volumetric flow rate is denoted by $\dot{Q}$, the number of moles is denoted by n, and the area of the nozzle exit is denoted by A_n. Since the nozzle-exit velocity is close to uniform, the average nozzle-exit velocity approximates the flow velocity at the nozzle exit.

$$\begin{aligned} \phi_{\mathrm{C_3H_8}} &= \left(\frac{\dot{Q}_{\mathrm{C_3H_8}}}{\dot{Q}_{air}}\right) \times \left(\frac{n_{air}}{n_{\mathrm{C_3H_8}}}\right)_{stoich} \qquad (2.1) \\ 23.8 &= \left(\frac{n_{air}}{n_{\mathrm{C_3H_8}}}\right)_{stoich} \\ v_{ave} &= \frac{\dot{Q}_{\mathrm{C_3H_8}} + \dot{Q}_{air}}{A_n} \qquad (2.2) \end{aligned}$$

The rotameters are calibrated after they are installed in the experimental apparatus to account for the flow resistance downstream from each flow meter. The propane flow meter is calibrated by timing the volumetric flow of bubbles through a graduated cylinder connected to the nozzle exit. The the air flow meter is calibrated using an electronic mass-flow meter (TSI Corp.).

Before each experiment, the flow meter calibrations are corrected for local variations in atmospheric temperature and pressure. Equation 2.3 shows the equations used to calculate the actual volumetric flow rate from variations in the local temperature and pressure.

$$\dot{Q}_{actual} = \dot{Q}_{calibration}\sqrt{\frac{p_{calibration}}{T_{calibration}}\frac{T_{actual}}{p_{actual}}} \qquad (2.3)$$

The average nozzle-exit velocity (equation 2.2) is chosen to report the flow condition in the experiment. Particle imaging velocimetry (PIV) shows an abrupt deceleration of a non-reacting Poiseuille flow impinging on a stagnation plane in the previous experimental work, Wiswall et al. [37]. Figure 2.4 shows these results. The actual

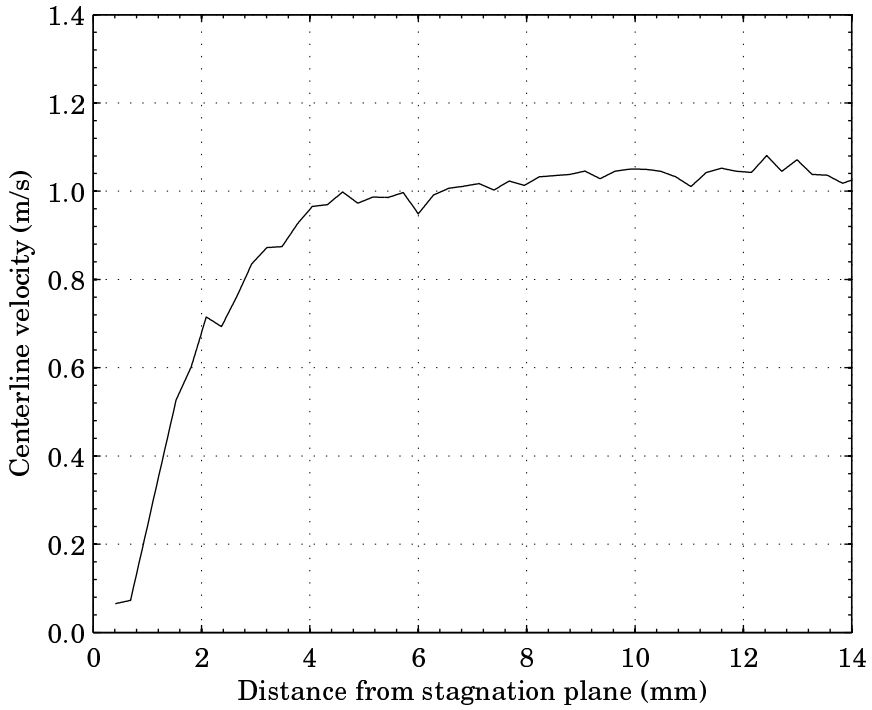

Figure 2.4 The local centerline velocity as a function of distance from the stagnation plane for a non-reacting Poiseuille flow (Wiswall [37]). The nozzle exit is located 45 mm from the stagnation plane.

nozzle-exit to stagnation-plane distance in Wiswall et al. [37] is $h = 45$ mm; however, the centerline velocity does not begin to decrease until approximately $h = 4$ mm. Thus, for purposes of mapping the results to the one dimensional stagnation flow analysis, an effective nozzle-exit to stagnation-plane distance must be determined. Because of this complexity in defining the effective h to map the flow conditions to a one dimensional stagnation flow, the average nozzle-exit velocity is used to define the the flow in the experiment.

A local increase in flow velocity downstream from the nozzle is caused by heating due to the stagnation plane and the presence of the flame. The buoyancy velocity is calculated by equation 2.4.

$$v_B = \sqrt{\left(\frac{\rho_\infty}{\rho} - 1\right) rg} \tag{2.4}$$

In equation 2.4, v_B is the buoyancy velocity, ρ is the density, r is nozzle radius, g is the acceleration of gravity, and ∞ indicates a free stream condition. Figure 2.5 shows the buoyancy velocity as a function of the stagnation-plane temperature. The flow condition, reported by average nozzle exit velocity, is the average nozzle exit velocity at room temperature, calculated by equation 2.2. This flow condition defines a mass flow rate for each experimental condition.

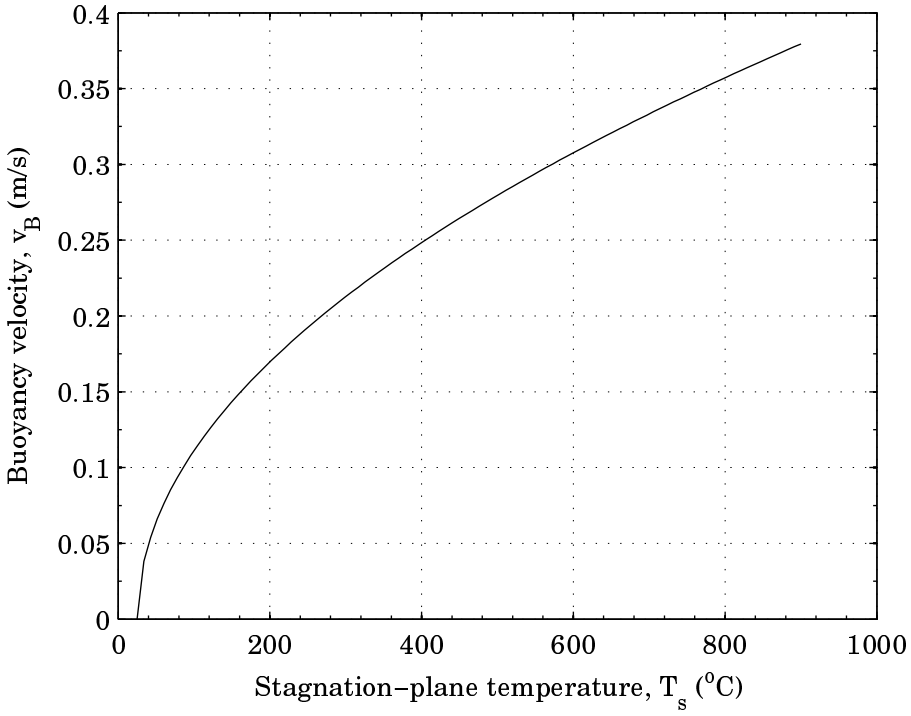

Figure 2.5 The buoyancy velocity as a function of stagnation-plane temperature

Comparing the average exit velocity for the conditions studied and the buoyancy velocity, the flow residence time is decreased due to the buoyant flow by approximately 30% at the higher stagnation-plane temperatures.

Figure 2.6 shows the relation between the rotameter float height and the resulting v_{ave} and ϕ in the experiment. For example, $v_{ave} = 120$ cm/s and $\phi = 1$ corresponds to an air float height of 102 mm and a propane float height of 105 mm at $p_{atm} = 990$ mb and $T = 22$ °C. The figure also shows the experimental range of v_{ave} and ϕ.

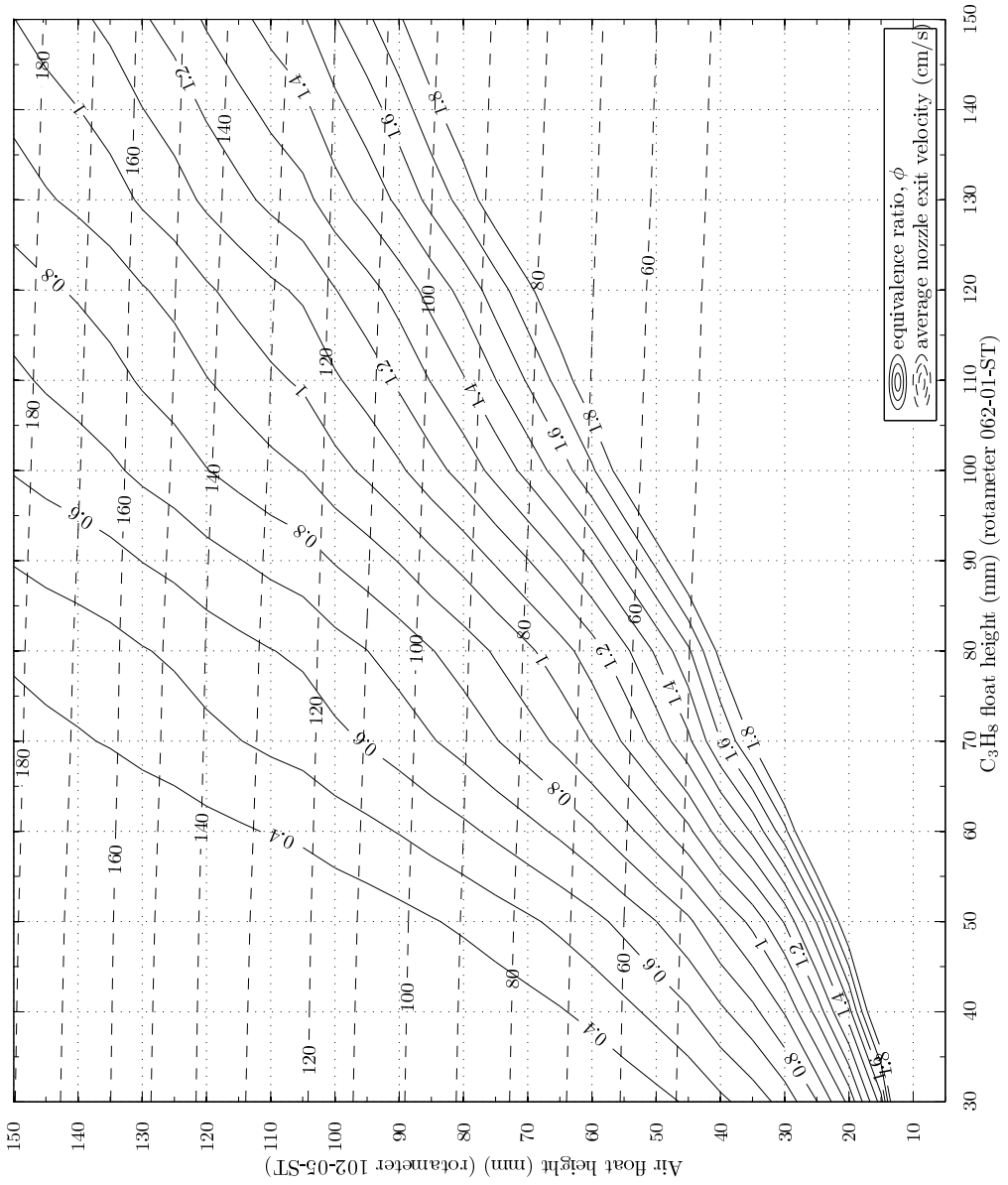

Figure 2.6 Contour plot showing the range of average-nozzle-exit-velocity and fuel-air-mixture possible with the flow control system. (p_{atm} = 990 mb, $T = 22^oC$)

2.1.3 Catalyst manufacture, mounting, and heating

Catalyst manufacture and mounting

Five stagnation-plane materials are investigated for catalytic propane oxidation: platinum, palladium, 90% SnO_2 – 10% Pt (by mass), SnO_2, and quartz. This dissertation also compares a platinum and quartz stagnation plane for the flame studies. The catalyst mount accepts catalyst wafers that are 25.4 mm × 25.4 mm square and of thickness 2 mm or less. The catalyst is mounted to the heated surface with clips made from 316 stainless steel. The clips and the platinum catalyst are visible in Fig. 2.3.

A bare quartz wafer, with dimensions 25.4 mm × 25.4 mm × 1 mm, is used as the quartz stagnation plane. The platinum, 90% SnO_2 – 10% Pt , and SnO_2 catalysts are applied to an identical quartz wafer. Palladium foil of dimensions 25 mm × 25 mm × 0.025 mm is used for the palladium catalyst. The quartz wafer has two material properties which make it a good choice as a mounting surface; it is resistant to large thermal gradients and remains stable at high temperature. The wafer is rigid enough to hold its shape while the stagnation plane mounting surface expands and contracts over the experimental temperature range.

The platinum catalyst is particle vapor deposited (PVD) on a quartz wafer. The PVD process is performed in *The Lurie Nanofabrication Facility* as follows. A 10 nm layer of titanium is deposited on the quartz wafer by PVD. A 100 nm layer of platinum is deposited on the titanium layer, and acts as the catalyst. The titanium layer is required to bond the platinum to the quartz surface. The wafer used in Fig. 2.3, is the PVD platinum-coated quartz wafer. The platinum used in the PVD process has a purity of 99.99%.

The palladium foil has 99.9% purity and is similarly mounted using the clips. The coefficient of linear thermal expansion for stainless steel is larger than for palladium [23]; therefore, if the temperature increases the palladium foil remains in contact with

the stagnation plane mounting surface. If the temperature decreases, the foil tends to bulge away from the stagnation plane mounting surface. Thus, for experiments using the palladium foil catalyst, the temperature must increase throughout the experiment.

The SnO_2 catalyst is prepared by drop evaporation of a 15% SnO_2 colloidal dispersion in H_2O solution on the quartz wafer. The solution is dropped on the wafer until the solution completely covers the wafer; then the wafer is placed in an oven at 110 °C to evaporate the water. The drop-evaporation procedure is performed three times. The SnO_2 is only weakly bonded to the surface; however, it is bonded well enough to remain on the surface during the experiment.

The 90% SnO_2 – 10% Pt (by mass) catalyst is prepared by mixing SnO_2 (99.9% purity) powder with Pt (99.9% purity) powder. The powder mixture is dispersed in methanol using a 60% powder – 40% methanol (by mass) mixing ratio to form a paste. The paste is spread on the quartz wafer and dried at 110 °C in an oven. Similar to the SnO_2 catalyst, the 90% SnO_2 – 10% Pt powder does not bond to the surface strongly, but remains adhered over the course of an experiment.

Catalyst heating

The stagnation plane mounting surface is heated by a pyrolytic graphite heating element (Momentive Ceramics) which is enclosed in a chamber flooded with nitrogen. Figure 2.7 shows a cross-sectional view of the heater enclosure. The catalyst is mounted on the bottom surface of the enclosure. Two K-type thermocouple probes (Omega Engineering Inc.) measure temperature. One thermocouple is embedded in the heater to measure the heater temperature. The other thermocouple is inserted into a groove between the bottom surface of the enclosure and the catalyst wafer. This thermocouple is used as the feedback in the control of the stagnation-plane temperature. The temperature measured by this thermocouple is denoted the "stagnation-plane temperature" (T_s). The thermocouple probe body is 0.01 inches in diameter and

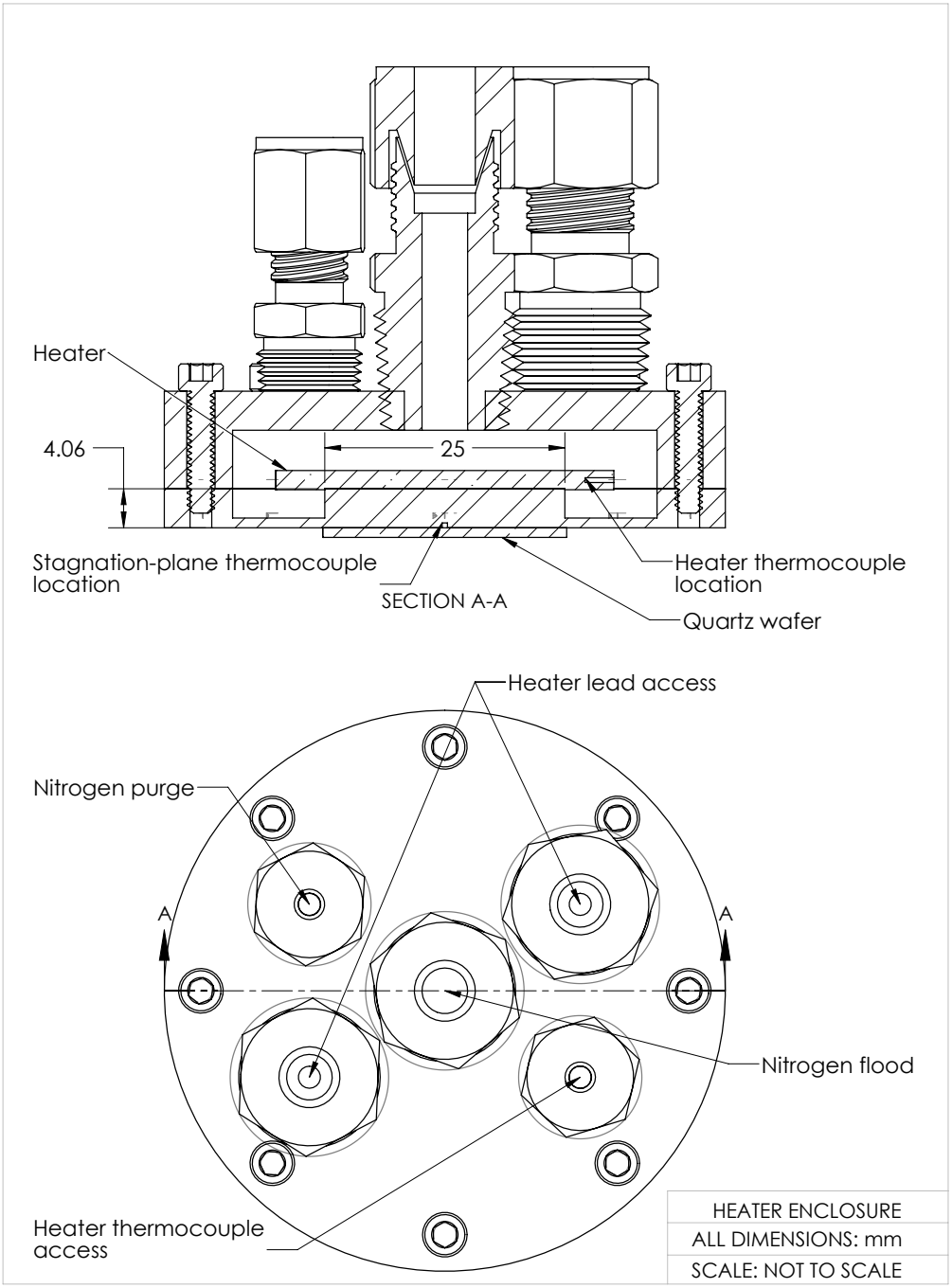

Figure 2.7 Cross-sectional view of the heater enclosure with important dimensions.

contains the thermocouple leads which are electrically insulated from the probe body. The thermocouple voltage is measured by a thermocouple reader (Omega Engineering Inc.) which has a built in cold-junction circuit, and displays the thermocouple bead temperature in °C. The maximum temperature the heating element can maintain is $T_s = 825$ °C for an average air-flow velocity of 1.3 m/s.

A proportional-integral-derivative (PID) approach controls the temperature of the catalyst. The output of the PID controller is given by equation 2.5, where m is the controller output, e is the difference between the set-point and the measured temperature, K_p, T_i, and T_d are controller parameters, and t is time.

$$m(t) = K_p \left(e(t) + \frac{1}{T_i} \int_{-\infty}^{t} e(\tau) d\tau + T_d \frac{de(t)}{dt} \right) \tag{2.5}$$

$$e(t) = T_{sp} - T(t) \tag{2.6}$$

$$K_p = \text{proportional gain}$$

$$K_i = K_p/T_i = \text{integral gain}$$

$$K_d = K_p T_d = \text{derivative gain}$$

The Ziegler-Nichols tuning method is used to tune the controller. The integral gain and derivative gain are input as 0, and the proportional gain is increased until a critical value is reached, K_{cr}, where the output first sustains a steady-state oscillation in temperature. The period of oscillation, P_{cr}, and K_{cr} are used to determine the parameter values: $K_p = 0.6K_{cr}$, $T_i = 0.5P_{cr}$, and $T_d = 0.125P_{cr}$. The heater is tuned at 750 °C while flowing air at $v_{ave} = 1.2$ m/s. The tuning parameters for the catalyst temperature control are, $1/K_p = 67\%$, $T_i = 13$, and $T_d = 3.3$.

The heater resistance is measured experimentally by the input current and voltage to the heater using ohms law (equation 2.7).

$$R = \frac{V}{I} \tag{2.7}$$

The heater resistance decreases with temperature. Figure 2.8 shows this behavior. The data is shown by the solid line in the figure. The dashed line is a least squares fit to the data using equation 2.8, where R is in ohm and T is in kelvin. The power delivered to the heater is denoted by "heater power" (P).

$$R = (-3.0363 \times 10^{-7})T^2 - (5.6228 \times 10^{-5})T + 5.3829 \tag{2.8}$$

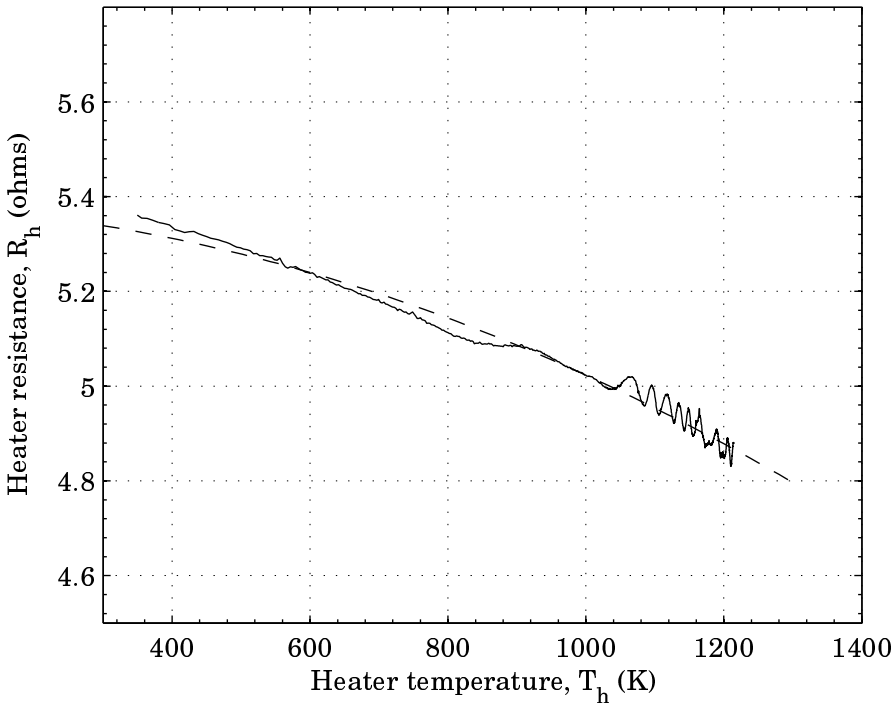

Figure 2.8 Heater resistance as a function of heater temperature. The dashed line is a least squares fit to the data of the solid line (equation 2.8).

The power delivered to the heater is calculated using the measured heater voltage and heater temperature. The resistance of the heater is calculated from the measured heater temperature using the curve fit (equation 2.8). Finally, the power is calculated using equation 2.9.

$$P = V^2/R \tag{2.9}$$

2.1.4 Gas sampling

There are two sampling tubes, one placed on either side of the stagnation plane. The placement of the sampling tubes is symmetric about nozzle axis centerline to minimize disturbance to the reactor flow. The symbol χ denotes the mole fraction of the gas species. For example, χO_2 denotes the oxygen mole fraction. In the exhaust flow, ideal gas behavior is assumed, and the mole fraction and volume fraction are assumed to be equal.

Nondispersive-infrared (NDIR) sensors (Horiba MEXA-584L) are used to measure the volume fractions of O_2, CO, CO_2, NO and unburned hydrocarbons (HC) in the exhaust. The HC in the exhaust is reported as a propane equivalent volume fraction; however, no distinction is possible between different hydrocarbon species. The exhaust stream is brought to room temperature before entering the gas sensing unit, by coiled aluminum tubing 7.5 m in length exposed to the room air. Water sometimes condenses from the exhaust stream as it cools to room temperature, and is filtered from the flow. In this case it is assumed that flow entering the gas sensing unit has 100% humidity at room temperature.

The unburned hydrocarbon, and CO_2 measurements from the sensing unit require additional calibration. The HC value is calibrated to show the n-hexane equivalent volume fraction. The propane equivalent volume fraction is calculated by the propane equivalence factor (0.519). Equation 2.10 shows the calculation of propane equivalent volume fraction given the n-hexane equivalent volume fraction, where PEF is the propane equivalent factor.

$$\%\ C_3H_8\ \text{eq.} = \%\ \text{n-hexane eq.}/\text{PEF} \tag{2.10}$$

The propane equivalent hydrocarbon measurement is not calibrated for high propane volume fractions; therefore, a calibration curve is generated at room temperature and

pressure for high propane volume fraction. The flow meters are used to measure the actual volume fraction of propane in the flow, and the gas sensing unit is calibrated to that measured value. Figure 2.9 shows the calibration data along with a third order least squares polynomial fitted to the data, which is shown by Equation 2.11.

$$\begin{aligned} C_3H_8\% = 0.02196 C_3H_{8eq}\%^3 + 0.07345 C_3H_{8eq}\%^2 \\ +0.5055 C_3H_{8eq}\% + 0.01105 \end{aligned} \tag{2.11}$$

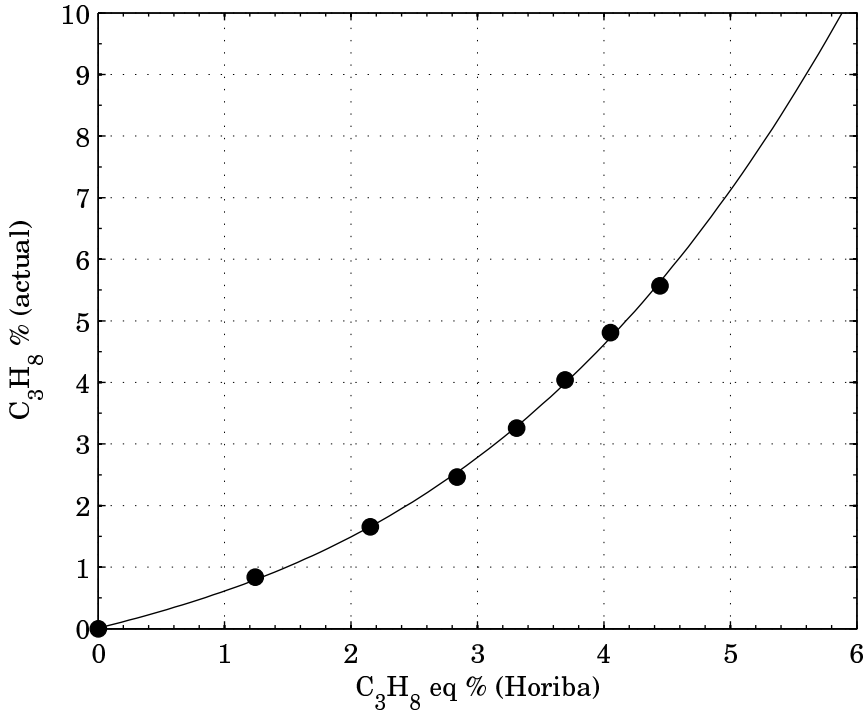

Figure 2.9 Calibration of the unburned hydrocarbon sensor. The curve fitted to the data is given by equation 2.11.

Propane interacted with the CO_2 sensor, and is quantified by flowing a known mixture of air and propane and recording the CO_2 response. Figure 2.10 shows the CO_2 reading due to a certain volume fraction of propane. A fourth order least squares polynomial is fitted to the data, and is used to correct the CO_2 measurement when

known fractions of propane are included in the flow stream. Equation 2.12 shows the fourth order polynomial fitted to the CO_2 sensor interaction with propane.

$$\begin{aligned} CO_2\% = &-6.364 \times 10^{-5} C_3H_8\%^4 + 5.992 \times 10^{-3} C_3H_8\%^3 \\ &-0.07375 C_3H_8\%^2 + 0.4213 C_3H_8\% - 0.03328 \end{aligned} \tag{2.12}$$

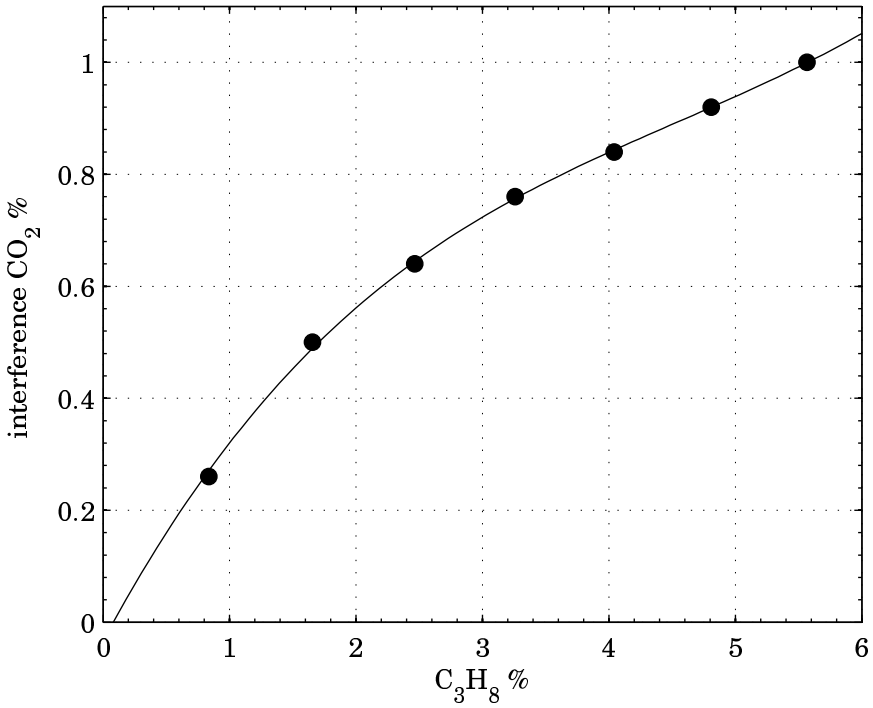

Figure 2.10 Interference of propane with CO_2 sensor. The curve fitted to the data is given by equation 2.12.

2.1.5 Experimental uncertainty

Reactant flow uncertainty

The uncertainty in the reactant flow rate is due to the uncertainty of the flow meters. Recall, the flow meters are corrected for local atmospheric pressure and temperature variations. The mass-flow meter used to calibrate the air flow meter has an uncertainty

of 2% of the reading. The propane flow meter uncertainty is calculated by two standard deviations of five repeated calibrations, giving a 95% confidence level. The fractional uncertainty calculation is shown in equation 2.13, where $\overline{\dot{Q}}$ is the arithmetic mean of the volumetric propane flow rate, and σ is the standard deviation of the volumetric propane flow rate measured in the five repeated calibrations. Figure 2.11 shows the fractional uncertainty of the propane flow as a function of the flow rate.

$$\text{fractional uncertainty} = \frac{2\sigma}{\overline{\dot{Q}}} \tag{2.13}$$

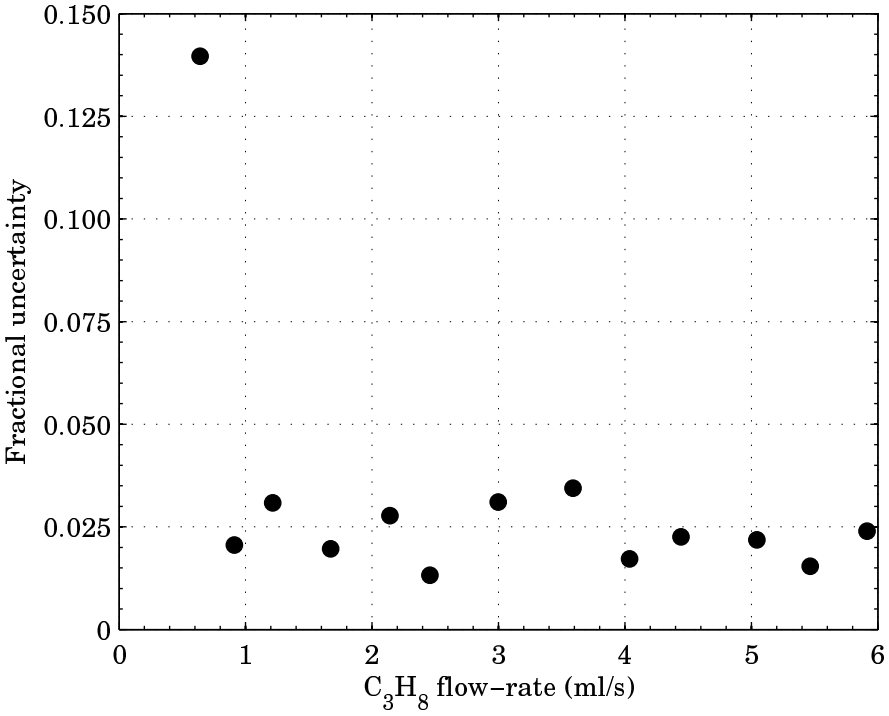

Figure 2.11 Fractional flow-uncertainty (95% confidence level) of propane as a function of flow rate. The uncertainty for the experimental conditions is less than 3.5% of the flow-rate. (P = 995 mb, $T = 23^o$C, rotameter 062-01-ST)

The uncertainty calculation for the equivalence ratio and average nozzle-exit velocity is due to the uncertainty in the volumetric reactant flow rates, the purity of the reactants (Table 2.1), and the mixture uncertainty of oxygen and nitrogen.

The uncertainty of the oxygen and nitrogen purities are an order of magnitude less than the volumetric flow rate uncertainty and are neglected. The resulting fractional uncertainties of the equivalence ratio and the average nozzle-exit velocity are listed in Table 2.2. The symbol U followed by a parameter denotes the uncertainty of that parameter.

Table 2.1 Purity of the reactants

Reactant	Purity
C_3H_8	99%
O_2	99.995%
N_2	99.995%

Table 2.2 Uncertainty of the reactant flow

Parameter	Uncertainty
O_2% in synthetic air	21.00 $\pm$0.005%
$U\dot{Q}_{air}$	$\pm 0.02\dot{Q}_{air}$
$U\dot{Q}_{propane}$	$\pm 0.035\dot{Q}_{propane}$
$U\phi$	$\pm 0.08\phi$
Uv_{ave}	$\pm 0.04v_{ave}$

The equivalence ratio and average nozzle-exit velocity uncertainties are calculated using a numerical statistical analysis from the propane purity, oxygen fraction, and reactant flow rates. All uncertainties are assumed to follow a normal distribution. The reported uncertainty of ϕ and v_{ave} is double the standard deviation calculated in the numerical statistical analysis giving a 95% confidence level. The program used to calculate the uncertainty of ϕ and v_{ave} is written in MATLAB and is included in Appendix C.1.

Temperature uncertainty

The uncertainty in the stagnation-plane temperature is due to thermocouple uncertainty and the temperature variation across the thickness of the catalyst wafer. The K-type thermocouple has an uncertainty of the larger of 2.2 °C or 0.75% of the reading (Omege Engineering Corp.). The temperature variation across the thickness of the

quartz wafer is estimated based on the conductivity of quartz and the heat transfer across its thickness. The conductivity of quartz is 1.4 W/m-K. Recall the dimensions of the quartz wafer are 25.4 mm × 25.4 mm × 1 mm. Thus, the thermal resistance of the quartz wafer is 1.1 K/W (equation 2.14). The quartz wafer thickness is denoted by l; the quartz conductivity is denoted by k, and the quartz wafer area is denoted by A in equation 2.14.

$$R_T = \frac{l}{kA} = \frac{0.001 \text{ m}}{(1.4 \text{ W/m-K})\,(6.45 \times 10^{-4} \text{ m}^2)} = 1.1 \text{ K/W} \tag{2.14}$$

The maximum power the heater produces is 200 W. The heater enclosure surface area is larger than the quartz wafer surface area by a factor of approximately 12.8. Thus, approximately 15.6 W must be dissipated through the wafer assuming no heat release from chemical reaction and an equal dissipation in heater power to the entire enclosure. The temperature difference across the wafer thickness is approximately 17 °C.

This is a good approximation of the upper limit of the temperature difference across the wafer thickness. For lower temperatures and no heat release due to chemical reaction the temperature difference across the wafer thickness will be less than the 17 °C calculated above. For heat release due to chemical reaction, the wafer is heated from both sides. If less than 15.6 W is transferred through the wafer, the temperature difference across the wafer thickness will be less than the 17 °C calculated above.

The total stagnation plane temperature uncertainty is determined by the statistical combination of the uncertainties in the thermocouple measurement and the temperature difference across the wafer thickness. As a worst-case scenario the temperature uncertainty is calculated using the highest temperature investigated, 900 °C. It is assumed the uncertainties are statistically independent and the resulting uncertainty is given by the square root of the sum of each uncertainty squared. Table 2.3 shows the

resulting temperature uncertainty given the contributing factors of the thermocouple uncertainty and the temperature difference across the thickness of the wafer.

Table 2.3 The measurement uncertainty contributing to the stagnation-plane temperature uncertainty.

Parameter	Uncertainty
UT (thermocouple)	$\pm$6.75 °C
UT (wafer thickness)	$\pm$17 °C
UT_s	$\pm$18 °C

Heater power uncertainty

The uncertainty in the heater power is due to the uncertainties of the heater temperature, the polynomial fit of the resistance as a function of heater temperature, the input voltage, and the input current. Table 2.4 presents the uncertainty of the contributions to the heater power uncertainty. The heater voltage and current are measured using a multimeter (Fluke 45).

Table 2.4 The measurement uncertainty contributing to the heater-power uncertainty.

Parameter	Uncertainty
UV	$\pm 0.002V$
UI	$\pm 0.0005I$
UR	$\pm 0.004R$
UR_{fit}	$\pm$0.27 Ohm
UT_h	$\pm$ larger of 2.2 °C or 0.0075 T_h
UP	$\pm 0.11P$

The uncertainty in the heater power is predominantly due to the polynomial fit of the resistance as a function of heater temperature. The polynomial fit uncertainty is the maximum absolute value of the curve-fit residuals. The heater-power uncertainty is calculated numerically using the constituent uncertainties. The reported uncertainty of P is double the standard deviation of the numerically calculated statistical variation, giving a 95% confidence level. The program used to calculate the uncertainty is included in Appendix C.2.

Gas-sampling uncertainty

The uncertainties of the exhaust gas species measurements are due to the gas sensing unit uncertainty, the uncertainty in the propane curve fit, and the uncertainty in the CO_2 curve fit. The maximum absolute value of the curve-fit residuals is an order of magnitude less than the uncertainties of the gas sensing unit. Thus, the uncertainty in the C_3H_8 and CO_2 volume fractions due to the curve fits are neglected. Table 2.5 lists the uncertainties of the exhaust gas species measurements.

Table 2.5 Gas species measurement uncertainties

Gas species	Uncertainty
CO	$\pm 0.025\%$
C_3H_8[1]	$\pm 2.5\% C_3H_8$
CO_2	$\pm 0.15\%$
O_2	$\pm 1.5\% O_2$
NO	25 ppm (detection limit)

1 C_3H_8 equivalent fraction

Uncertainties of the flame study measurements

The distance between the disk flame and the stagnation plane is denoted by the disk-flame separation distance, x_{sep}. The disk-flame separation distance is determined by measuring a calibrated image of the flame. Figure 2.12 shows a magnified image of the disk flame at the condition $v_{ave} = 1.2$ m/s and $\phi = 0.77$. Measurement of disk-flame separation distance showing its uncertainty is labeled on the figure. The disk-flame separation distances reported are the distance between the stagnation plane and the top of the flame surface. The uncertainty in the measurement is due to determining the location of the stagnation plane and top of the flame on the figure. The uncertainty in x_{sep} is determined to be ± 0.26 mm.

The repeatability of the lean-extinction limit is determined by double the standard deviation of the lean-extinction limit of five repeated experiments. This results in ± 0.02 and gives a confidence level of 95%. The repeatability of ϕ_{min} and the uncertainty

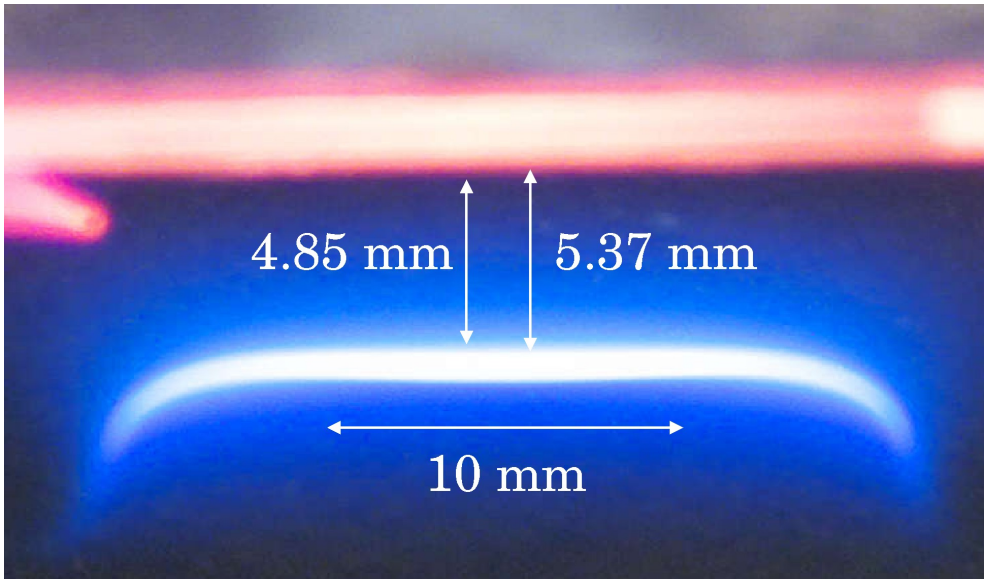

Figure 2.12 The uncertainty in the disk-flame separation distance.

of ϕ both contribute to the uncertainty of the lean-extinction limit. It is assumed that the repeatability of ϕ_{min} and the uncertainty of ϕ are normally distributed and independent from each other. The uncertainty of ϕ_{min} for the experiments is $\pm\sqrt{0.02^2 + (0.08\phi)^2}$.

2.2 Experimental procedure

This dissertation contains two experimental studies: catalysis of propane oxidation and flame catalyst interaction. The experimental procedures for the catalysis of propane oxidation study and flame catalyst interact ion study are described in this section.

2.2.1 Catalysis of propane oxidation

The independent parameters of the catalytic oxidation of propane studies are the equivalence ratio, the average nozzle-exit velocity, and the stagnation-plane temperature; the dependent parameters are the heater power and the exhaust species volume fractions.

The data is recorded by several pieces of equipment. The temperature controller measures and controls the stagnation plane temperature. A thermocouple reader (Omega Engineering Corp.) is used to measure the heater temperature, and a multimeter (Fluke 45 dual display multimeter) is used to measure the input voltage to the heater. Recall, the heater temperature and heater voltage determine the power delivered to the heater. The equivalence ratio, and the average nozzle-exit velocity are measured by the propane and air rotameters (Omega Engineering Inc.). The exhaust species are measured using NDIR gas sensors (Horiba).

There are several preparations required before data is recorded. Starting with the apparatus at room temperature, the catalyst is mounted on the heater enclosure, and the experimental apparatus is assembled. After the apparatus is assembled, the heater enclosure is flooded with nitrogen at 5 psi. The float heights of the air and propane rotameters are calculated based on the room pressure and temperature for the desired ϕ and v_{ave} to be studied, and using the calculated float heights, the reactant flow is initiated. Finally, the gas-sampling unit is allowed to warm up for five minutes.

Data is recorded over the temperature range $T_s = 22$ °C to $T_s = 800$ °C. For the prescribed ϕ and v_{ave} the dependent parameters are recorded over 50 °C increments, except over the catalyst light-off temperature range, where the temperature is varied by 25 °C increments. For each temperature increment, data is recorded after the apparatus reaches steady state operation which takes 10 minutes. For the prescribed flow condition, separate data sets are recorded by increasing or decreasing temperature: data is recorded starting at high temperature and incrementally decreasing the stagnation-plane temperature, and data is recorded starting at low temperature and incrementally increasing the stagnation-plane temperature. The apparatus is always allowed to cool to room temperature before the catalytic activity of a different equivalence ratio and/or average nozzle-exit velocity is recorded.

2.2.2 Flame-catalyst interaction

The independent parameters of the flame catalyst interaction studies are the equivalence ratio, the average nozzle-exit velocity; the dependent parameters are the electrical power delivered to the heater, the lean-extinction limit, the disk-flame separation distance, and flame structure.

The heater power, stagnation-plane temperature, equivalence ratio, and average nozzle-exit velocity are recorded by the same equipment used to record data for the catalysis oxidation of propane study. The rotameters are used to record the lean-extinction limit. The the flame-stagnation-plane separation distance, and flame structure are recorded using a digital camera.

The preparation to record data is similar to the catalysis of propane oxidation study. Starting with the apparatus at room temperature, the catalyst is mounted on the heater enclosure, and the experimental apparatus is assembled. After the apparatus is assembled, the heater enclosure is flooded with nitrogen at 5 psi. Different from the catalysis of propane oxidation studies, the equivalence ratio varies throughout the experiment. The air rotameter float height is calculated based on the room pressure and temperature for the desired v_{ave} to be studied.

Data is recorded starting with an ignited stable disk flame and a prescribed average nozzle-exit velocity. The disk flame is ignited using a small propane air torch. Recall, the stagnation-plane is open to the atmosphere for the flame-catalyst interaction studies. After the stable flame is ignited, the temperature controller is used to prescribe the stagnation-plane temperature. The equivalence ratio is decreased in approximately $\phi = 0.04$ increments until flame extinction occurs. The equivalence ratio is decreased by decreasing the fuel flow rate while leaving the air flow rate constant. For each increment in ϕ, data is recorded after the system reaches steady state.

Chapter 3

Catalysis of propane oxidation

Five materials are examined for catalytic propane oxidation: platinum, palladium, 90% SnO_2 – 10% Pt (by mass), SnO_2, and quartz. The platinum propane-oxidation results are presented in Section 3.1. In this section, key terms and general catalytic behavior are defined. Section 3.2 presents the results for the the palladium, 90% SnO_2 – 10% Pt, SnO_2, and quartz catalysts, and compares them with the platinum behavior. Finally, Section 3.3 discusses the results. The platinum results from this chapter have been presented at *The 6th U.S. National Combustion Meeting* and the paper published in the proceedings is included in Appendix B.

For all cases the average nozzle-exit velocity is 1.2 m/s. Three propane-air mixtures are investigated: a fuel-rich, stoichiometric and fuel-lean mixture. The three propane-air mixtures are defined by three different values of the normalized equivalence ratio ($\Phi = \phi/(1+\phi)$): $\Phi = 0.6$, 0.5, and 0.4 ($\phi = 1.50$, 1.00, and 0.67). The heater power, CO_2, O_2, C_3H_8, CO and NO volume fractions quantify the reactivity of the catalysts. Tables 3.1-3.5 show the experimental data using platinum, palladium, 90% SnO_2 – 10% Pt , SnO_2, and quartz as catalysts. Table 3.6 shows the constituent-species volume fraction of the inlet flow for the three fuel-air mixtures.

Table 3.1 Exhaust-gas analysis for platinum (PVD) catalytic-oxidation activity on C_3H_8-air mixtures: $v_{ave} = 1.2$ m/s. P denotes the power required to maintain the stagnation-plane temperature, and T_s denotes the stagnation-plane temperature. All species measurements are provided on a volume-fraction basis.

T_s °C	P (W)	CO_2 %	O_2 %	C_3H_8 %	CO %	NO ppm
			$\phi = 1.50$, ($\Phi = 0.6$)			
100	22	0.08	21.41	5.76	0.01	0
200	43	0.08	21.49	5.83	0.01	0
250	47	0.09	21.32	5.94	0.01	0
275	49	0.11	21.25	5.96	0.01	0
300	50	0.21	21.13	6.04	0.01	0
325	50	0.41	20.89	6.01	0.01	0
350	46	0.65	20.56	5.97	0.01	0
375	41	0.92	20.19	5.92	0.02	0
425	0	2.55	17.60	5.30	0.02	0
450	0	2.84	17.25	5.24	0.02	0
500	10	3.11	16.85	5.29	0.04	0
600	34	3.28	16.58	5.25	0.09	0
700	67	3.34	16.46	5.22	0.12	0
800	95	3.38	16.42	5.21	0.13	0
			$\phi = 1.00$, ($\Phi = 0.5$)			
100	23	0.01	21.01	4.01	0.00	0
200	43	0.02	21.60	4.18	0.02	0
250	49	0.02	21.64	4.20	0.01	0
275	50	0.06	21.61	4.22	0.02	0
300	51	0.08	21.26	4.22	0.01	0
325	48	0.29	20.95	4.16	0.02	0
350	29	0.98	19.93	3.91	0.02	0
375	23	1.37	19.34	3.79	0.02	0
425	21	1.82	18.65	3.62	0.02	0
450	25	1.93	18.46	3.57	0.02	0
500	33	2.07	18.25	3.52	0.02	0
600	55	2.17	18.09	3.48	0.02	0
700	81	2.21	18.00	3.46	0.02	0
800	115	2.26	17.93	3.44	0.03	0
			$\phi = 0.67$, ($\Phi = 0.4$)			
100	23	-0.02	21.75	2.92	0.01	0
200	44	-0.02	21.83	2.93	0.02	0
250	47	-0.04	21.85	2.94	0.01	0
275	51	0.00	21.81	2.94	0.02	0
300	54	0.04	21.76	2.93	0.02	0
325	54	0.12	21.63	2.90	0.02	0
350	42	0.64	20.87	2.72	0.02	0

Continued on next page

Table 3.1 – continued from previous page

T_s ^{o}C	P (W)	CO_2 %	O_2 %	C_3H_8 %	CO %	NO ppm
$\phi = 0.67$, ($\Phi = 0.4$)						
372	36	0.94	20.39	2.61	0.02	0
425	39	1.27	19.87	2.49	0.02	0
450	41	1.36	19.72	2.46	0.02	0
500	47	1.46	19.56	2.42	0.02	0
600	75	1.55	19.43	2.39	0.02	0
700	106	1.61	19.33	2.37	0.02	0
800	131	1.63	19.27	2.35	0.02	0

Table 3.2 Exhaust-gas analysis for palladium foil catalytic-oxidation activity on C_3H_8-air mixtures: $v_{ave} = 1.2$ m/s. P denotes the power required to maintain the stagnation-plane temperature, and T_s denotes the stagnation-plane temperature. All species measurements are provided on a volume-fraction basis.

T_s ^{o}C	P (W)	CO_2 %	O_2 %	C_3H_8 %	CO %	NO ppm
$\phi = 1.50$, ($\Phi = 0.6$)						
23	0	0.14	20.45	6.71	0.01	0
100	25	0.11	20.41	6.44	0.01	0
150	37	0.10	19.99	6.35	0.01	0
200	46	0.09	19.87	6.28	0.01	0
250	54	0.11	19.85	6.24	0.01	0
300	61	0.10	19.89	6.12	0.00	0
350	71	0.12	20.00	6.13	0.01	0
427	0	2.82	15.82	5.24	0.03	0
450	1	3.16	15.20	5.10	0.12	0
475	1	3.20	15.14	5.06	0.12	0
500	10	3.19	15.27	5.10	0.12	0
550	30	3.27	15.11	5.08	0.12	0
600	40	3.31	15.09	5.06	0.13	0
700	73	3.31	14.97	5.02	0.15	0
800	103	3.33	14.86	4.99	0.16	0
$\phi = 1.00$, ($\Phi = 0.5$)						
22	0	0.04	20.28	4.00	0.01	0
100	30	0.03	20.27	4.05	0.02	0
150	39	0.02	20.22	4.02	0.01	0
200	50	0.01	20.01	4.05	0.00	0
250	57	0.03	19.97	4.06	0.02	0
300	65	0.02	19.98	4.05	0.02	0
350	72	0.02	19.97	4.05	0.02	0

Continued on next page

Table 3.2 – continued from previous page

T_s ^{o}C	P (W)	CO_2 %	O_2 %	C_3H_8 %	CO %	NO ppm
$\phi = 1.00$, ($\Phi = 0.5$)						
375	75	0.00	20.16	4.02	0.01	0
400	81	0.00	20.13	4.01	0.01	0
425	77	0.02	20.20	4.00	0.01	0
450	85	0.08	20.13	3.97	0.02	0
475	83	0.21	19.83	3.89	0.01	0
500	72	0.63	19.36	3.74	0.02	0
525	69	0.93	18.81	3.62	0.02	0
550	61	1.42	18.08	3.42	0.02	0
575	66	1.61	17.81	3.35	0.02	0
600	65	1.88	17.37	3.23	0.02	0
625	70	2.02	17.19	3.19	0.02	0
650	76	2.06	17.09	3.15	0.02	0
700	92	2.13	17.07	3.13	0.02	0
800	135	1.88	17.34	3.18	0.02	0
$\phi = 0.67$, ($\Phi = 0.4$)						
26	0	-0.04	20.34	2.88	0.01	0
100	25	-0.04	20.36	2.86	0.01	0
200	52	-0.03	20.28	2.84	0.01	0
250	59	-0.02	20.33	2.85	0.02	0
300	64	-0.02	20.37	2.86	0.02	0
350	72	0.00	20.38	2.86	0.02	0
400	81	0.04	20.31	2.85	0.02	0
425	83	0.06	20.29	2.84	0.02	0
450	77	0.14	20.20	2.81	0.02	0
475	85	0.24	20.04	2.77	0.02	0
500	83	0.43	19.76	2.71	0.02	0
525	77	0.75	19.26	2.58	0.02	0
550	73	1.12	18.69	2.44	0.02	0
575	78	1.32	18.00	2.32	0.01	0
600	76	1.44	17.83	2.29	0.01	0
625	85	1.51	17.75	2.27	0.01	0
650	93	1.55	17.69	2.26	0.01	0
700	111	1.61	17.53	2.23	0.01	0
800	157	1.54	17.38	2.19	0.01	0

Table 3.3 Exhaust gas analysis for 90% SnO_2 – 10% Pt (by mass) catalytic-oxidation activity on C_3H_8-air mixtures: $v_{ave} = 1.2$ m/s. P denotes the power required to maintain the stagnation-plane temperature, and T_s denotes the stagnation-plane temperature. All species measurements are provided on a volume-fraction basis.

T_s °C	P (W)	CO_2 %	O_2 %	C_3H_8 %	CO %	NO ppm
$\phi = 1.50$, ($\Phi = 0.6$)						
22	0	0.14	20.68	6.79	0.01	0
100	26	0.11	20.13	6.46	0.01	0
150	35	0.12	20.12	6.36	0.01	0
200	43	0.11	19.70	6.32	0.00	0
250	51	0.13	19.66	6.29	0.01	0
361	0	2.60	15.95	5.46	0.02	0
380	0	2.66	15.92	5.28	0.02	0
400	2	2.68	16.02	5.25	0.02	0
425	9	2.72	15.96	5.22	0.02	0
450	16	2.73	15.91	5.21	0.03	0
500	28	2.77	15.79	5.16	0.02	0
550	39	2.79	15.76	5.12	0.03	0
600	54	2.81	15.76	5.10	0.03	0
650	68	2.81	15.74	5.06	0.02	0
700	84	2.85	15.73	5.04	0.03	0
800	118	2.85	15.63	5.00	0.04	0
$\phi = 1.00$, ($\Phi = 0.5$)						
100	27	0.02	20.61	4.24	0.01	0
150	38	0.03	20.56	4.29	0.02	0
200	48	0.00	20.20	4.25	0.01	0
250	54	0.02	20.27	4.25	0.01	0
300	63	0.01	20.24	4.22	0.01	0
325	49	0.55	19.28	4.02	0.01	0
350	49	0.75	18.98	3.95	0.02	0
375	50	0.87	18.83	3.91	0.02	0
400	50	0.93	18.72	3.88	0.02	0
425	54	1.00	18.65	3.84	0.01	0
450	57	1.06	18.66	3.83	0.02	0
500	68	1.11	18.55	3.82	0.02	0
600	92	1.19	18.42	3.77	0.02	0
700	121	1.38	18.15	3.70	0.02	0
800	158	1.44	18.00	3.65	0.02	0
$\phi = 0.67$, ($\Phi = 0.4$)						
22	0	-0.02	20.83	2.92	0.01	0
100	29	-0.02	20.65	2.86	0.01	0
150	39	-0.04	20.59	2.84	0.01	0
200	49	-0.03	20.58	2.82	0.02	0

Continued on next page

Table 3.3 – continued from previous page

T_s ^{o}C	P (W)	CO_2 %	O_2 %	C_3H_8 %	CO %	NO ppm
			$\phi = 0.67$, ($\Phi = 0.4$)			
250	55	-0.05	20.35	2.80	0.01	0
300	62	-0.04	20.52	2.80	0.01	0
325	64	-0.02	20.54	2.80	0.01	0
350	60	0.15	20.04	2.73	0.01	0
375	63	0.28	19.91	2.68	0.01	0
400	63	0.43	19.73	2.54	0.01	0
425	65	0.51	19.58	2.60	0.01	0
450	69	0.57	19.55	2.58	0.01	0
500	76	0.63	19.43	2.55	0.01	0
600	100	0.71	19.23	2.51	0.01	0
700	129	0.79	19.15	2.49	0.01	0
800	167	0.88	19.02	2.45	0.02	0

Table 3.4 Exhaust-gas analysis for SnO_2 catalytic-oxidation activity on C_3H_8-air mixtures: $v_{ave} = 1.2$ m/s. P denotes the power required to maintain the stagnation-plane temperature, and T_s denotes the stagnation-plane temperature. All species measurements are provided on a volume-fraction basis.

T_s ^{o}C	P (W)	CO_2 %	O_2 %	C_3H_8 %	CO %	NO ppm
			$\phi = 1.50$, ($\Phi = 0.6$)			
600	100	0.07	21.00	6.18	0.02	0
700	128	0.17	21.34	6.18	0.01	0
800	171	0.29	21.14	6.10	0.02	0
820	182	0.31	21.05	6.06	0.01	0
			$\phi = 1.00$, ($\Phi = 0.5$)			
600	97	0.06	21.80	4.26	0.02	0
700	128	0.08	21.76	4.25	0.02	0
800	172	0.18	21.60	4.23	0.02	0
820	181	0.21	21.54	4.13	0.02	0
			$\phi = 0.67$, ($\Phi = 0.4$)			
600	92	0.00	22.06	2.92	0.01	0
700	132	0.02	22.02	2.92	0.02	0
800	171	0.09	21.89	2.83	0.02	0
820	181	0.11	21.84	2.82	0.02	0

Table 3.5 Exhaust-gas analysis for quartz catalytic-oxidation activity on C_3H_8-air mixtures: $v_{ave} = 1.2$ m/s. P denotes the power required to maintain the stagnation-plane temperature, and T_s denotes the stagnation-plane temperature. All species measurements are provided on a volume-fraction basis.

T_s ^{o}C	P (W)	CO_2 %	O_2 %	C_3H_8 %	CO %	NO ppm
$\phi = 1.50$, ($\Phi = 0.6$)						
100	19	0.09	21.24	5.94	0.01	0
200	40	0.07	21.31	5.93	0.01	0
300	57	0.07	21.31	5.98	0.01	0
400	72	0.11	21.34	6.03	0.01	0
500	91	0.11	21.35	6.05	0.01	0
600	112	0.11	21.36	6.06	0.01	0
700	138	0.13	21.37	6.08	0.02	0
800	173	0.13	21.37	6.08	0.02	0

Table 3.6 Inlet flow composition. All species fractions are provided on a volume-fraction basis.

ϕ	Φ	O_2 %	C_3H_8 %	N_2 %
1.50	0.6	19.76	5.93	74.31
1.00	0.5	20.16	4.03	75.81
0.67	0.4	20.44	2.72	76.84

3.1 Platinum propane-oxidation results

Figures 3.1, 3.2, and 3.3 show the volume-fractions of CO_2, O_2, and C_3H_8 in the exhaust flow as a function of the stagnation-plane temperature, T_s, for PVD platinum catalysed oxidation of propane. The bars in the figures denote the uncertainty in the data; recall, the uncertainty of the data is discussed in Chapter 2.1.5 on page 28. Each figure shows the results for the three fuel-air mixtures at $v_{ave} = 1.2$ m/s.

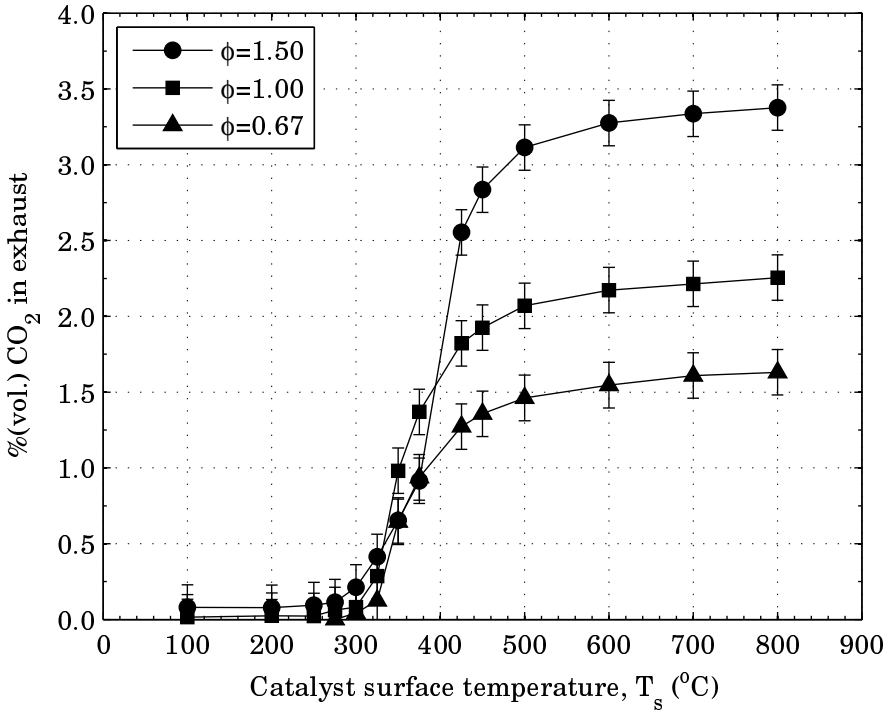

Figure 3.1 Platinum CO_2 activity for propane-air mixtures at $v = 1.2$ m/s.

The three figures show an abrupt change of the exhaust-gas chemical composition. At low temperatures, the CO_2, O_2, and C_3H_8 fractions are stable, and as a check on the system, the O_2 and C_3H_8 inlet mixture fractions (Table 3.6) are within the experimental uncertainty of their measured values. As the temperature increases, the O_2 and C_3H_8 fractions begin to decrease, and the CO_2 fraction begins to increase. The sensitivity of the exhaust-gas composition to T_s does not continue indefinitely for increasing T_s. For high temperatures, the CO_2, O_2, and C_3H_8 volume fractions

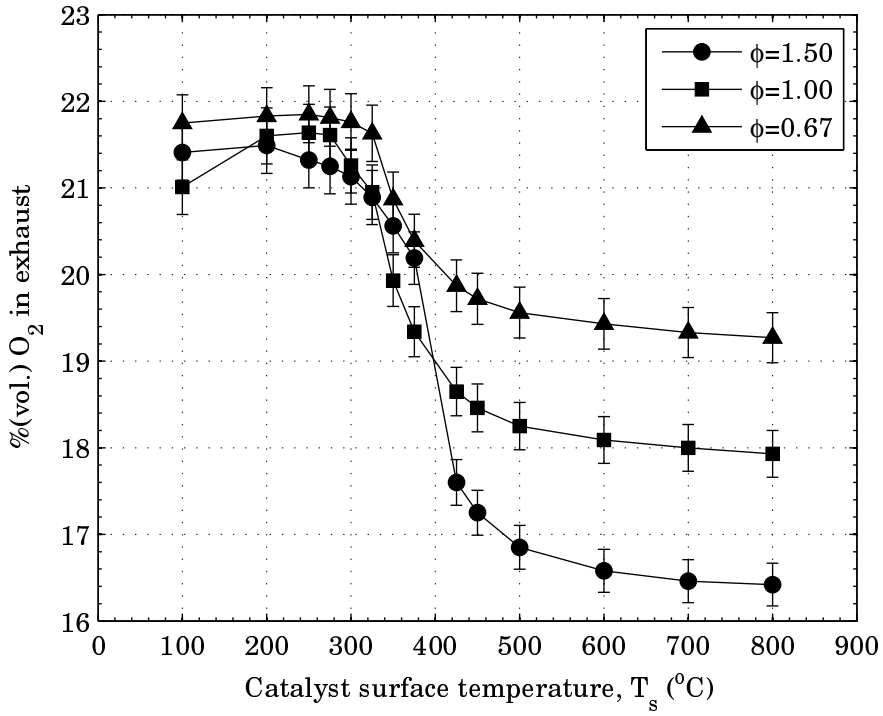

Figure 3.2 Platinum O_2 activity for propane-air mixtures at $v = 1.2$ m/s.

stabilize.

Complete oxidation does not occur in this system. This is most obvious in Fig. 3.3 where C_3H_8 is present in the exhaust for the fuel-lean and stoichiometric cases, which would not be present for complete oxidation. The presence of the fuel in the exhaust sample is attributed to a portion of the flow bypassing the stagnation plane without having opportunity to react. Figure 3.1 shows that the largest fraction of CO_2 in the exhaust is present for the fuel-rich case.

There are two critical temperatures defined for these results. The lowest temperature where CO_2 is detectable in the exhaust is named the "catalyst-activation temperature" (T_{sa}). This temperature is determined based on a piecewise linear interpolation of the CO_2 data, and is defined as the lowest temperature where the CO_2 in the exhaust is greater than 0.15%. The stagnation-plane temperature where the first derivative of the CO_2 fraction with respect to the stagnation plane temperature

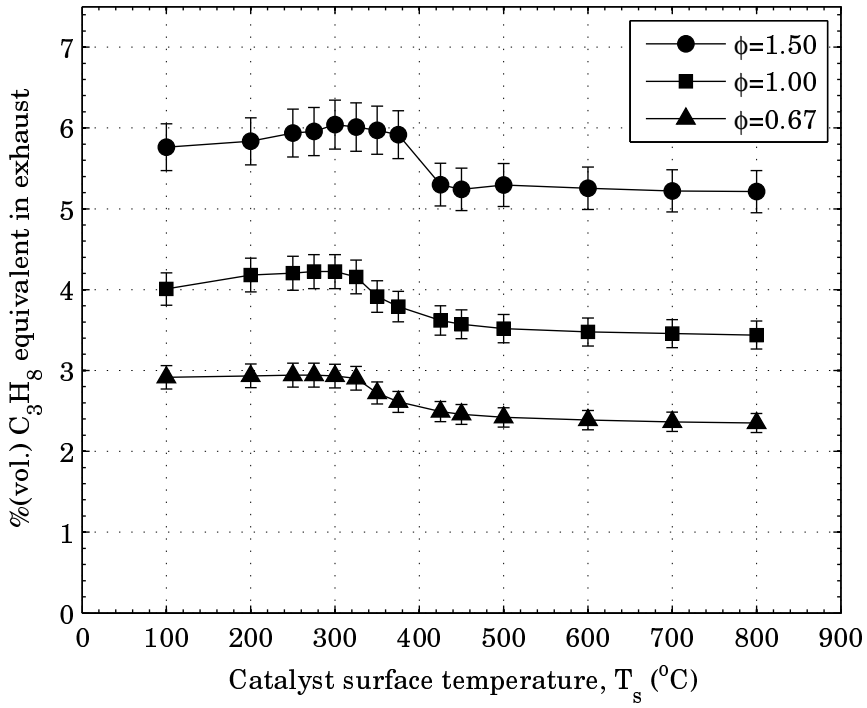

Figure 3.3 Platinum C_3H_8 activity for propane-air mixtures at $v = 1.2$ m/s.

$(d(\chi CO_2)/dT_s)$ is at a maximum (the inflection point of the curve) is named "CO_2 inflection temperature" ($T_{i\ CO_2}$).

The derivative curve is calculated by equation 3.1 using a piecewise linear interpolation of the data points with a resolution of 1 °C.

$$\frac{d\left(\chi CO_2(T)\right)}{dT_s} \approx \frac{\chi CO_2\left(T + 1°C\right) - \chi CO_2\left(T\right)}{1°C} \tag{3.1}$$

Figure 3.4 shows the CO_2 fraction and its derivative for $\phi = 1.50$. The catalyst-activation and CO_2 inflection temperatures are labeled on the figure: $T_{sa} = 285$ °C and $T_{i\ CO_2} = 400$ °C.

Figure 3.5 shows the electric power (P) required to maintain the stagnation-plane temperature at a given value. The heater power using a quartz stagnation-plane is also plotted on the figure, and it monotonically increases for increasing T_s. Using the PVD platinum catalyst, a local maximum and minimum in P occur. The temper-

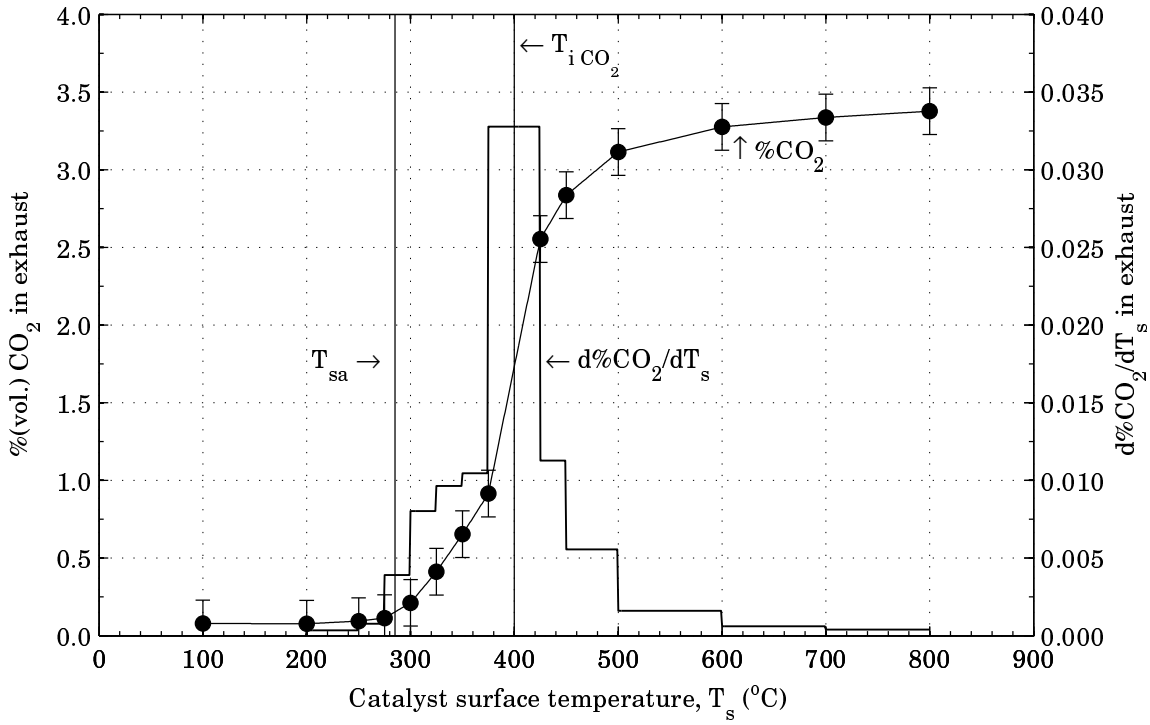

Figure 3.4 The first derivative of the CO_2 fraction with respect to the stagnation plane temperature for platinum oxidized propane-air at $\phi = 1.5$ and $v = 1.2$ m/s.

ature where the local maximum in P as a function of T_s occurs is denoted by "the local-maximum-power temperature" ($T_{P\ max}$), and the temperature where the local minimum in P as a function of T_s occurs is denoted by "the local-minimum-power temperature" ($T_{P\ min}$). Both $T_{P\ max}$ and $T_{P\ min}$ are labeled on the figure for each fuel-air mixture.

The heater power increases for increasing stagnation-plane temperature until the local maximum occurs. As the temperature is further increased, the heater power decreases for increasing temperature until the local minimum. For temperatures greater than the local-minimum-power temperature, the power increases monotonically with increasing temperature. For the platinum stagnation plane and $\phi = 1.50$, the local-maximum-power and local-minimum-power temperatures occur at $T_s = 325$ °C and $T_s = 437$ °C. For T_s between 325 and 437 °C, the heater power abruptly decreases for increasing stagnation-plane temperature.

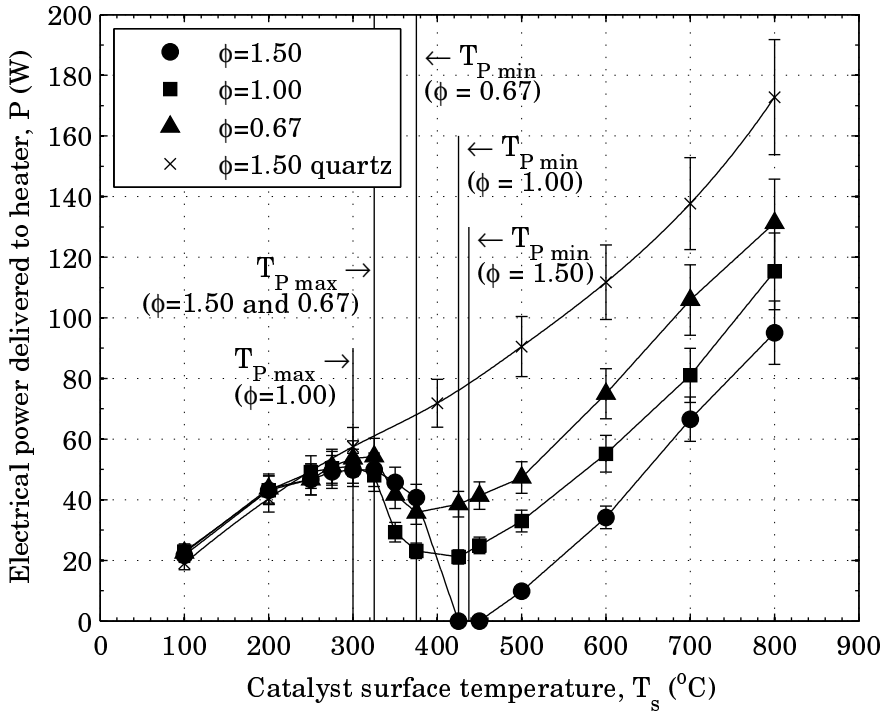

Figure 3.5 Power delivered to heater for platinum catalyzed propane-air mixtures at $v = 1.2$ m/s.

The largest difference in power between the local maximum and minimum occurs at the fuel-rich condition, and the smallest difference in power between the local maximum and minimum occurs at the fuel-lean condition. In particular, for $\phi = 1.50$ the catalytic reaction is sufficient to maintain the stagnation plane at both 425 °C and 450 °C with no electrical power input to the heater.

Figure 3.6 shows the CO volume fraction in the exhaust-gas flow. The CO volume fraction is most apparent for the fuel-rich ($\phi = 1.50$) condition. At low temperature, CO is not present in the exhaust. For a large enough temperature, the CO fraction begins to increase. The temperature where CO is first detectable in the experiment is denoted by "the CO inception temperature" (T_{CO}). The CO inception temperature is determined by the lowest temperature where the CO fraction increases above 0.025%, and is determined by a piecewise linear interpolation. The CO inception temperature is labeled in the figure: $T_{\mathrm{CO}} = 463$ °C for $\phi = 1.50$ and $T_{\mathrm{CO}} = 751$ °C for $\phi = 1.00$. Using

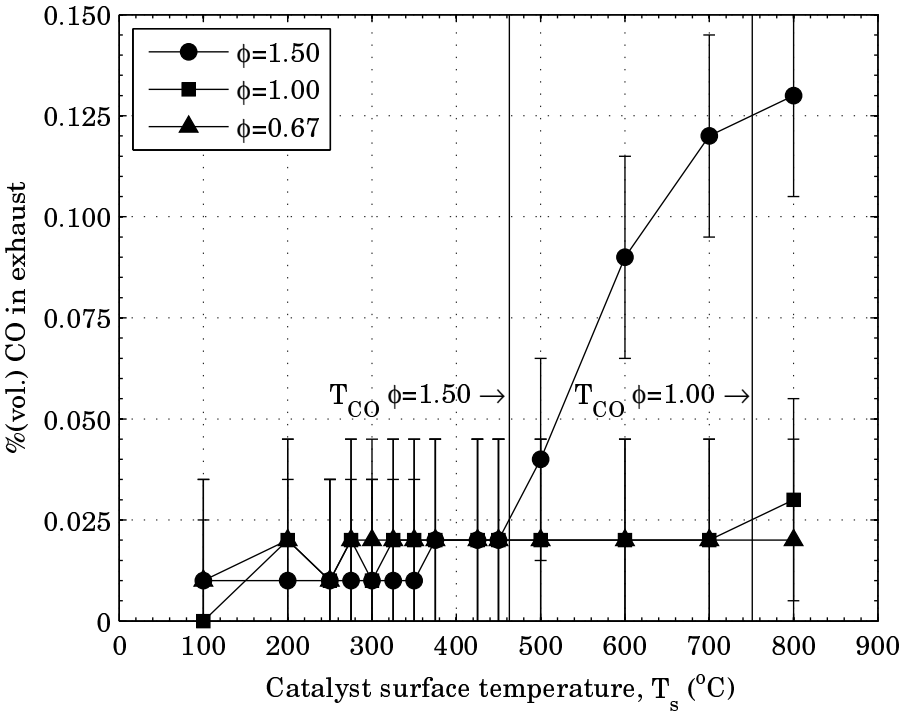

Figure 3.6 Platinum CO activity for propane-air mixtures at $v = 1.2$ m/s.

a quartz stagnation-plane, the CO volume fraction is undetectable at the fuel-rich condition. The CO fraction is also undectable for the fuel-lean case ($\phi = 0.67$).

3.2 Comparison of catalyst performance

The critical temperatures introduced (T_{sa}, $T_{i\ CO_2}$, $T_{P\ max}$, $T_{P\ min}$, and T_{CO}) are presented in Table 3.7 for the platinum, palladium, 90% SnO_2 – 10% Pt, and SnO_2 catalysts. The values of the derivative of the CO_2 fraction ($d\chi CO_2\left(T_{i\ CO_2}\right)/dT_s$), maximum power ($P_{max}$), and minimum power ($P_{max}$) at $T_{i\ CO_2}$, $T_{P\ max}$, and $T_{P\ min}$ are also included in Table 3.7.

Table 3.7 The critical catalyst temperatures for the platinum, palladium, 90% SnO_2 – 10% Pt (by mass), and SnO_2 catalysts. Temperatures are reported in °C, and power is reported in watts (W).

	T_{sa}	$T_{i\ CO_2}$	$\frac{d\chi CO_2(T_{i\ CO_2})}{dT_s}$	$T_{P\ max}$	P_{max}	$T_{P\ min}$	P_{max}	T_{CO}
$\phi = 1.50$, ($\Phi = 0.6$)								
Pt	285	400	0.033	313	50	438	0	463
Pd	351	391	0.035	350	71	450	1	408
90% SnO_2 – 10% Pt	252	303	0.022	250	51	371	0	438
SnO_2	682	–	–	–	–	–	–	–
$\phi = 1.00$, ($\Phi = 0.6$)								
Pt	309	339	0.028	300	51	425	21	751
Pd	464	536	0.020	450	85	550	61	–
90% SnO_2 – 10% Pt	307	312	0.021	300	54	338	49	–
SnO_2	769	–	–	–	–	–	–	–
$\phi = 0.67$, ($\Phi = 0.6$)								
Pt	327	340	0.021	313	54	372	36	–
Pd	453	532	0.015	475	85	550	73	–
90% SnO_2 – 10% Pt	350	363	0.006	325	64	350	60	–

3.2.1 The fuel-rich condition, $\phi = 1.50$

Figures 3.7, 3.8, and 3.9 show the CO_2 volume fraction, heater power, and CO volume fraction for the palladium, 90% SnO_2 – 10% Pt (by mass), SnO_2, quartz and platinum catalysts at the fuel-rich condition ($\phi = 1.50$). The palladium, and 90% SnO_2 – 10%

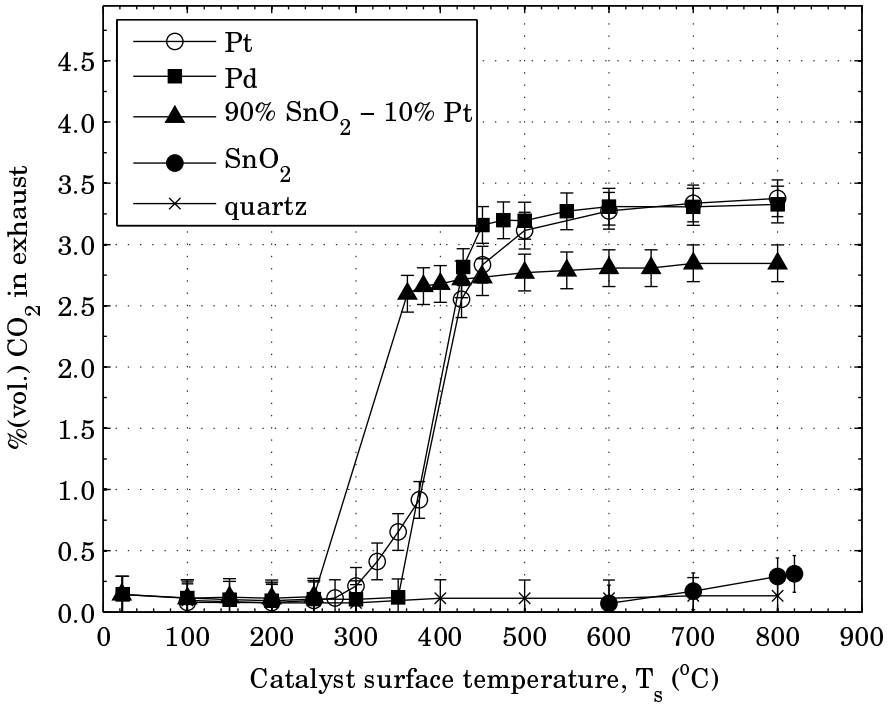

Figure 3.7 Catalytic CO_2 production for a propane-air mixture at $v = 1.2$ m/s and $\phi = 1.50$ using a platinum, palladium 90% SnO_2 – 10% Pt (by mass), SnO_2, or quartz catalyst.

Pt catalysts show the same general behavior as platinum. At low temperature, the CO_2 is below its detectivity limit, and as the catalyst temperature increases, the CO_2 fraction increases rapidly. As the temperature increases further, the CO_2 fraction passes through an inflection point (the CO_2-inflection temperature) and begins to stabilize. At high temperature there is very little increase in propane oxidation for increasing temperature.

The power required to maintain T_s also behaves similarly to platinum for the palladium, and 90% SnO_2 – 10% Pt catalysts. The power increases until it reaches a local

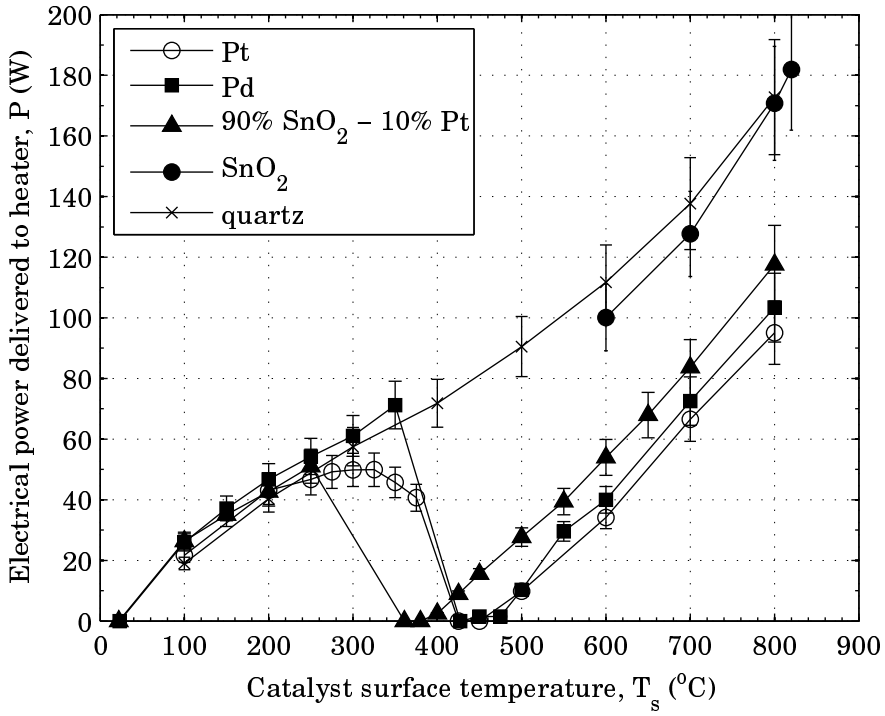

Figure 3.8 The power required to maintain the catalyst temperature for a propane-air mixture at $v = 1.2$ m/s and $\phi = 1.50$ using a platinum, palladium 90% SnO_2 – 10% Pt (by mass), SnO_2, or quartz catalyst.

maximum for increasing T_s, the local-maximum-power temperature. As T_s increases further, the power decreases until it reaches a local minimum. Finally, for increasing T_s the heater power increases for temperatures greater than the local-minimum-power temperature.

The quartz stagnation plane does not exhibit the catalyst-activation and CO_2-inflection temperatures, or the local-maximum and local-minimum in heater power that exist for platinum. The SnO_2 catalyst shows minimal catalytic activity; however, the CO2 volume fraction becomes detectable at $T_{sa} = 682$ °C. Higher temperature experiments are required to determine whether the SnO_2 catalyst shows similar trends to platinum. Using a quartz stagnation-plane, there is no detectable CO_2 in the exhaust-gas flow. For both the SnO_2 and quartz catalysts, there is no detectable CO in the exhaust-gas flow. Also, the power curves overlap for the SnO_2 and quartz catalysts,

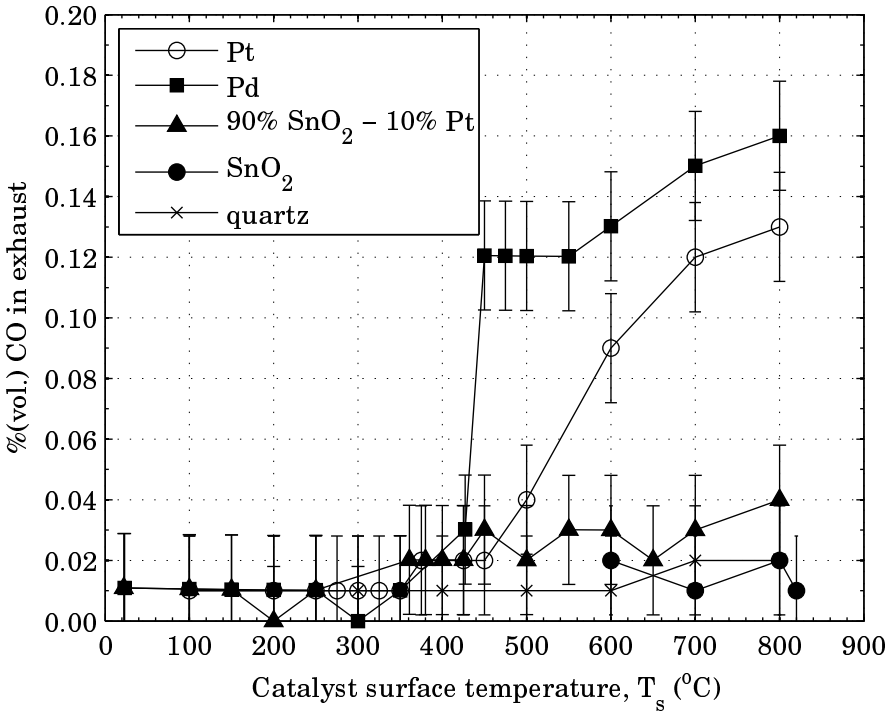

Figure 3.9 Catalytic CO production for a propane-air mixture at $v = 1.2$ m/s and $\phi = 1.50$ using a platinum, palladium 90% SnO_2 – 10% Pt (by mass), SnO_2, or quartz catalyst.

and the curve monotonically increases for increasing stagnation-plane temperature.

For palladium, the catalyst-activation temperature is higher than for platinum (Fig. 3.7), and the CO_2 inflection temperatures are approximately equal. Consistent with the catalyst-activation temperature, the local-maximum-power temperature is higher for palladium than platinum (Fig. 3.8). For both palladium and platinum the local minimum in P is near zero; in other words, the stagnation-plane temperature is sustained without electric heating. The stabilized CO_2 volume fraction in the exhaust is equal for both palladium and platinum, except near the catalyst-activation and CO_2 inflection temperatures. Consistent with this, an equal CO_2 volume fraction in the exhaust corresponds to an equal P for palladium and platinum, and a lower CO_2 volume fraction corresponds to a higher P for palladium than for platinum. The CO-inception temperature is lower for palladium than for platinum.

The 90% SnO_2 – 10% Pt catalyst has a lower catalyst-activation temperature and

CO_2-inflection temperature than platinum (Fig. 3.7); in other words, the behavior of the 90% SnO_2 – 10% Pt catalyst is similar to the platinum catalyst and is shifted to a lower temperature when compared to the platinum catalyst. Similarly, the local-maximum-power and local-minimum-power temperatures are lower for the 90% SnO_2 – 10% Pt catalyst than for platinum (Fig. 3.8). The stabilized CO_2 volume fraction is smaller for 90% SnO_2 – 10% Pt than for platinum. The smaller CO_2 volume fraction corresponds to a larger P for temperatures greater than the catalyst-stabilization temperature. The CO-inception temperature for the 90% SnO_2 – 10% Pt catalyst is $T_{CO} = 438$ °C; however, the CO fraction does not continue to increase as drastically as it does for the platinum or palladium catalysts.

3.2.2 The stoichiometric and fuel-lean conditions, $\phi = 1.0$ and $\phi = 0.67$

Figures 3.10 and 3.11 show the CO_2 volume fraction and the heater power for each catalyst material at $\phi = 1.00$. The quartz catalyst is non-reactive for the fuel-rich case and also shows non-reactive behavior for the stoichiometric and fuel-lean cases; therefore, data for quartz is not presented.

The SnO_2 catalyst shows a minimal, but non-zero, CO_2 volume fraction at the highest temperatures investigated. The catalyst-activation temperature is $T_{sa} = 769$ °C for the stoichiometric case. The SnO_2 catalyst did not exhibit the CO_2-inflection temperature or the local-maximum-power and local-minimum-power temperatures for either the stoichiometric or fuel-lean case. For the fuel-lean case the CO_2 volume fraction is always below 0.15% for the SnO_2 catalyst; therefore, no catalyst-activation temperature is reported for the SnO_2 for the fuel-lean case.

The palladium catalyst becomes active at a higher temperature than platinum. This is quantitatively compared by the larger catalyst-activation and CO_2-inflection temperatures for palladium than for platinum for the stoichiometric fuel-air mixture

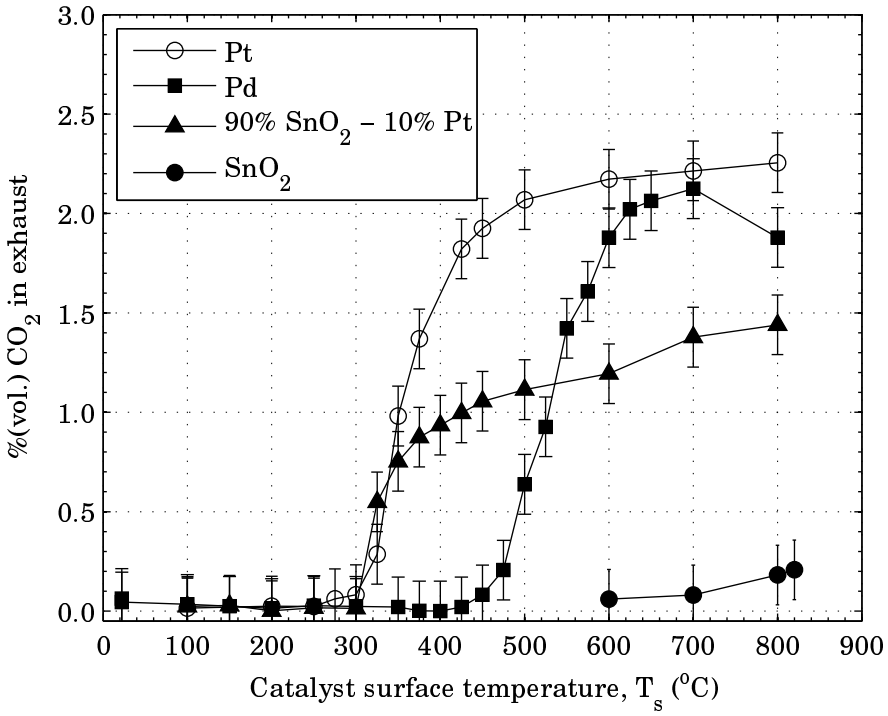

Figure 3.10 Catalytic CO_2 production for a propane-air mixture at $v = 1.2$ m/s and $\phi = 1.00$ using a platinum, palladium 90% SnO_2 – 10% Pt (by mass), SnO_2, or quartz catalyst.

(Fig. 3.10). Consistent with this, the local-maximum-power and local-minimum-power temperatures are also larger for palladium than for platinum (Fig. 3.11). Recall, for the fuel-rich case the palladium and platinum behavior almost overlaps (Figs. 3.7 and 3.8). This shows a decrease, for palladium, in the catalyst-activation and CO_2-inflection temperatures, and the local-maximum-power and local-minimum-power temperatures for increasing ϕ. The stabilized CO_2 volume fraction in the exhaust appears to approach the same value using the platinum or palladium catalyst; however, at 800 °C, there is a decline in the CO_2 volume fraction using palladium which is not present for platinum. Consistent with these two trends, an equal CO_2 volume fraction in the exhaust corresponds to an equal heater power for palladium and platinum. Likewise, a smaller CO_2 volume fraction corresponds to a larger heater power for palladium when compared with platinum.

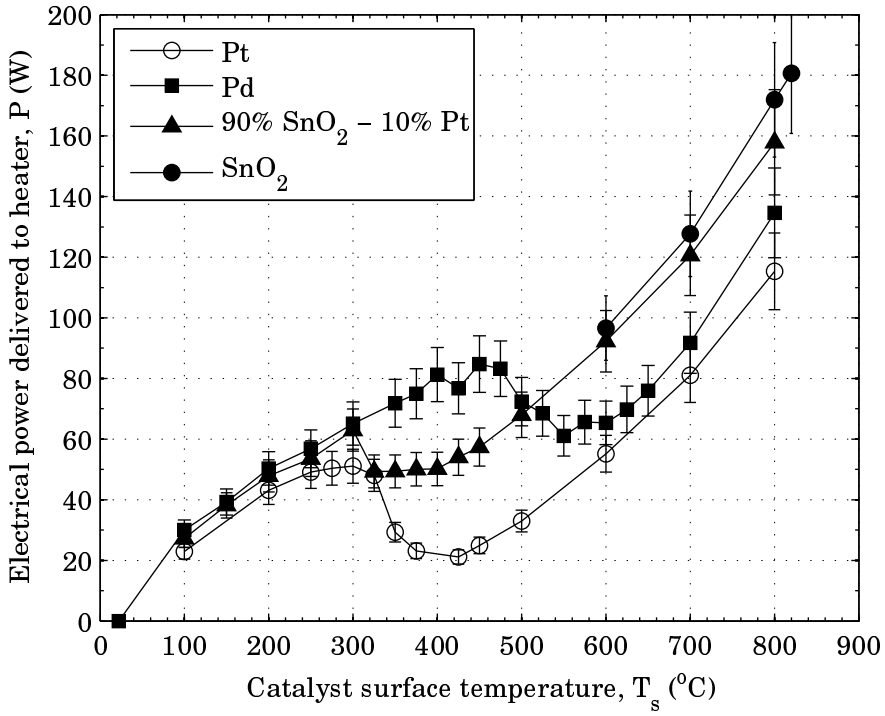

Figure 3.11 The power required to maintain the catalyst temperature for a propane-air mixture at $v = 1.2$ m/s and $\phi = 1.00$ using a platinum, palladium 90% SnO_2 – 10% Pt (by mass), SnO_2, or quartz catalyst.

The 90% SnO_2 – 10% Pt and platinum catalysts become active at similar temperatures; in other words, the catalyst-activation and CO_2-inflection temperatures are approximately equal for the stoichiometric fuel-air mixture for the 90% SnO_2 – 10% Pt and platinum catalysts (Fig. 3.10). Similarly, the local-maximum-power temperature is approximately equal for both catalysts, but the local-minimum-power temperature is lower for 90% SnO_2 – 10% Pt than for platinum. The stabilized CO_2 volume fraction is substantially lower for 90% SnO_2 – 10% Pt than for platinum. Consistent with this, the lower CO_2 volume fraction corresponds to a larger heater power for temperatures greater than the catalyst-stabilization temperature.

The platinum, palladium, and 90% SnO_2 – 10% Pt catalysts show similar behavior for the fuel-lean case as the stoichiometric and fuel-rich cases; in particular, the fuel conversion and power as a function of stagnation-plane temperature curves show

similar trends. Figures 3.12 and 3.13 show the CO_2 volume fraction and the heater power for each catalyst material at $\phi = 0.67$. The fuel lean case has the lowest CO_2 production, of the three equivalence ratios tested, which corresponds to the lowest difference between the local-maximum and local-minimum power, of the three equivalence ratios tested.

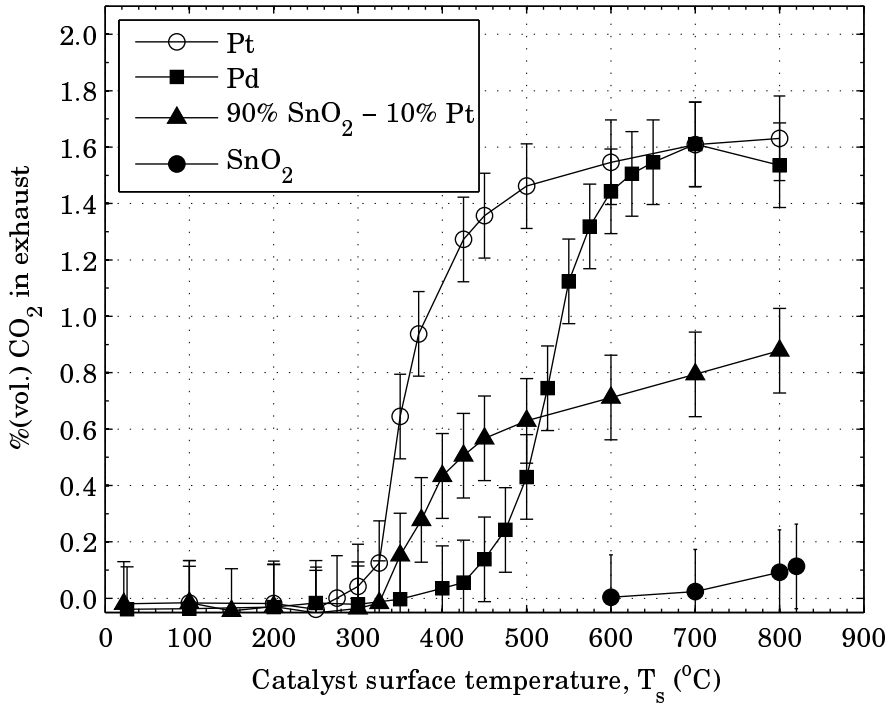

Figure 3.12 Catalytic CO_2 production for a propane-air mixture at $v = 1.2$ m/s and $\phi = 0.67$ using a platinum, palladium 90% SnO_2 – 10% Pt (by mass), SnO_2, or quartz catalyst.

For all fuel-air mixtures, the catalyst-activation, CO_2-inflection, local-maximum-power, and local-minimum-power temperatures are used to compare the behavior between the catalyst materials. Figure 3.14 shows the catalyst-activation and CO_2-inflection temperatures as a function of the equivalence ratio, and Fig. 3.15 shows the local-maximum-power and local-minimum-power temperatures as a function of the equivalence ratio, for the platinum, palladium, and 90% SnO_2 – 10% catalysts.

The palladium catalyst, denoted by the square symbols in the figures, exhibits decreasing catalyst-activation and CO_2-inflection temperatures for increasing equiv-

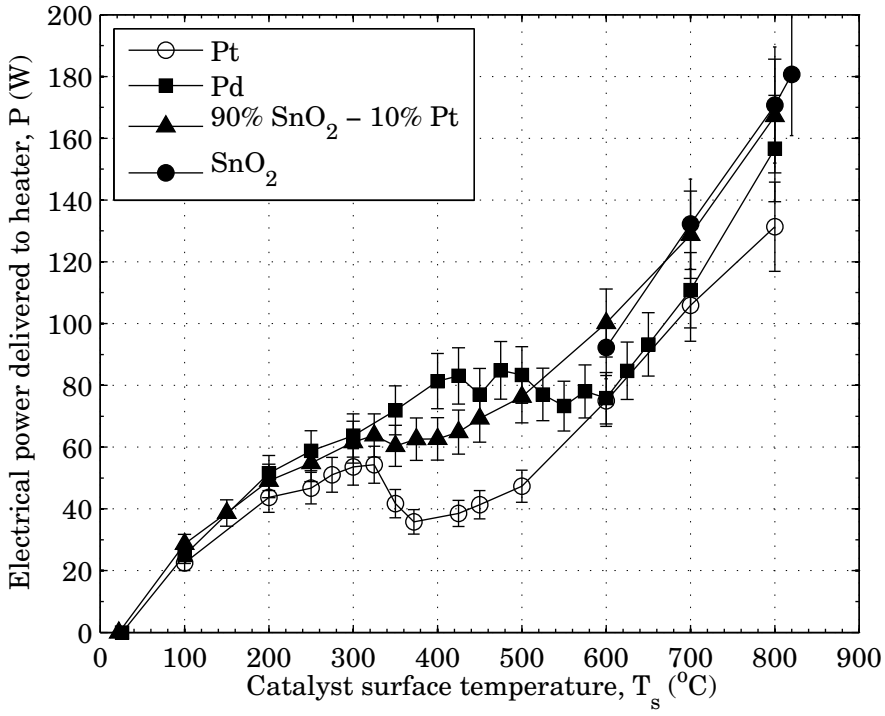

Figure 3.13 The power required to maintain the catalyst temperature for a propane-air mixture at $v = 1.2$ m/s and $\phi = 0.67$ using a platinum, palladium 90% SnO_2 – 10% Pt (by mass), SnO_2, or quartz catalyst.

alence ratio. The 90% SnO_2 – 10% Pt catalyst, denoted by the triangle symbols in the figures, exhibits the same trend as palladium for the catalyst-activation temperature; however, the CO_2-inflection temperature remains approximately constant for increasing equvalence ratio for the 90% SnO_2 – 10% Pt catalyst.

The platinum catalyst, denoted by the circle symbols in the figures, exhibits an approximately constant catalyst-activation temperature and a slightly increasing CO_2-inflection temperature for increasing equivalence ratio.

These trends are coincident with similar trends in the local-maximum-power and local-minimum-power temperatures. The palladium and platinum behavior are close to overlap at the fuel-rich condition; however, for the stoichiometric and fuel-lean conditions the palladium catalyst must be brought to a higher temperature to show the same activity levels as the platinum catalyst.

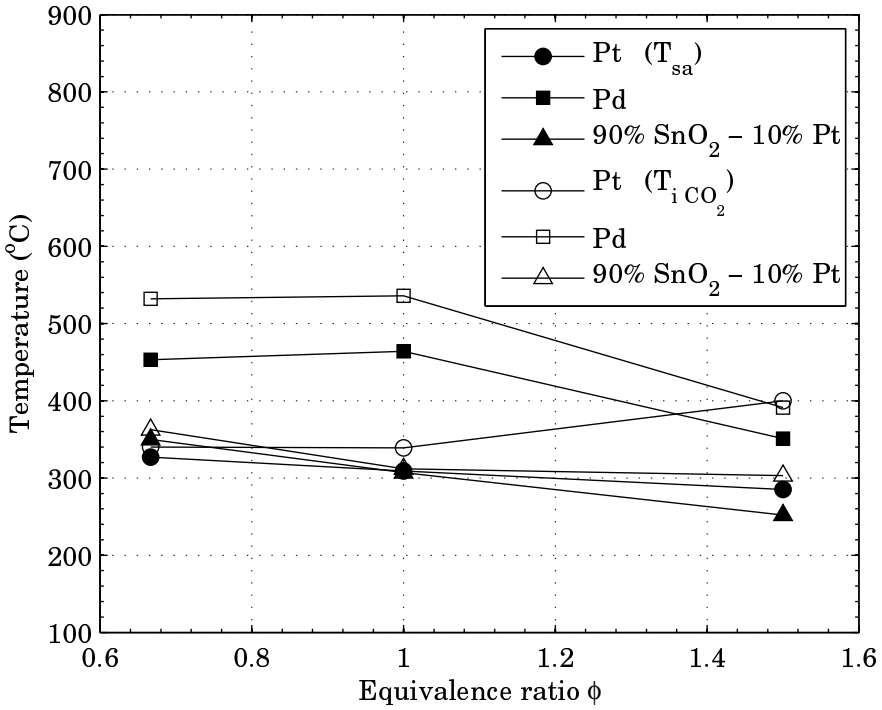

Figure 3.14 The catalyst-activation and CO_2-inception temperatures for the platinum, palladium, and 90% SnO_2 – 10% Pt catalysts. The filled symbols show T_{sa} and the open symbols show $T_{i\ CO_2}$.

The 90% SnO_2 – 10% Pt catalyst shows reactivity at lower temperatures than the platinum catalyst for the fuel-rich condition. For the stoichiometric and fuel-lean condition, the sensitivity of the 90% SnO_2 – 10% Pt and platinum catalysts are approximately equal in catalyst temperature. The absolute conversion of the 90% SnO_2 – 10% Pt catalyst at high temperature is always lower than for the platinum catalyst.

Both the 90% SnO_2 – 10% Pt and the palladium catalysts show sensitivity at lower temperature as the equvalence ratio is increased. This trend is not observed for the platinum catalyst.

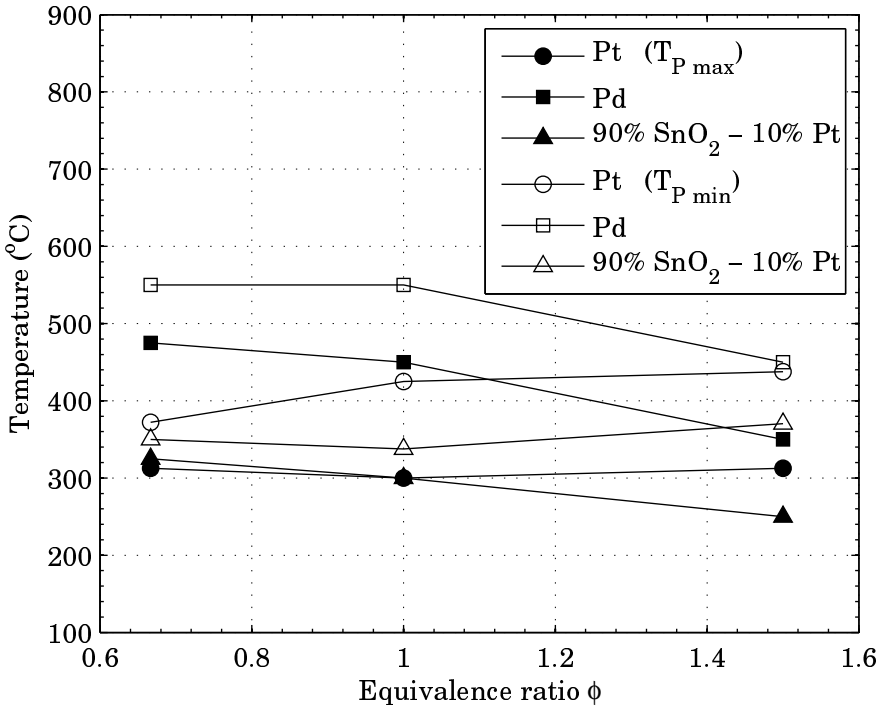

Figure 3.15 The local-maximum-power and local-minimum-power temperatures for the platinum, palladium, and 90% SnO_2 – 10% Pt catalysts. The filled symbols show $T_{P\ max}$ and the open symbols show $T_{P\ min}$.

3.3 Discussion

Quartz is non-reactive as a propane-oxidation catalyst for the temperatures investigated. Further, there is no chemical reaction due to the hot support structure in the experiment. The following evidence supports these claims. The O_2 and C_3H_8 volume-fraction measurements are unchanged from the unreacted room-temperature condition for the range of stagnation-plane temperature studied (T_s = 100 °C – 800 °C), and CO_2, CO, and NO are undetectable in the exhaust flow when using a quartz stagnation-plane (Figs. 3.7 and 3.9). Finally, the power to maintain the stagnation-plane temperature monotonically increases for increasing T_s, which implies minimal changes in reaction heat release over the experimental range (Fig. 3.8). Thus, propane oxidation is negligible when using a quartz stagnation-plane for the range of stagnation-plane temperature investigated. The non-reactivity of quartz also shows

there is minimal fuel oxidation due to contact of the flow with the hot support structures of the experimental apparatus. Most importantly, the non-reactive behavior of quartz, shows the reactivity of the platinum, palladium, 90% SnO_2 – 10% Pt, and SnO_2 catalysts, is due to reaction on the catalysts.

The platinum results can be compared to a study done by Veser and Schmidt [34], who reported the heterogeneous ignition temperatures of propane-air mixtures impinged on a heated platinum foil. In their experiments, the heater power is indpendently controlled, and the catalyst temperature is the dependent parameter. Figure 3.5 is replotted in Fig. 3.16 showing the heater power on the horizontal axis. For an

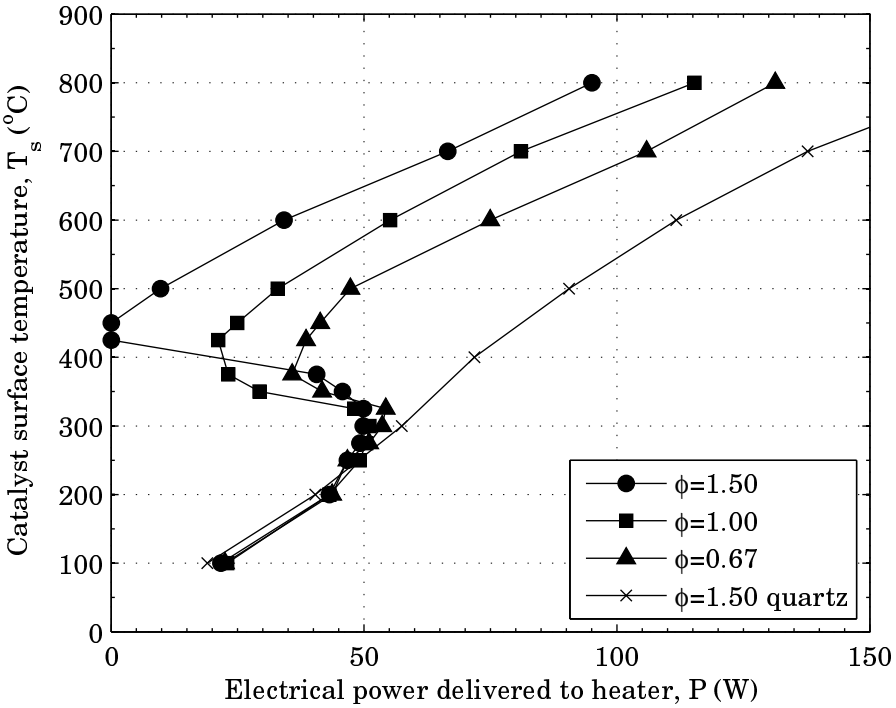

Figure 3.16 Figure 3.5 replotted showing the heater power on the horizontal axis

experiment where the power is indpendently controlled, as the power increases, the stagnation-plane temperature will show an abrupt increase at the local-maximum-power temperature. As power decreases from a high value, the stagnation-plane temperature will show an abrupt decrease at the local-minimum-power temperature. Thus, the results of the current work can be compared with the Veser and Schmidt

data, by considering the local-maximum-power temperature the point of catalytic ignition (where an increase in heater power causes catalytic light off), and the local-minimum-power temperature the point of catalytic extinction (where a decrease in heating power causes an extinction in the catalytic reaction).

Figure 3.17 shows the comparison of the local-maximum-power and local-minimum-power temperatures in the current work, with the catalytic ignition and extinction points reported by Veser and Schmidt [34]. The self-sustaining heat release conditions

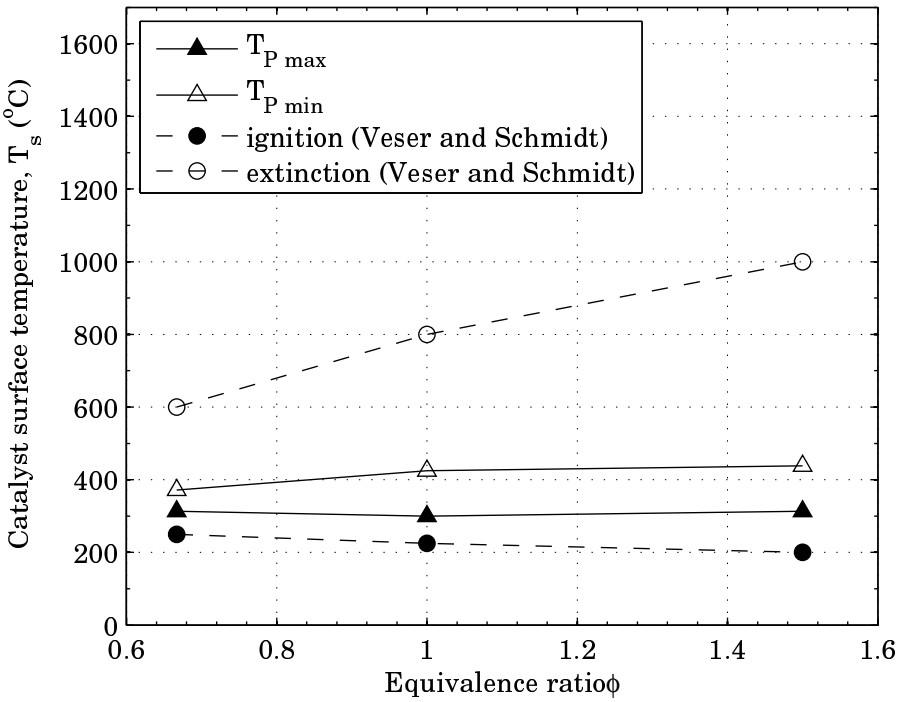

Figure 3.17 Comparison of the platinum propane oxidation results with the heterogeneous ignition and extinction data of Veser and Schmidt [34]

correspond to the auto thermal conditions observed in the Veser and Schmidt study. Note that this condition is highly dependent on the heat transfer properties of the catalyst stagnation surface.

The ignition point of propane on the platinum foil is slightly lower than that indicated by the local maximum in power measured in the current work. The extinction branch measured by Veser and Schmidt is at a much higher temperature than the

local minimum in the current work. The larger difference between the ignition and extinction temperatures is likely due to a lower heat loss from the catalyst for the Veser and Schmidt data. The quartz data in Fig. 3.16 shows the heater power required to maintain the stagnation plane temperature without reaction. A lower heat loss from the catalyst will cause the slope of the curves in Fig. 3.16 to increase; in other words, the stagnation plane will achieve a higher temperature for a given heater power. This shift in the curve will cause the difference between the local-maximum-power and local-minimum-power temperatures to increase. The differences in heat transfer between the Veser and Schmidt study, and the current work, are likely due to differences in the experimental conditions: the foil system in Veser and Schmidt compared with the current apparatus, and the factor of 5 higher flow velocities in the current experiments.

The platinum, palladium, and 90% SnO_2 – 10% Pt catalysts are most active at the fuel-rich condition. The results show that both the palladium and 90% SnO_2 – 10% Pt catalysts have a decrease in the catalyst-activation and CO_2-inflection temperatures for the fuel-rich condition (Fig. 3.14). The difference between the local-maximum and local-minimum power is greatest for the fuel-rich case; suggesting, the heat release due to propane oxidation increases for increasing fuel-air mixtures, for all three catalysts (Figs. 3.5, 3.8, and 3.11).

The fraction of carbon atoms in the exhaust in the form of CO_2 and CO is defined to compare the activity of the catalyst over the range of equivalence ratio. The fraction of carbon in the exhaust as CO_2 and CO is denoted by the "reacted-carbon fraction" ($\chi_c(CO_2+CO)$) and defined by equation 3.2. Recall, the symbol χ denotes the mole fraction of a particular gas species. In the exhaust flow, ideal gas behavior is assumed, and the mole fraction and volume fraction are assumed to be equal. The mole fractions

in equation 3.2 are measured from the exhaust flow.

$$\chi_c\,(\mathrm{CO_2{+}CO}) = \frac{\chi\mathrm{CO_2} + \chi\mathrm{CO}}{\chi\mathrm{CO_2} + 3\chi\mathrm{C_3H_8} + \chi\mathrm{CO}} \tag{3.2}$$

By approximating the number of moles to be equal for the products and reactants, equation 3.3 can be used to relate the inlet flow to the exhaust flow of carbon atoms. Since inlet propane flow provides the carbon into the system, the reacted-carbon fraction shows the fraction of the inlet mixture which reacts.

$$(\chi\mathrm{CO_2} + 3\chi\mathrm{C_3H_8} + \chi\mathrm{CO})_{\mathrm{products}} = (3\chi\mathrm{C_3H_8})_{\mathrm{reactants}} \tag{3.3}$$

The constant-mole reaction approximation is valid for propane-air oxidation. For complete stoichiometric oxidation, the number of moles in the products is larger than the number of moles in the reactants by a factor of 1.04. In the current experiment, only a fraction of the inlet flow reacts; therefore, the number moles in the products will deviate from the moles in the reactants less than for complete oxidation.

Figure 3.18 and 3.19 show the reacted-carbon fraction for the platinum, palladium, and 90% SnO_2 – 10% Pt catalysts. The reacted-carbon fraction is approximately equal for all three fuel-air mixtures and for both the palladium and platinum catalysts (Fig. 3.18). Since the inlet carbon is entirely supplied by propane, the mass of propane oxidized must be greatest for the fuel-rich case for an equal reacted-carbon fraction for the three fuel-air mixtures.

The 90% SnO_2 – 10% Pt catalyst shows an even greater increase in the catalytic activity for increasing equivalence ratio (Fig. 3.19). The stabilized reacted-carbon fraction does not approach one value for the range of equivalence ratio; the stabilized reacted-carbon fraction increases for increasing equivalence ratio. This shows an even stronger sensitivity to fuel-rich mixtures.

An analysis of the activation energy in the system also shows the platinum catalyst

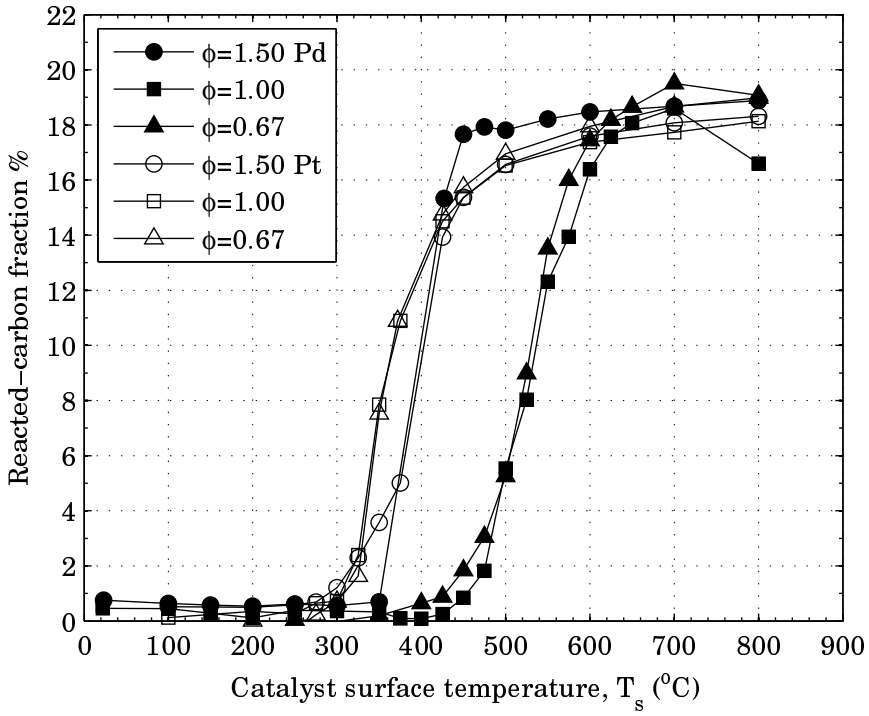

Figure 3.18 The reacted-carbon % for propane-air mixtures at $v_{ave} = 1.2$ m/s using a platinum or palladium catalyst.

is most active at the fuel-rich condition. In the surface reaction-rate-limited regime, the CO_2 volume fraction in the exhaust follows Arrehnius behavior, with respect to catalyst temperature. Equation 3.4 describes the Arrehnius behavior, where A_0 is a constant, E_a is the activation energy, R_g is the universal ideal gas constant, and T_s is the catalyst temperature.

$$\chi \mathrm{CO}_2 = A_0 e^{-\frac{E_a}{R_g T_s}} \tag{3.4}$$

Figure 3.20 shows the ratio of the activation energy to the ideal gas constant (E_a/R_g) for platinum for the three fuel-air mixtures studied. A linear least squares fit to the data, of the form shown in equation 3.5, determines E_a/R_g. The activation energy decreases for increasing fuel air mixture, which shows the fuel-rich case has the

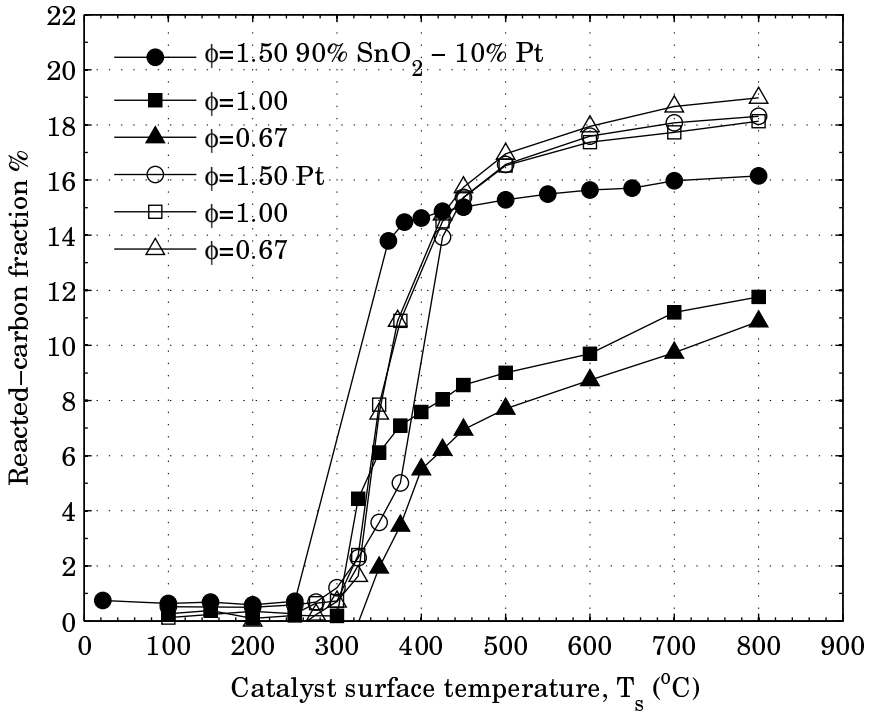

Figure 3.19 The reacted-carbon % for propane-air mixtures at $v_{ave} = 1.2$ m/s using a platinum or 90% SnO_2 – 10% Pt (by mass) catalyst.

highest catalytic activity.

$$\ln(\chi CO_2) = \ln(A_0) - \frac{E_a}{R_g}\frac{1}{T_s} \tag{3.5}$$

The CO_2-inflection temperature shows the transition from surface-kinetics to diffusion limitation of the heterogeneous reaction. There is a rapid increase in CO_2 volume fraction, and a rapid decrease in O_2 and C_3H_8 volume fractions for lower temperatures approaching the CO_2-inflection temperature (Figs. 3.1, 3.2, and 3.3). The rapid increase in propane oxidation is consistent with the highly temperature sensitive surface-kinetically limited heterogeneous oxidation. For temperatures greater than the CO_2-inflection temperature, the CO_2, O_2, and C_3H_8 volume fractions approach stable values for increasing T_s. The stable volume fractions imply that the diffusion of gas

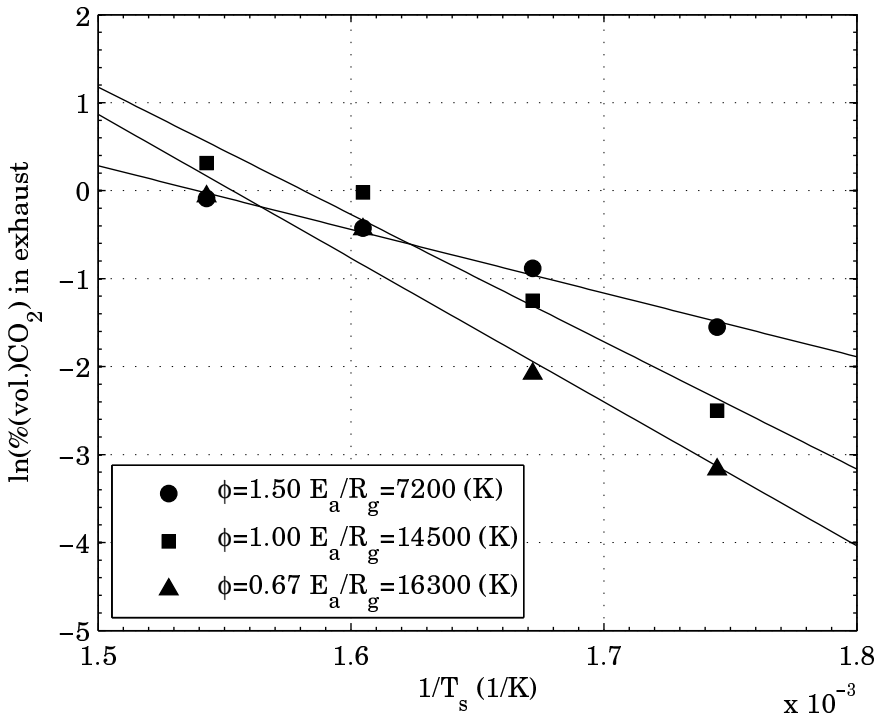

Figure 3.20 The activation energy for the three fuel-air mixtures studied, for platinum, in the surface reaction-rate-limited regime.

species to and from the surface limit the propane oxidation reaction. The diffusion rate of the gas species to and from the stagnation-plane is weakly influenced by the stagnation-plane temperature; therefore, heterogeneous reaction limited by diffusion is expected to be stable for increasing T_s.

Stable volume fractions for increasing T_s may also be due to complete oxidation where all the reactants are consumed and the volume fractions are therefore stable for increasing T_s; however, this is not the case in the current results. The stable volume fractions in T_s are not due to complete oxidation. This is most apparent for the fuel-lean and stoichiometric cases where the C_3H_8 volume fraction stabilizes above zero and for the fuel-rich case where the O_2 volume fraction stabilizes above zero. The stabilized level of CO_2 volume fraction is also below its complete reaction value for all fuel-air cases.

There is a significant portion of the flow which does not react, even at the highest

temperatures and most reactive catalyst in the experiment. This claim is analogous to the claim that the heterogeneous reaction is limited by diffusion and is again supported by the non-zero stabilization of the C_3H_8 and O_2 volume fractions, and the CO_2 fraction being below the theoretical complete oxidation value (Figs. 3.1, 3.2, and 3.3). The flow further from the nozzle centerline in the stagnation-flow geometry, has a shorter residence time on the catalyst. Some of the reactants in this flow may not have a chance to react. It is expected that a slower flow velocity will result in more complete oxidation, because the residence time of the flow will increase for decreasing velocity.

An increase in the CO_2 volume fraction in the exhaust corresponds to an increase in the heat release due to the propane oxidation. This claim is supported by the inverse relationship between the power required to maintain the catalyst temperature and the CO_2 volume fraction in the exhaust, and the inverse relationship between the power and the heat release of the reaction (Figs. 3.7 and 3.8). The temperature at the local maximum in power occurs coincidentally with the catalyst-activation temperature, and the decrease in power is coincident with the increase in the CO_2 volume fraction. The lower stabilized CO_2 volume fraction in the exhaust for 90% SnO_2 – 10% Pt than platinum corresponds to a higher power required to maintain T_s.

Although CO is produced for the fuel-rich case for platinum, palladium, and 90% SnO_2 – 10% Pt, the amount of CO produced when compared with the amount of CO_2 produced is low. Approximating the carbon in the fuel to react to either CO_2 or CO, the carbon dioxide to reacted carbon fraction (χ_{rc} CO_2) is defined by equation 3.6. The carbon dioxide to reacted carbon fraction provides a means to compare the relative production of CO and CO_2.

$$\chi_{rc}\mathrm{CO_2} = \frac{\mathrm{CO_2}}{\mathrm{CO_2} + \mathrm{CO}} \tag{3.6}$$

Figure 3.21 shows a contour plot of the gas-phase equilibrium values of χ_{rc} CO_2, for the range of inlet mixtures used in the experiments, at atmospheric pressure. The equilibrium χ_{rc} CO_2 is calculated using the gas-phase thermodynamic data in GRI-Mech 3.0 [16]. The equilibrium CO values increase as the equivalence ratio

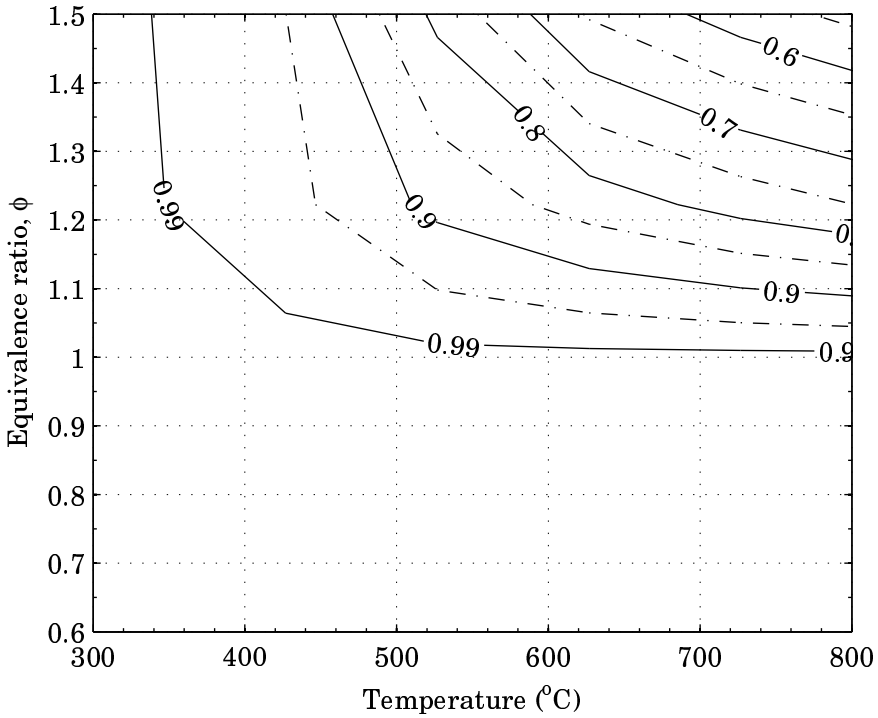

Figure 3.21 Gas-phase equilibrium contours of χ_{rc} CO_2, as a function of temperature and equivalence ratio, at $p = 1$ atm.

increases and the temperature increases. For $T < 340$ °C or $\phi < 1$, there is virtually no CO in a mixture in chemical equilibrium.

Figure 3.22 shows the gas-phase equilibrium data compared with catalytic CO production data at the fuel-rich condition. The catalyst produces much less CO in relation to CO_2 than chemical equilibrium. This may occur for several reasons. Most likely, the gas phase chemistry is too slow to allow equilibrium to be established before the exhaust temperatures decrease is the sampling apparatus. Also, some of the CO produced by the catalyst may react with the remaining O_2 in the gas-phase adjacent to the catalyst reducing the relative amount of CO produced in relation to CO_2. The

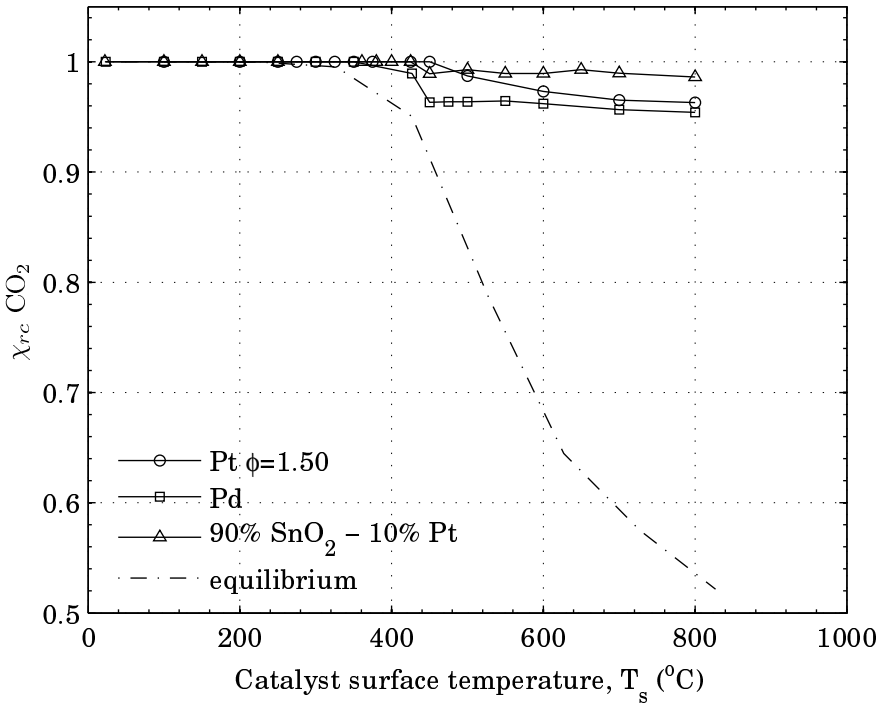

Figure 3.22 Experimental results of χ_{rc} CO_2 for $\phi = 1.50$, compared with the gas-phase equilibrium data, at $p = 1$ atm

catalyst may preferentially oxidize to CO_2 thereby limiting the CO produced.

Chapter 4

Catalysis of premixed propane-air flames

The flame studies of propane-air mixtures impinging on a platinum or quartz stagnation surface are presented in this chapter. Recall, the experimental procedure is to ignite a stable flame in the stagnation flow and incrementally decrease the equivalence ratio until the fuel-lean extinction limit is identified, while holding the average nozzle-exit velocity constant. For each equivalence-ratio increment, the dependent data are the heater power, the flame-plate separation distance, and the flame image. The fuel-lean extinction limit is defined as the average of the ϕ where a flame is present and the next increment in ϕ where the flame extinguishes. Tables 4.1 and 4.2 present the experimental data using a quartz and platinum stagnation plane, and Table 4.3 and 4.4 present the fuel-lean extinction limits for quartz and platinum.

The following sections describe the effects of the catalyst on the flame structure and the lean-extinction limits for these experiments. Images of the observed flame structures in the experiment are presented in Section 4.1. The results of the data are presented in Section 4.2, and the results are discussed in Section 4.3.

Table 4.1 Flame location and extinction data using a quartz stagnation plane with a constant stagnation-plane temperature.

v_{ave}(cm/s)	ϕ	P (W)	x_{sep} (mm)	T_s (°C)
59.7	0.395	188	6.13	875
59.7	0.381	188	4.40	875
59.6	0.360	197	0[1]	875
59.6	0.353	–	–	–
79.9	0.563	191	6.03	900
79.7	0.501	188	3.99	900
79.7	0.483	197	0[1]	900
79.7	0.474	196	0[1]	900
79.6	0.450	197	0[1]	900
79.5	0.433	–	–	–
99.1	0.659	157	4.85	900
99.0	0.630	162	3.45	900
98.9	0.608	–	0[2]	–
120	0.771	140	5.11	900
119	0.715	143	4.12	900
119	0.636	150	3.08	900
119	0.624	–	0[2]	–
140	0.804	128	3.91	900
140	0.764	134	3.18	900
139	0.718	141	2.35	900
139	0.711	–	–	–
162	0.876	115	3.34	900
161	0.824	123	2.92	900
161	0.789	127	2.35	900
161	0.785	–	–	–

[1]ring flame

[2]unstable ring flame

Table 4.2 Flame location and extinction data for a platinum stagnation plane with a constant stagnation-plane temperature.

v_{ave} (cm/s)	ϕ	P (W)	x_{sep} (mm)	T_s (°C)
59.8	0.444	180	6.17	875
59.7	0.388	181	5.32	875
59.7	0.374	–	–	–
80.0	0.581	179	5.00	900
79.9	0.545	181	4.12	900
79.8	0.510	184	3.54	900
79.7	0.492	186	3.07	900
79.7	0.483	–	–	–
99.0	0.644	147	3.59	900
99.0	0.630	150	2.86	900
98.9	0.600	152	2.42	900
98.8	0.593	–	–	–
119	0.771	130	4.76	900
119	0.736	131	4.32	900
119	0.715	134	3.87	900
119	0.687	137	3.65	900
118	0.645	141	2.35	900
118	0.628	146	2.10	900
118	0.615	149	1.73	900
118	0.611	–	–	–
139	0.804	128	2.56	900
139	0.751	131	2.05	900
139	0.704	140	1.60	900
139	0.698	–	–	–
161	0.856	111	2.43	900
161	0.832	115	2.05	900
161	0.805	123	1.76	900
160	0.772	134	1.53	900
160	0.767	–	–	–
181	0.947	90	2.37	900
181	0.903	108	2.09	900
181	0.869	110	1.87	900
180	0.827	124	1.59	900
180	0.822	–	–	–

Table 4.3 The fuel-lean extinction limits, ϕ_{min} using a quartz stagnation plane with a constant stagnation-plane temperature.

v_{ave}(cm/s)	ϕ_{min}	(T_s °C)
59.6	0.357	875
79.5	0.441	900
98.9	0.608	900
119	0.624	900
139	0.714	900
161	0.787	900

Table 4.4 The fuel-lean extinction limits, ϕ_{min} using a platinum stagnation plane with a constant stagnation-plane temperature.

v_{ave}(cm/s)	ϕ_{min}	T_s (°C)
59.7	0.381	875
79.7	0.487	900
98.8	0.596	900
118	0.613	900
139	0.701	900
160	0.770	900
180	0.825	900

4.1 Flame-structure imaging results

Figure 4.1 presents images of the flame structures observed in the current study for two flow conditions over the range of equivalence ratio $\phi = 0.5$–1.5. Previous research by Zhang and Bray [39], and Fernandes and Leandro [9] investigated similar propane-air stagnation-flow flames and described the basic flame structures as the cool-core-envelope flame, cone flame, envelope flame, disk flame, and ring flame. The flame images in Fig. 4.1 are classified using these descriptions.

The flame structures spontaneously change as ϕ decreases or increases for a constant nozzle-exit velocity. For the images in Fig. 4.1, the flame is ignited at $\phi = 1.5$, and the flame structure spontaneously changes as ϕ decreases until the fuel-lean extinction limit occurs. The equivalence ratio where the transition occurs depends on whether ϕ is increasing or decreasing; this indicates there is hysteresis of the flame-structure transition points.

There are several important characteristics of each of the flame structures. The cool-core-envelope flame is present only at the most fuel-rich conditions. As the equivalence ratio is decreased a cone flame is stabilized. The cone flame can be stabilized for both fuel-rich and fuel-lean equivalence ratios. As the flame speed decreases, the height of the cone flame increases. The envelope flame occurs near $\phi = 1$ for $v_{ave} = 0.9$ m/s and did not occur for any ϕ for $v_{ave} = 1.2$ m/s. As ϕ decreases further into the fuel-lean mixture regime, the cone flame spontaneously changes to the disk flame. The separation distance from the stagnation-plane to the disk flame (denoted by the disk-flame separation distance, x_{sep}) is sensitive to ϕ and v_{ave}. As ϕ decreases in the fuel-lean mixture regime, the disk flame stabilizes closer to the stagnation-plane. There were audible acoustic vibrations when the disk flame was present. The acoustic vibrations were not present for any of the other flame structures or for a non-ignited flow. Finally, the ring flame is present only at the most fuel-lean conditions, and exhibits turbulence.

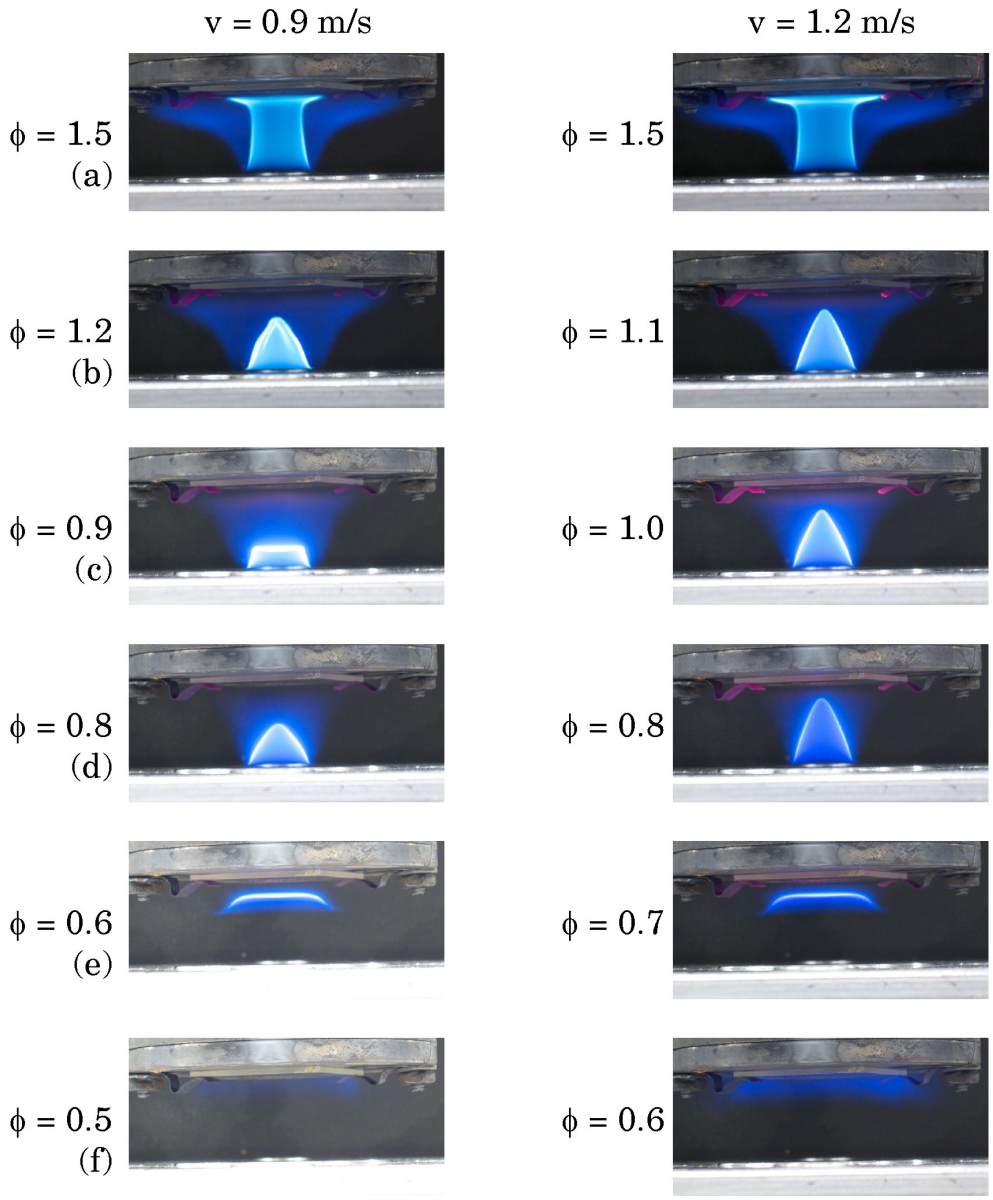

Figure 4.1 Progression in flame structure while decreasing ϕ from fuel-rich to fuel-lean mixtures. The $v = 0.9$ m/s column shows the five flame structures observed in the current work: (a) cool-core-envelope flame, (b,d) cone flame, (c) envelope flame, (e) disk flame, (f) and ring flame.

4.2 Catalysis of premixed, fuel-lean propane-air flames results

The geometry and proximity of the disk flame to the stagnation-plane makes it amenable to catalyst-flame interaction studies. The flatness of the disk flame results in radial uniformity of x_{sep}. This simplifies analysis and modeling of the flame-catalyst

interaction. Moreover, as ϕ decreases, the disk flame is forced closer to the stagnation-plane. This maximizes the catalytic influence on the lean-extinction limit, ϕ_{min}, and the flame-catalyst interaction when using a catalytic stagnation-plane.

Figures 4.2 and 4.3 show flame images for decreasing ϕ for several nozzle-exit velocity conditions. Figure 4.2 shows flame images using a bare quartz stagnation-plane, and Fig. 4.3 shows flame images using a Pt coated stagnation-plane. Tables 4.1 and 4.2 show the data associated with each image: v_{ave}, ϕ, P, and x_{sep}.

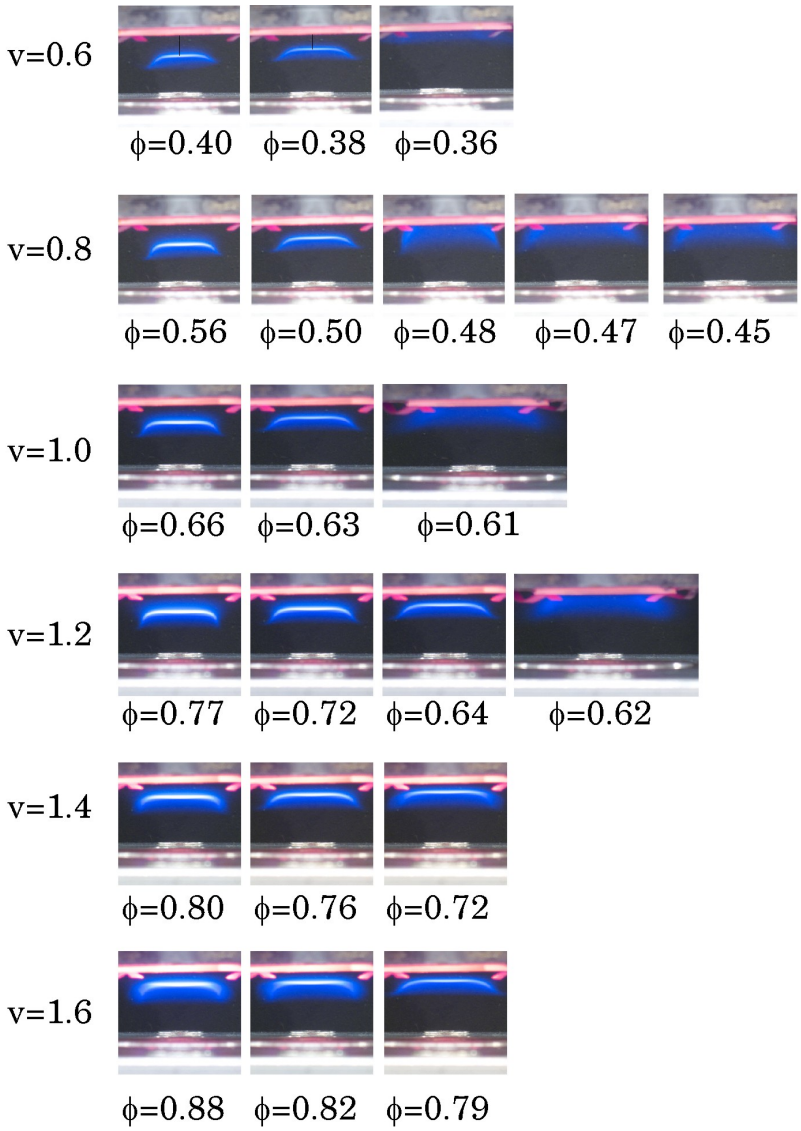

Figure 4.2 Images of the disk flame progressing to extinction while reducing equivalence ratio for a bare quartz wafer.

For the quartz stagnation-plane, the flame structure spontaneously changes from a

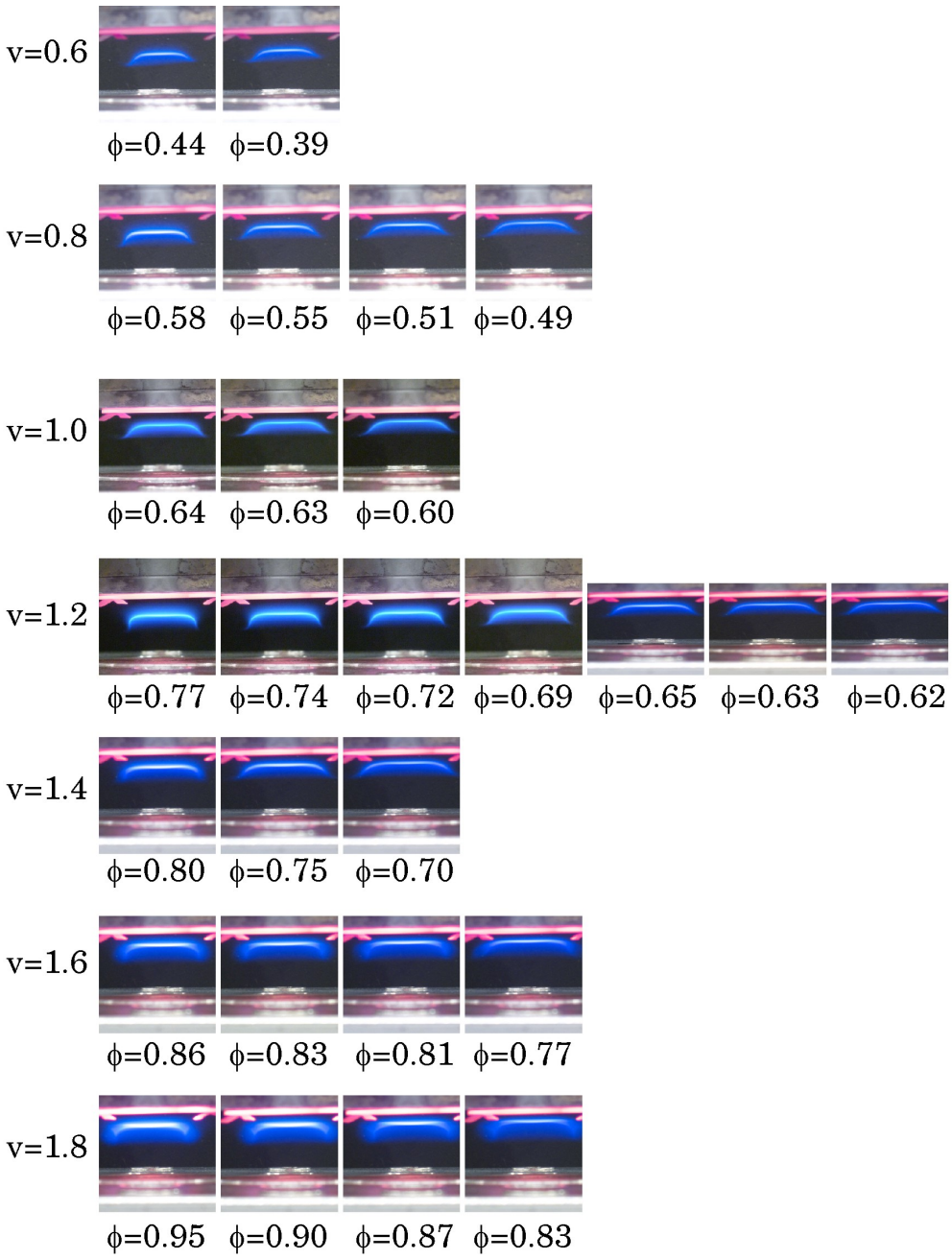

Figure 4.3 Images of the disk flame progressing to extinction while reducing equivalence ratio for a Pt coated quartz wafer.

disk flame to a ring flame as ϕ decreases while maintaining a constant v_{ave} in the range 0.6 m/s to 1.2 m/s. The equivalence ratio where the disk flame spontaneously changes to the ring flame is denoted by "disk-to-ring flame transition (ϕ_r)", and the values for ϕ_r are listed in Table 4.5. The disk-to-ring flame transition is the average of the ϕ

Table 4.5 The disk flame to ring flame transition, ϕ_r using a quartz stagnation plane with a constant temperature of 900 ^{o}C for $v \geq 0.8$ m/s and 875 ^{o}C for $v = 0.6$ m/s.

v_{ave}(cm/s)	ϕ_{min}
59.7	0.371
79.7	0.492
98.9	0.619
119	0.630

where the ring flame is first observed and previous ϕ where the disk flame is observed. The ring flames for $v_{ave} = 1.0$ m/s and $v_{ave} = 1.2$ m/s eventually extinguish after several seconds of stable combustion, and the ring flame structure is not observed for $v_{ave} = 1.4$ m/s and $v_{ave} = 1.6$ m/s. There are audible acoustic vibrations for $v_{ave} = 1.4$ m/s and $v_{ave} = 1.6$ m/s. Only slightly audible acoustic vibrations occur for the lower average nozzle-exit velocity conditions. Fernandes and Leandro [9] quantified similar acoustic vibrations. No audible acoustic vibrations exist in the flow without a flame, also the acoustic vibrations occurred for the disk flame only.

For the Pt coated stagnation-plane, Fig. 4.3, no ring flame structure is ever observed. Audible acoustic vibrations occur for $v_{ave} = 1.4$ m/s and $v_{ave} = 1.6$ m/s, similar to the quartz stagnation plane. As expected for both the platinum and quartz stagnation planes, for fuel-lean mixtures, the flame speed decreases for decreasing ϕ and the disk flame moves closer to the stagnation-plane.

Figures 4.4, 4.5, and 4.6 compare the flame properties of the platinum and quartz stagnation-planes in terms of x_{sep}, ϕ_{min}, ϕ_r, and P. The stagnation-plane temperature is maintained at 900 °C for $v_{ave} \geq 0.8$ m/s, and at 875 °C for $v_{ave} = 0.6$ m/s. The lower the stagnation-plane temperature for $v_{ave} = 0.6$ m/s is because, the heater at full power cannot maintain the stagnation-plane temperature at 900 °C for all $v_{ave} = 0.6$ m/s conditions. The filled symbols show data using the platinum coated stagnation-plane, and the open symbols show data using the bare quartz stagnation-plane.

Obtained from the images, values for x_{sep} are listed in Tables 4.1 and 4.2. The

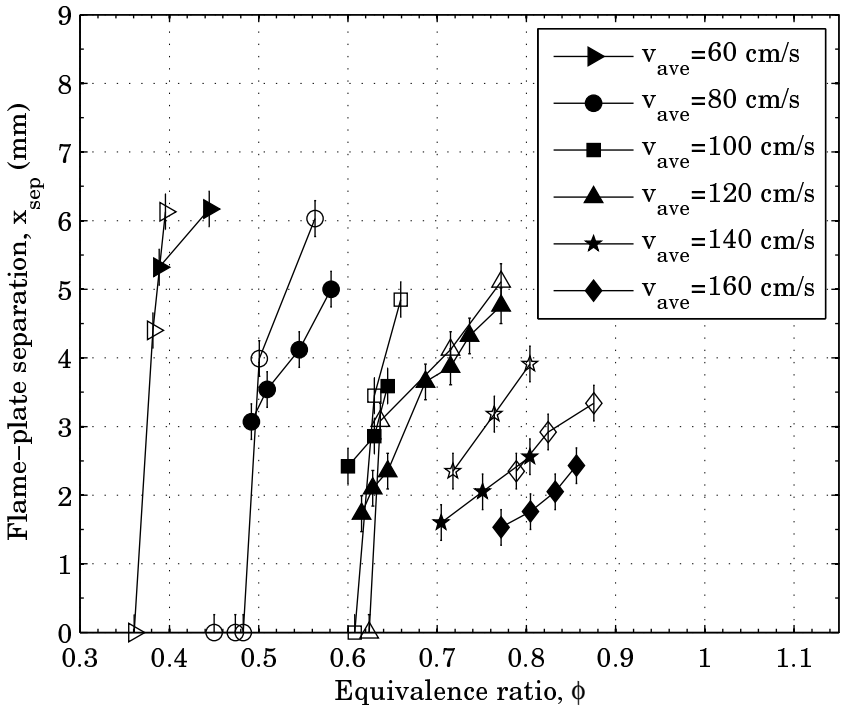

Figure 4.4 The flame separation from the stagnation plane (x_{sep}) as a function of the equivalence ratio (ϕ) and average nozzle-exit velocity (v_{ave}). $T_s = 900$ ^{o}C for $v \geq 0.8$ m/s and $T_s = 875$ ^{o}C for $v = 0.6$ m/s. The filled symbols denote the platinum surface data; the open symbols denote the quartz surface data.

results are consistent with the balance between the flame speed as a function of ϕ and the flow velocity; more specifically, the disk-flame separation distance decreases as ϕ decreases, or the average nozzle-exit velocity increases. Figure 4.4 also shows the fuel-lean extinction limit and the disk-to-ring flame transition. The separation distance between the ring flame and the stagnation plane is so small that it could not be distinguished in the flame images; therefore, points where $x_{sep} = 0$ show a stable ring flame on the figure.

The fuel-lean extinction limit and the disk-to-ring flame transition are shown in Fig. 4.5. The fuel-lean extinction limit decreases for decreasing v_{ave}. The disk-to-ring flame transition occurs only for the quartz stagnation plane and only for the range of average nozzle-exit velocity conditions $v_{ave} = 0.6$–1.2 m/s. For the larger average nozzle-exit velocity conditions ($v_{ave} = 1$–1.6 m/s), the lean-extinction limits for platinum and

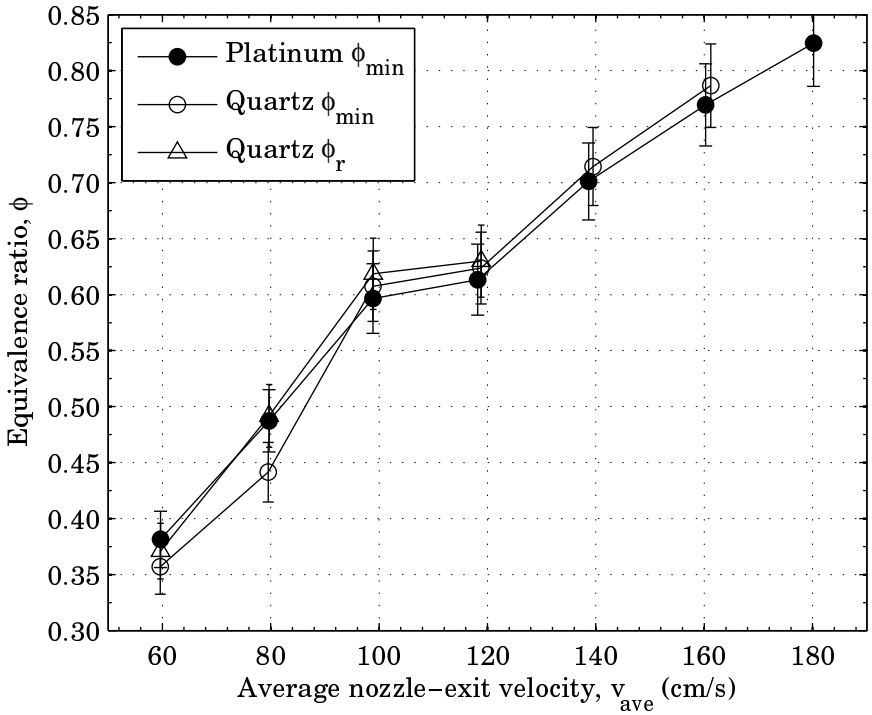

Figure 4.5 The lean-extinction limit,ϕ_{min}, and disk-to-ring flame transition, ϕ_r, as a function of the average nozzle-exit velocity (v_{ave}). $T_s = 900$ ^{o}C for $v \geq 0.8$ m/s and $T_s = 875$ ^{o}C for $v = 0.6$ m/s. The filled symbols denote the platinum surface data; the open symbols denote the quartz surface data.

quartz overlap. The disk-to-ring flame transition, using quartz and the lean extinction limit using platinum, overlap for the lower average nozzle-exit velocity conditions ($v_{ave} = 0.6$ and 0.8 m/s). For $v_{ave} = 0.6$ and 0.8 m/s the lean-extinction limit, using quartz, is lower than when using platinum.

The power to maintain the stagnation-plane temperature is a strong function of the equivalence ratio and a weaker function of v_{ave}. There is only slight overlap in stable ϕ among different v_{ave} conditions; however, P increases slightly as v_{ave} decreases for constant ϕ. The heater power decreases for increasing ϕ, and is slightly larger for the bare-quartz stagnation-plane than for the platinum-coated stagnation-plane.

The difference in the emissivity between the platinum and the quartz stagnation plane may account for the slight decrease in heater power for platinum when compared with quartz. This behavior is also observed in previous experiments using an unheated

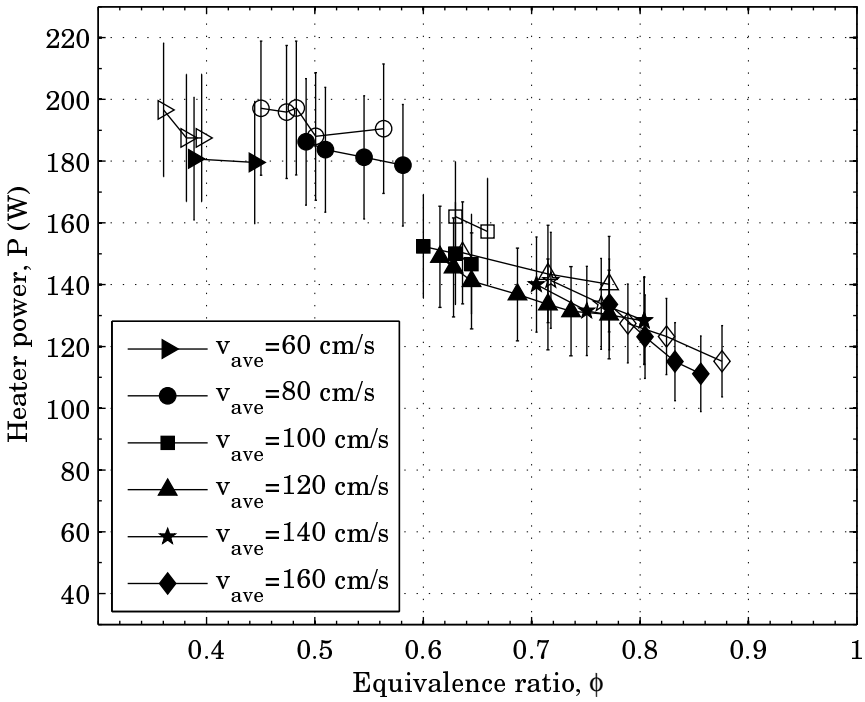

Figure 4.6 The electric power required to maintain a constant stagnation plane temperature (P) as a function of the equivalence ratio (ϕ) and average nozzle-exit velocity (v_{ave}). $T_s = 900$ ^{o}C for $v \geq 0.8$ m/s and $T_s = 875$ ^{o}C for $v = 0.6$ m/s. The filled symbols denote the platinum surface data; the open symbols denote the quartz surface data.

stagnation plane, Wiswall et al. [37, 38]. The lower emissivity of the platinum stagnation plane results in a lower heat transfer rate to the environment. The lower heat transfer rate results in a lower heater power required to maintain the stagnation plane temperature.

4.3 Discussion

The flame structure results from the balance between the flame speed, the average nozzle-exit velocity, and flow-geometry and diffusion effects. The height of the cone flame is inversely proportional to the flame speed and proportional to the average nozzle-exit velocity. The cool-core-envelope and envelope flames are likely derivatives of the cone flame. The cool-core-envelope flame is similar to a cone flame that stabilizes

at a height such that it interferes with the stagnation plane. The envelope flame is similar to a cone flame, where the center forms a flat top where the flame speed balances with the local jet velocity.

The disk flame first occurs when the cone flame destabilizes from the nozzle, and the flame lifts off the nozzle and stabilizes near the stagnation plane. A possible reason the disk flame occurs for fuel-lean conditions, and not for fuel-rich conditions, is at fuel-rich conditions, local atmospheric diffusion aids the stabilization of the flame on the nozzle exit. The diffusion of oxygen from the atmosphere strengthens the flammability of fuel-rich mixtures; therefore, the flame tends to stabilize at the interface of the nozzle flow and the atmosphere. At fuel-lean conditions, local atmospheric diffusion reduces the ability of the flame to stabilize at the nozzle exit. The diffusion of oxygen from the atmosphere weakens the flammability of fuel-lean mixtures; therefore, the flame tends to stabilize near the center of the nozzle flow. The disk flame stabilizes in the region near the stagnation plane where the impinging jet velocity balances with the flame speed, and stabilizes closer to the stagnation plane as the flame speed decreases, by decreasing ϕ, or the average nozzle-exit velocity increases.

The ring flame likely forms due to quenching of the disk flame as it is forced to the stagnation plane. The ring flame appeared to stabilize where the impinging laminar flow transitioned to turbulent flow in a ring, larger than the nozzle-exit diameter, on the stagnation plane. Both Zhang and Bray [39] and Fernandes and Leandro [9] observed the ring flame at fuel-rich conditions only. The heating of the stagnation plane in the current work may be why the ring flame stabilizes at fuel lean conditions. Even when the disk flame is locally extinguished, the propane-air mixture impinges on the heated quartz stagnation plane, which can affect the heat transfer losses allowing the ring flame to stabilize at $\phi < 1$.

The platinum catalyst inhibited the formation of the ring flame structure near ϕ_{min}. This is the greatest effect the catalyst had on the flame system. The inhibition

of the ring flame can be due to several mechanisms. It is possibly due to fuel oxidation on the platinum coated stagnation plane, which can render the flow noncombustible for conditions when the ring flame is stabilized for the quartz case. In other words, as the propane-air mixture impinges on the heated platinum stagnation plane, fuel oxidation occurs. The partially oxidized gases then may not stabilize a ring flame. It is also possible that radical scavenging of the catalyst may quench the flame. The ring flame is in much closer proximity to the stagnation plane than the disk flame; thus, interaction between the catalyst surface and the flame may reduce the free radical concentration necessary to sustain the flame.

The extinction of the disk flame is insensitive to the stagnation surface material. For the slower average nozzle-exit velocity conditions, $v_{ave} = 0.6$ m/s and $v_{ave} = 0.8$ m/s, the difference in ϕ_{min} between the platinum and the bare quartz stagnation plane is due to the stabilization of the ring flame for the quartz stagnation plane. Recall, ϕ_{min} is defined as the least ϕ where any flame can be stabilized. The minimum ϕ where a disk flame is stabilized is approximately equal for the quartz and platinum stagnation plane; in other words, $\phi_{min\ \mathrm{Pt}} \approx \phi_{r\ \mathrm{quartz}}$ or $\phi_{min\ \mathrm{Pt}} \approx \phi_{min\ \mathrm{quartz}}$ depending on if the disk flame transitions to a ring flame or not for the quartz stagnation plane. This further suggests that the surface chemistry plays a minor role in the gas-phase chemistry of the disk flame. The insensitivity of disk flames in a stagnation flow is consistent with previous research. Law et al. [19] and Ishizuka et al. [15] experimentally examined the lean-extinction limits of propane-air flames, in a stagnation-flow, subject to different boundary conditions on the stagnation-plane, including a platinum catalyst. They also found that the catalyst did not affect the lean-extinction limits at the conditions they considered.

Although catalytic extinction of lean-extinction limits of stagnation flow flames has not been realized experimentally, there is evidence to suggest an influence can occur. Law and Sivashinsky [20] performed a theoretical study and determined situations

where the presence of a catalyst is most likely to influence the lean-extinction limit in a stagnation flow. They theoretically determined for Lewis numbers (defined as $Le = \delta_t/\delta_m$ where δ_t is the thermal diffusivity and δ_m is the mass diffusivity) less than 1, the flame strengthens due to an increased flame temperature as it approaches the surface; and for Lewis numbers greater than 1, the flame extinguishes due to a decreased flame temperature as it approaches the surface. Their primary conclusion is that flames are much more likely to exhibit a catalytic extension of the lean extinction limit for a Lewis number greater than one.

More recently, Li and Im [21, 22] numerically investigated catalytic extension of the lean-extinction limit of disk flames in a stagnation-flow. Their numerical studies using platinum catalyzed methane-oxidation chemistry revealed that the lean-extinction limit can be extended provided that the characteristic time scales of the surface reactions are faster than those of the gas-phase reactions, as would be the case if the catalytic surface retains a high temperature with lower heat loss or if the gas-phase mixture is diluted.

Chapter 5

Conclusions and suggestions for future research

5.1 Conclusions

The experimental results show ways that catalysis can extend the useful operating conditions for hydrocarbon oxidation and combustion. The stagnation-flow reactor provides a platform to investigate the fundamental behavior of catalytic fuel oxidation and the catalysis of premixed flames. Exhaust gas sampling, and the heater power required to maintain the catalyst temperature, quantify catalytic fuel oxidation. The lean-extinction limit, and flame structure transition points, quantify the catalytic influence on premixed flames. Control of the catalyst temperature allows for investigation of the intertwined effects of gas-phase transport, catalyst heat transfer properties, and surface reaction rates.

The platinum, palladium, and 90% SnO_2 – 10% Pt catalysts transition from surface reaction limited operation to diffusion limited operation over the experimental conditions studied. Further, the platinum, palladium, and 90% SnO_2 – 10% Pt studies yield comparable fuel oxidation trends with respect to the stagnation-plane temperature. These results show, in the diffusion-limited regime, that different catalyst materials can yield comparable fuel conversion performance.

While varying equivalence ratio, the reaction heat release increases well into the fuel-rich regime. The platinum, palladium, and 90% SnO_2 – 10% Pt catalysts show the highest catalytic activity in the fuel-rich case, which is quantified by the heater power and the mass of fuel reacted to CO_2. Palladium and 90% SnO_2 – 10% Pt show an increasing catalyst-activation temperature for decreasing ϕ, and platinum shows an approximately constant catalyst-activation temperature for decreasing ϕ ($T_{sa} = 310$ °C). The 90% SnO_2 – 10% Pt catalyst shows the lowest catalyst-activation temperature of the experiments which occurs for the $\phi = 1.5$ mixture ($T_{sa} = 250$ °C).

Figures 5.1, 5.2, and 5.3 show % CO_2 and % CO contours for the platinum, palladium, and 90% SnO_2 – 10% Pt catalysts. These figures can be used to determine operating regimes where CO_2 production is maximized, while keeping CO production low.

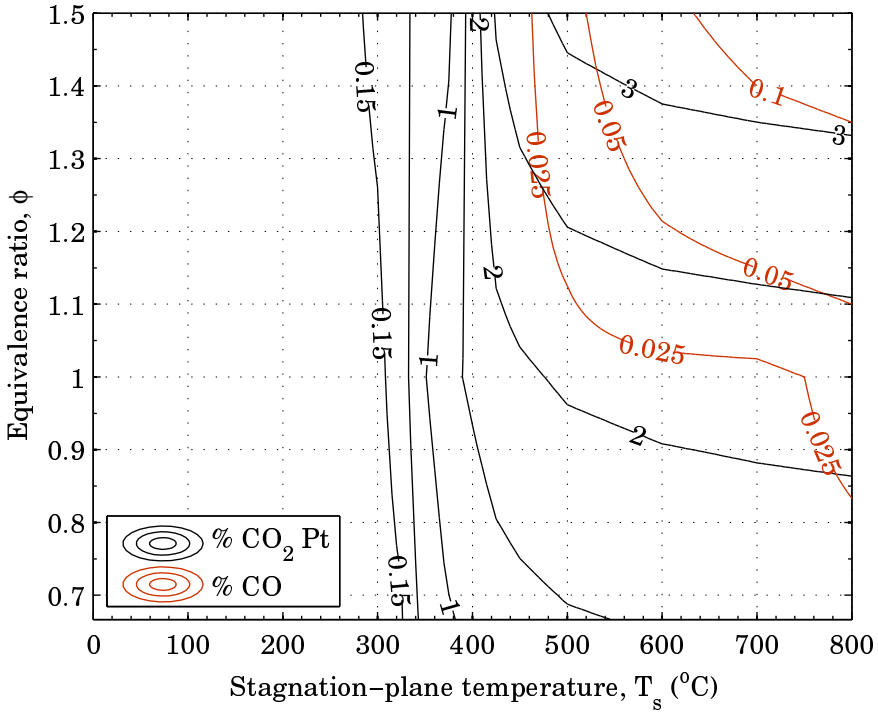

Figure 5.1 % CO_2 and % CO contours for platinum over the experimental range of equivalence ratio and stagnation-plane temperature

The results of the fuel oxidation catalysis studies contribute to combustion device

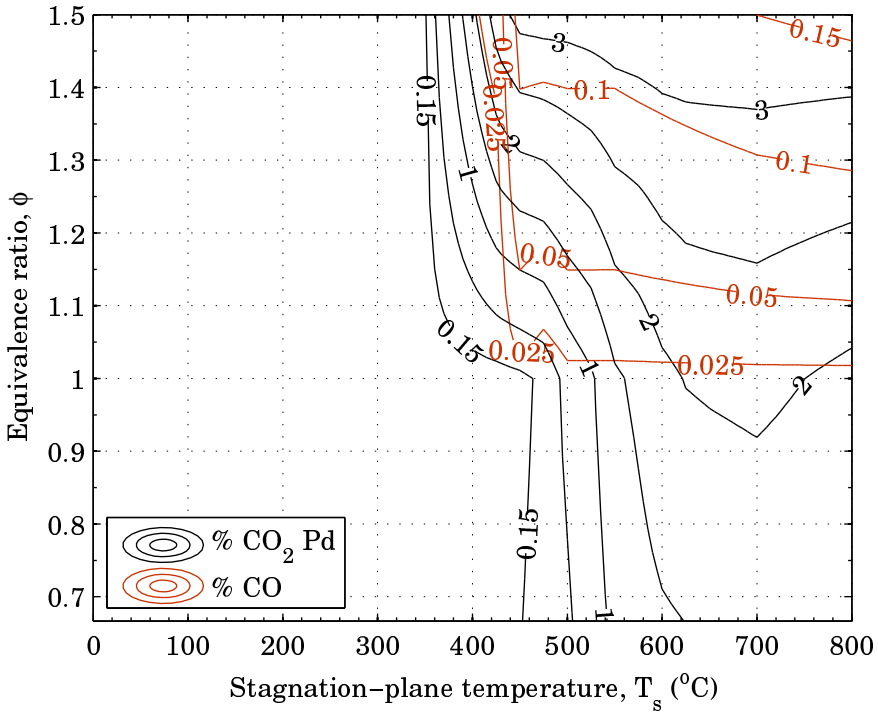

Figure 5.2 % CO_2 and % CO contours for palladium over the experimental range of equivalence ratio and stagnation-plane temperature

design. One such example is described in Lyubovsky et al. [25]. In a gas-turbine combustor, a small fraction of the inlet fuel, mixed with air in a fuel-rich mixture, can be passed through a catalyst. The heat release due to the catalytic reaction can be used to preheat the remaining inlet reactant flow of the combustor. Further, the catalyst partially reacts the fuel which is reintroduced to the inlet reactant flow. Lower peak combustion temperatures are allowed by the high temperature inlet flow of the combustor. The lower peak temperatures in the combustor can reduce the formation of pollutants such as nitrogen oxides.

The lean extinction limits of propane-air flames are insensitive to the stagnation plane material, for the experimental conditions studied. This suggests the disk flame is insensitive to the catalyst, and the reaction rate is much larger for premixed flames, than for diffusion limited catalytic oxidation. The comparatively lower reaction rate for the diffusion limited catalytic oxidation is evidenced by partial propane oxidation

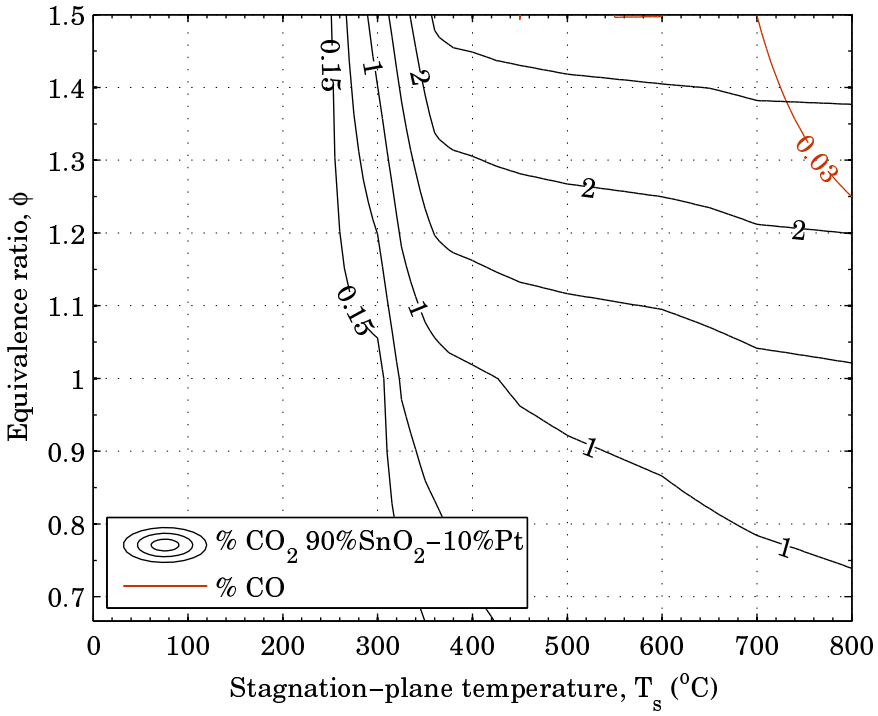

Figure 5.3 % CO_2 and % CO contours for 90% SnO_2 – 10% Pt over the experimental range of equivalence ratio and stagnation-plane temperature

in the diffusion-limited propane-oxidation catalysis studies. The insensitivity of the reaction rate to increased temperature of diffusion-limited catalytic operation suggests that increasing the catalyst temperature will not increase its influence on the flame.

Although flame reactions tend to dominate catalytic reactions, a catalyst can influence the structure of gas phase flames. This is shown by the inhibition of the ring flame for a platinum catalyst in the stagnation-flow reactor. This result is the only catalytic influence found in the premixed flame catalysis studies. The mechanism of the ring flame inhibition is not completely understood; however, the results show the inhibition is due to the presence of a platinum stagnation plane.

5.2 Suggestions for future research

The results set directions for development of improved catalyst systems. Research and development of lean NO_x catalysts can help decrease the pollutants emitted from high-efficiency diesel engines. The important parameters such as catalyst light-off can be compared among different catalysts in the stagnation-flow reactor by comparing the catalyst-activation temperature. Development of a functioning lean NO_x catalyst can allow more widespread use of high-efficiency diesel engines which will reduce fuel consumption.

Catalyst aging and poisoning is another important area to study for the industrial implementation of catalysts. Many industrial catalysts are exposed to impurities that may reduce catalytic reactivity. Impurities can be introduced into the reactant mixture to investigate their effects on the catalyst performance over time. The experimental apparatus can also be thermally cycled to study the thermal stability of the catalyst.

Catalytic fuel decomposition can provide insight into ways to use a catalyst to pre-react a fuel to allow, low polluting, high efficiency combustion in a gas-phase combustor. Fuel decomposition studies will improve understanding of catalytic fuel reforming to manipulate hydrocarbon fuel sources into different forms. One such example is conversion of plant matter into ethanol by pyrolysis. If developed into a transportable device, waste plant matter can be converted into ethanol at its source. This eliminates the costly transportation of biomass to a refining facility. Studies of fuel-rich or diffusion flames on a catalyst surface may yield stronger flame-catalyst interaction. Such research may also connect with catalytic fuel decomposition studies.

Fundamental reaction on the catalyst surface is also a future research path. Information about radical and short lived species near the catalyst surface can be accomplished by using spectroscopy techniques. The one dimensionality of the stagnation-flow reactor is suited to line-of-sight laser spectroscopy near the surface. Using these techniques both diffusion rates and the species present can be obtained.

Appendices

Appendix A

An experimental study of the effects of platinum on methane/air and propane/air mixtures in a stagnation-point-flow reactor

James T. Wiswall, Margaret S. Wooldridge, and Hong G. Im

The ASME Journal of Heat Transfer,
November 2009, Vol. 131

An Experimental Study of the Effects of Platinum on Methane/Air and Propane/Air Mixtures in a Stagnation Point Flow Reactor

James T. Wiswall

Margaret S. Wooldridge

Hong G. Im

Department of Mechanical Engineering,
University of Michigan,
2350 Hayward Street,
Ann Arbor, MI 48109

A stagnation-flow burner facility was used to study the catalytic surface reactions of premixed combustion systems at atmospheric pressure. The configuration serves as an important platform to investigate the interaction between homogeneous and heterogeneous reactions with independent control of the characteristic chemical and physical residence time scales. Methane/oxygen/nitrogen and propane/oxygen/nitrogen mixtures were examined with and without the presence of a platinum catalyst located at the stagnation surface. The effects of oxidizer composition and nitrogen dilution were investigated. Lean flame extinction limits were determined for the two fuels and were found to be unaffected by the presence of the catalytic surface. The flame extinction data indicated that the systems were controlled by gas phase combustion with negligible contributions from heterogeneous reactions. The catalytic activity of the heated surface in response to the direct impingement of fuel/air mixtures onto the stagnation surface, without the presence of a flame, was quantified by the increase in the surface temperature. The methane/air mixtures demonstrated no catalytic activity for these conditions, whereas propane/air mixtures demonstrated temperature increases of over 100 K. The data indicate that the surface reaction was transport limited for the propane/air system.
[DOI: 10.1115/1.3156788]

Keywords: catalytic combustion, platinum, propane, methane, lean extinction limit

1 Introduction

Catalytically assisted combustion can greatly improve the performance of combustion devices and aid the development of new energy generation technologies. For the past 3 decades, over 85% of the global energy demand has been supplied by combustion sources [1]. Considering such large usage, improvements in combustion efficiencies and pollutant emissions will have a dramatic impact on our efforts toward extending existing fuel resources and transitioning to sustainable energy while reducing environmental impact. Catalysts can allow lower-temperature combustion, which directly reduces some pollutants, such as nitric oxides (NO_x), as well as improve the overall conversion efficiency, stability, and range of operating conditions [2].

Catalysts are particularly important to the development of small scale combustion devices. Despite the large energy density of hydrocarbon fuels, combustion at small dimensions with high surface-to-volume ratios often suffers from excessive heat losses that prevents sustained exothermic reactions. Surface reactions can overcome these challenges by increasing reaction rates at lower temperatures and by extending the range of stable combustion. However, the quantitative benefit of surface reactions on combustion properties, such as extending flammability limits for practical device operating conditions, remains uncertain primarily due to the uncertainties in the homogeneous and heterogeneous reaction rate chemistries. Catalyst chemistry also introduces uncertainties due to variability in surface properties.

The overall objective of this research program is thus to broaden our fundamental understanding of the interactions between gas-phase and surface combustion in a well defined combustion system and to use such knowledge to improve combustion performance. This work specifically explored the feasibility of using catalysts to extend the lean extinction limits of methane and propane fueled flames and to quantify the surface reactivity for conditions when no flame is present.

The stagnation-flow reactor used in this work is particularly well suited to fundamental studies of catalyst performance, as the stagnation-flow reactor allows independent control of the characteristic time scales for chemical reaction and flow. The stagnation-flow reactor simplifies temperature and species profiles to nominally one dimension where the thermal and concentration gradients occur in the axial direction only. The gas residence time on the surface and surface reaction rate can be independently controlled by the flow velocity and surface heating, respectively. The stagnation surface also provides a physical support, which can be used to examine a broad range of catalyst materials and properties, and many types of catalyst/fuel combinations can be tested in such a system. In the present study, the stagnation plane was chosen to be either platinum or silicon, so the effects of surface reactions can be quantitatively compared relative to two levels of surface reactivity (where the silicon surface is considered as a reference condition with negligible surface reaction). The lean extinction limits and surface reactivity were examined for a range of parametric conditions of surface heating, mixture equivalence ratio, and strain rates. For each set of experimental conditions, both catalytically active and baseline systems were examined.

Contributed by the Heat Transfer Division of ASME for publication in the JOURNAL OF HEAT TRANSFER. Manuscript received November 20, 2008; final manuscript received April 2, 2009; published online August 25, 2009. Review conducted by Walter W. Yuen. Paper presented at the 2007 ASME International Mechanical Engineering Congress (IMECE2007), Seattle, WA, November 10–16, 2007.

2 Scientific Background

There are two processes (surface reaction kinetics and gas-phase species diffusion) that can limit the heterogeneous reaction rate. Pfefferle and Pfefferle [3] among many other sources discussed the relative contributions of these processes. The transition from surface-kinetics-limited to diffusion-limited operation of a catalyst sometimes yields an observable step change in behavior. For example, as the temperature of the inlet reactant flow on a catalytic reactor is increased, the catalyst temperature may show a large increase in temperature as the reaction limitation transitions from surface kinetically limited to diffusion limited. Consistent with other studies (e.g., Ref. [4]), this transition is called "light-off" or heterogeneous ignition in the current work. Further heating will eventually lead to homogeneous ignition of the gas-phase reactants.

In general, both homogeneous and heterogeneous reactions contribute to extinction and ignition phenomena when a catalyst is present. As described earlier, this coupling can yield two distinct ignition events: heterogeneous and homogeneous ignitions. This often causes catalyst performance metrics to be intertwined with the parameters of the specific facility used to study the catalyst (e.g., the flow geometry, the form of the catalyst (e.g., foil, wash-coat, etc.), the heat transfer properties of the catalyst support, etc.). Thus, it is often difficult to compare results between different experimental facilities, and it is critical to establish clear baselines for conditions where a catalytic surface is not present.

The stagnation-flow configuration has served as a canonical geometry to investigate catalyst phenomena for many years. Researchers have used such experimental methods to develop and validate heterogeneous reaction mechanisms [4,5], to investigate light-off and the effects of catalysts on homogeneous flammability limits and ignition phenomena [4,6,7], to quantify fuel conversion efficiencies [8], and to compare catalyst properties, to name a few research topics. Among the most relevant papers, Veser and Schmidt [6] experimentally studied ignition of methane, ethane, propane, and isobutane flames in a stagnation flow. Williams et al. [7] studied methane and propane light-off and homogeneous ignition in a stagnation flow. In these studies, each fuel was found to have different ignition characteristics when the catalyst ignition temperature was considered as a function of fuel-air ratio. Ethane had the lowest homogeneous ignition temperature at 950°C, and methane had the highest at 1200°C. Law et al. [9] examined the lean extinction limits of propane/air flames in stagnation-point-flow subjected to different boundary conditions on the stagnation surface, including a platinum catalyst. They found that the catalyst did not affect the lean extinction limits at the conditions they considered.

More recent studies by Li and Im [10,11] specifically focused on the catalytic extension of lean extinction limit. Their numerical studies of methane/platinum stagnation-point-flow reactor revealed that lean extinction limit can be extended provided the characteristic time scales of the surface reactions are faster than those of the gas-phase reactions, as would be the case if the catalytic surface retains a high temperature with lower heat loss or if the gas-phase mixture is diluted. It remains to be seen, however, if the observed catalytic benefit of flammability extension can be realized experimentally.

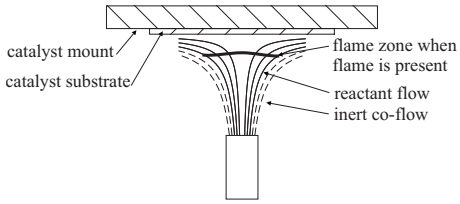

Fig. 1 Schematic of the stagnation-point-flow reactor configuration

Therefore, the goal of the present experimental study is to identify the practical extent to which heterogeneous reaction can alter and improve reactor performance and thereby verify the findings from the earlier modeling studies [10,11]. In particular, we investigate the effects of platinum catalyst on lean extinction limits of methane and propane in air, with and without the presence of gas-phase premixed flames. The consideration of different fuels, as well as the nonreacting and catalytic surfaces, allows comprehensive coverage of conditions at which gas-phase and heterogeneous reactions interact at varying degrees of relative dominance. For reference, a schematic of the flow configuration is shown in Fig. 1. A stream of gas-phase reactant mixture impinges onto a solid surface, which can be nonreacting (bare silicon) or catalytic (platinum). First, we consider the cases in which a gas-phase flame is present initially, such that the flow impinging on the stagnation surface consists predominantly of the combustion products. The lean extinction limits are then determined by varying the reactor conditions, such as the fuel/air equivalence ratio. In the second part of experiments, a fuel/air mixture at room temperature and pressure is directed onto the heated surface of the stagnation plane, such that surface-only reaction modes are investigated. For these experiments, the rate of heat release at the surface is monitored by measuring the time dependent temperature of the stagnation surface.

3 Experimental Approach

3.1 Experimental Facility. The experimental facility is schematically shown in Fig. 2. A mixture of fuel, oxygen (O_2), and nitrogen (N_2) was impinged on a flat plate to achieve a stagnation flow. The flow was directed upward with the fuel, O_2 and N_2 mixture in the inner tube, and nitrogen flowing through the outer

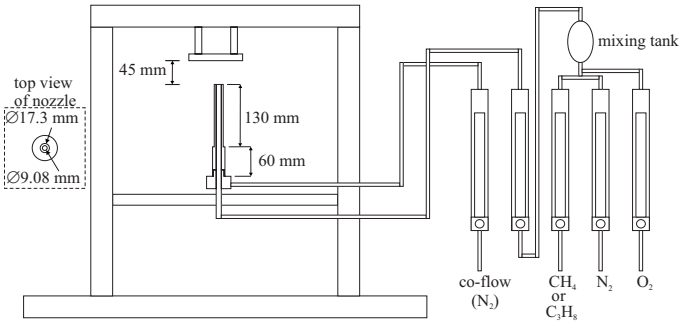

Fig. 2 Schematic showing gas flow measurement, control, and important reactor dimensions

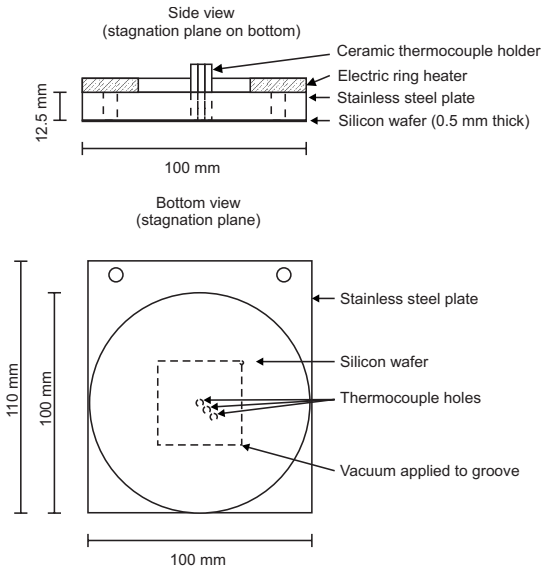

Fig. 3 Dimensions of stagnation plane and support

coflow tube. The nitrogen coflow minimizes the entrainment of the ambient air into the reactant mixture in the inner tube. The volume flow rates of the fuel, O_2 and N_2, and the total mixture were regulated using calibrated rotameters. The relative levels of the flow rates were used to set the stoichiometric ratios and levels of nitrogen dilution of the combustible mixtures. The total mixture rotameter was used to adjust the overall exit velocity from the nozzle, and the coflow rotameter was used to adjust the exit velocity of shroud flow of N_2. Each rotameter had an uncertainty of $\pm 2\%$ of the reading.

The coflow nozzle consists of the inner tube (reactant mixture) with 9.08 mm inner diameter and 0.265 mm wall thickness. The coflow tube was 17.3 mm inner diameter. The length of the coflow tube was 130 mm. Type 304 stainless steel was used for all tubing. Dry compressed air (79% N_2, 21% O_2) was used for some experiments instead of mixing O_2 and N_2.

Figure 3 shows the dimensions of the stagnation plane and the support. The support for the stagnation plane was constructed from type 304 stainless steel and was located 45.5 mm above the nozzle exit such that the stagnation plane was 45 mm above the nozzle exit. The plate was mounted on a translation stage, which had a 60 mm range and dimensions of 100×110 mm^2, by 12.5 mm thick. A 0.5 mm thick wafer of silicon with a diameter of 100 mm was used as the stagnation surface. The silicon wafer was mounted on the supporting stainless steel plate using a vacuum seal. Insulating washers made from ceramic were placed between the supporting structure and the stainless steel plate to reduce heat loss by conduction.

Platinum was used as the catalyst and was deposited on the silicon wafer by physical vapor deposition (PVD). To achieve a stable deposition of platinum, a 30 nm layer of titanium was first deposited on the silicon. A layer of platinum 100 nm thick was then deposited on the titanium. A bare silicon wafer was used as the reference nonreactive case of a surface with no catalytic activity. The platinum was deposited by PVD to ensure similar heat transfer parameters would exist between the catalytic and nonreactive cases.

A 0.2 mm diameter B-type thermocouple (Pt/30%Rh–Pt/6%Rh, Omega Engineering Inc.) was used to measure the stagnation plane temperature (T_s). It was possible to measure T_s in three locations radially outward from the centerline of the flow (see Fig. 3), and the variation over the radial measurement locations was less than 20 K. The thermocouples were in physical contact with the nonstagnation plane side of the silicon wafer, leaving no part of the thermocouples exposed to the reactant flow. The thermocouple bead temperature was considered equivalent to that of the stagnation plane and surrounding support. The thermocouple voltage was measured using a multimeter (Fluke 45) and was recorded at a rate of 2.5 Hz, using a data acquisition system (LABVIEW 8). T_s was calculated using the polynomial fit for B-type thermocouples [12].

Table 1 Uncertainty of the experimental parameters

Uncertainty
$U\phi = \pm 0.028\phi$
$U\chi_{N_2} = \pm 0.0057\chi_{N_2}$
$Uv_{ave} = \pm 0.036v_{ave}$
$U\phi_{min} = \pm 0.04\phi$
$UT_s = \pm 15$ K

The equivalence ratio (ϕ) is determined based on the measured flow rates for the fuel and O_2 flow rates (Eq. (1)). The dilution with N_2 is defined relative to the total N_2+O_2 flow rates (Eq. (2)). The nozzle exit velocity (v_{ave}) is the calculated average exit velocity of the total flow exiting the nozzle (Eq. (3)).

$$\phi = \frac{(\dot{Q}_{fuel}/\dot{Q}_{O_2})}{(\dot{Q}_{fuel}/\dot{Q}_{O_2})_{stoich}} \tag{1}$$

$$\chi_{N_2} = \frac{\dot{Q}_{N_2}}{\dot{Q}_{N_2} + \dot{Q}_{O_2}} \tag{2}$$

$$v_{ave} = \frac{\dot{Q}_{fuel} + \dot{Q}_{O_2} + \dot{Q}_{N_2}}{A_n} \tag{3}$$

The parameters ϕ, χ_{N_2}, and v_{ave} are controlled independently. Each flow meter was calibrated and corrected for atmospheric pressure variations during each experiment. The temperature in the laboratory varied by less than 10°C. The uncertainty in each flow meter was determined to be two standard deviations based on the calibration testing, to give a 95% confidence level. The reported uncertainty for ϕ, χ_{N_2}, and v_{ave} was determined using the square root of the sum of the uncertainty of each flow meter squared. The minimum equivalence ratio ϕ_{min} and stagnation plane temperature T_s were determined for each extinction experiment. The uncertainty in T_s was the uncertainty reported by the manufacturer of the thermocouple. The uncertainty in ϕ_{min} was based on the variability in results obtained from identical test conditions and the uncertainty in the measurement of ϕ. Table 1 shows the independent and dependent parameters and the associated uncertainties.

Each fuel was studied with and without an ignited gas-phase flame. For the flame extinction experiments, the fuel/air mixture was ignited using an external premixed propane/air flame brought into the proximity of the stagnation plane. The starter flame was removed after the stagnation flame was ignited. To measure the lean extinction limit (ϕ_{min}), the average nozzle exit velocity (v_{ave}) and the nitrogen mole fraction in the oxidizer (χ_{N_2}) were held constant while ϕ was decreased until extinction occurred. The lean extinction limit, ϕ_{min}, was defined as the average between the lowest measured ϕ yielding a stable flame and the slightly lower ϕ yielding an unstable condition. The resolution of controlling ϕ in the experimental setup was 0.008. The surface temperature (T_s) was recorded for each stable flame condition. In the studies of extinction limit, the independent parameters were v_{ave}, ϕ, and χ_{N_2},

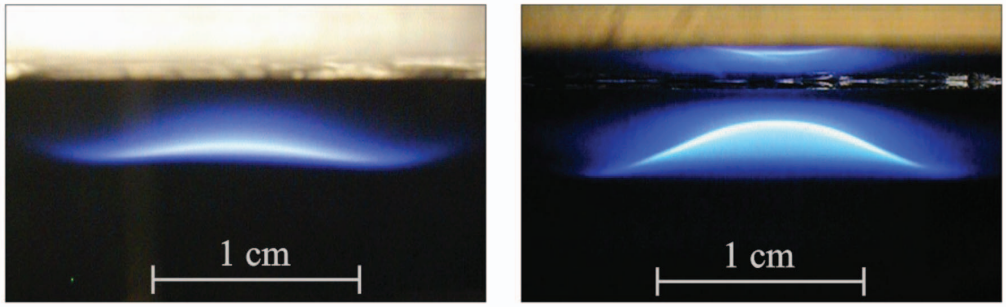

(a) CH_4/air ($\phi = 0.62$; $v_{ave} = 0.5$ m/s) (b) C_3H_8/air ($\phi = 0.77$; $v_{ave} = 0.8$ m/s)

Fig. 4 Typical methane and propane stagnation-flow flames

and the dependent parameters were $\phi_{\min}$ and T_s.

To measure the catalytic activity in the absence of a gas-phase flame, the air and coflow were impinged on the heated plate until a steady state temperature was reached. For these experiments, the back side of the plate was insulated using an alumina fiber based insulation paper (Cotronics Corp.). After the steady state temperature was reached (T_{s0}), the fuel was added to the mixture and the plate temperature was monitored until a steady state temperature with the fuel mixture was reached (T_{sf}). A change in surface temperature after the fuel was introduced indicates heat release due to the reaction of the fuel on the catalyst. For unburned reactants impinging on the heated plate, the independent parameters were v_{ave}, ϕ, χ_{N_2}, and the initial plate temperature T_{s0}, and the dependent parameter was the increase in the plate temperature $\Delta T_s = T_{sf} - T_{s0}$.

4 Experimental Results and Discussion

4.1 Extinction Limits for $CH_4/O_2/N_2$/Air and $C_3H_8/O_2/N_2$/Air Flames. Figure 4 shows the images of typical premixed flames for the methane/air and propane/air systems. The blue emission at the top of Fig. 4 is a reflection from the stagnation surface. For the conditions presented here, the distance from the stagnation surface to the center of the flame was approximately 4 mm for methane/air flames and 2 mm for propane/air flames. The propane/air flames in general have higher flame speeds; hence they required higher nozzle exit velocities to establish stable flames. The higher curvature of the propane/air flames is attributed to the fact that the higher nozzle exit velocity leads to a more nonuniform velocity profile in the radial direction.

For the stagnation-point-flow configuration under study, the impinging gases decelerate as they approach the stagnation plane, and the flame stabilizes at a location where the flame speed balances with the local gas velocity. A larger flame speed for a given v_{ave} will cause the flame to be farther away from the plate. Starting with a stabilized flame at a given condition, the extinction limits were measured by gradually decreasing the mixture equivalence ratio until the flame is extinguished on the stagnation surface.

4.1.1 Premixed $CH_4/O_2/N_2$ Stagnation-Flow Flames on Pt and Si. The experimental results for the methane extinction limits are presented in Figs. 5 and 6, while the raw data values are shown in Table 2. Figure 5 shows the minimum equivalence ratio at extinction and the corresponding surface temperature as a function of v_{ave}, while holding χ_{N_2} constant at 0.79 (as in air). The results for both unheated (filled symbols) and heated (open symbols) surface conditions are shown. It is evident that both $\phi_{\min}$ and T_s increase as v_{ave} increases, implying that the flame can be more easily extinguished due to the decreased residence time for complete combustion. The higher T_s at extinction for higher v_{ave} further confirms that faster chemical reactions are needed in order to sustain combustion under reduced flow residence time. The range of velocities presented here were practical limitations of the experimental facility used in this study: A lower flow rate would result in flashback and a higher flow rate would yield flame quenching.

Figure 6 shows $\phi_{\min}$ and corresponding T_s as a function of χ_{N_2}, while holding v_{ave} constant at 0.74 m/s. Results for the heated condition (open symbols) are shown. As χ_{N_2} increases, the flame speed is decreased due to dilution, causing a larger $\phi_{\min}$ at extinction. However, the plate temperature, T_s, is relatively constant

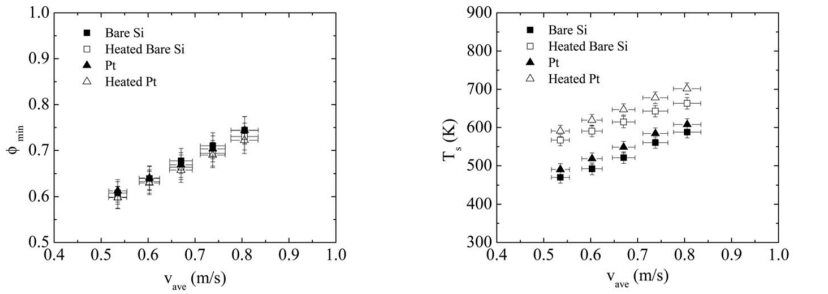

(a) ϕ_{min} as a function of v_{ave} (χ_{N_2}=0.79) (b) T_s at ϕ_{min} as a function of v_{ave} (χ_{N_2}=0.79)

Fig. 5 Lean extinction limits of CH_4 flames as a function of the nozzle exit velocity for fixed dilution level

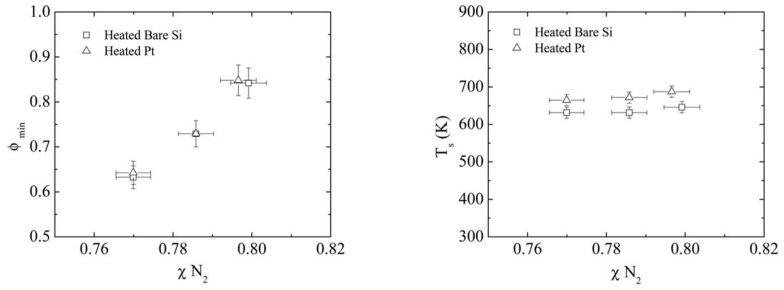

(a) ϕ_{min} as a function of χ_{N_2} (v_{ave}=0.74 m/s) (b) T_s at ϕ_{min} as a function of χ_{N_2} (v_{ave}=0.74 m/s)

Fig. 6 Lean extinction limits for CH_4 flames as a function of dilution for fixed levels of stretch

with respect to increasing χ_{N_2}, unlike the results shown in Fig. 5. This is expected because, for a given v_{ave} with the same residence time, extinction occurs at the same chemical reactivity. The decreased enthalpy of the reactants for increased dilution is offset by the increased enthalpy at higher equivalence ratio to achieve the same chemical reactivity at the extinction condition. The range of dilution with χ_{N_2} was limited at high concentrations by the lack of stable conditions and at low concentrations by flashback. The overall results in Figs. 5 and 6 suggest that the combustion characteristics at these conditions are primarily controlled by the gas-phase combustion.

Table 2 Measured extinction limits for methane flames

v_{ave} (m/s)	χ_{N_2}	ϕ_{min}	T_s (K)
	Bare Si wafer		
0.54	0.79	0.62	470
0.61	0.79	0.64	492
0.67	0.79	0.68	521
0.74	0.79	0.71	560
0.81	0.79	0.74	588
	Heated bare Si wafer		
0.54	0.79	0.60	567
0.61	0.79	0.63	590
0.67	0.79	0.66	614
0.74	0.79	0.69	642
0.81	0.79	0.73	663
0.74	0.77	0.63	631
0.74	0.79	0.73	632
0.75	0.80	0.84	646
	Pt coated wafer		
0.54	0.79	0.61	490
0.61	0.79	0.64	518
0.67	0.79	0.67	548
0.74	0.79	0.70	584
0.81	0.79	0.74	607
	Heated Pt coated wafer		
0.54	0.79	0.60	591
0.61	0.79	0.63	619
0.67	0.79	0.66	647
0.74	0.79	0.69	678
0.81	0.79	0.72	701
0.74	0.77	0.64	665
0.74	0.79	0.73	672
0.74	0.80	0.85	688

Figures 5(*b*) and 6(*b*) further show that T_s is slightly higher for the platinum surface case compared with that for the bare silicon surface case. The magnitude of the temperature difference was clearly greater than the experimental uncertainty. The increase in the temperature for the platinum case is attributed to the difference in the radiative heat loss associated with the two surface conditions, which is primarily attributed to differences in surface emissivity. Within the observed temperature range, the emissivities of platinum, silicon wafer, and stainless steel are estimated to be 0.26 [13], 0.76 [14], and 0.9 [15], respectively. There are also visible variations in the surface finish with aging of the catalyst, which can further modify the emissivity. Consistent temperature increases with platinum surfaces were observed regardless of the surface heating conditions, suggesting that surface reactions were not activated significantly in all cases.

Despite the small differences in the surface temperature, the presence of platinum hardly affected the lean extinction limits for the methane flames. There is a slight decrease in ϕ_{min} as the plate is heated, as shown in Fig. 5(*a*), which is attributed to the enhanced gas-phase reactions. However, the overall effect was found to be insignificant compared with the difference in T_s between the heated and unheated conditions (Fig. 5(*b*)). Therefore, for the conditions studied, catalytic activities were negligible, and the combustion and surface heating behavior were dictated by gas-phase reaction and transport.

4.1.2 Premixed $C_3H_8/O_2/N_2$ Stagnation-Flow Flames on Pt and Si. Anticipating that surface reactions can be more active with propane/air mixtures, we also conducted experiments to measure the lean extinction limits of propane/air impinging on the platinum surface. The results for the lean extinction limits are presented in Fig. 7 and Table 3. Figure 7 shows ϕ_{min} and corresponding T_s as a function of v_{ave} for χ_{N_2}=0.79. Only heated surface conditions were considered at a comparable heating level as in the methane flame cases. Similar to the methane results, T_s increases with increasing v_{ave}, while the difference in T_s, as well as in ϕ_{min}, between different surface conditions is very small. These results indicate that the extinction process for the propane flames was also dictated by the gas-phase reactions.

The results for the propane lean extinction limits are found to be consistent with the results by Law et al. [9], in which the effects of platinum on the extinction limits of premixed propane/air stagnation flames were investigated. They also found that the propane air flames stabilized on the heated stagnation surface (T_s=630–800 K) were insensitive to the presence or the absence of platinum of the stagnation surface. If the characteristic value for flame stretch is defined as $S_L=v_a vg/d$, where d is the distance from the luminous flame sheet to the stagnation surface, the values for S_L for the current work range from 2651/s to 3351/s for the

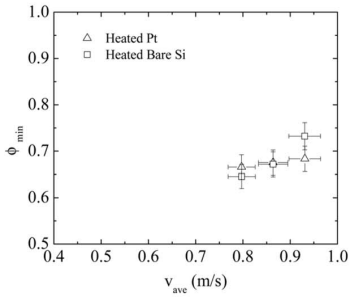

(a) ϕ_{min} as a function of v_{ave} (χ_{N_2}=0.79)

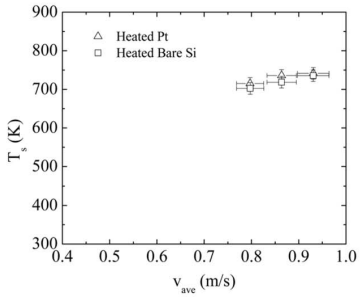

(b) T_s at ϕ_{min} as a function of v_{ave} (χ_{N_2}=0.79)

Fig. 7 Lean extinction limits for C_3H_8 flames as a function of the nozzle exit velocity for fixed dilution level

propane flames (where d=3 mm). The stretch values for the study by Law et al. [9] range from 1401/s to 11301/s. The results for the lean extinction limits as a function of the average nozzle exit velocity are plotted in Fig. 8 along with the experimental results by Law et al. [9]. The results agree well in the low velocity range considered in the present study. Law et al. [9] also studied the location of the flame at extinction. They found the flame location at extinction was slightly farther from the stagnation plane with decreasing mixture velocity. For the experimental conditions tested in the current work, the flame location at extinction was approximately constant; however, note that the range of velocities considered is much smaller than that of Law et al. [9].

Table 3 Measured extinction limits for propane flames

v_{ave} (m/s)	χ_{N_2}	ϕ_{min}	T_s (K)
	Bare Si wafer		
0.80	0.79	0.65	702
0.87	0.79	0.67	718
0.93	0.79	0.73	735
0.87	0.80	0.76	678
0.94	0.80	0.76	671
	Pt coated Si wafer		
0.80	0.79	0.67	715
0.87	0.79	0.68	735
0.93	0.79	0.68	741
0.87	0.80	0.76	678
0.94	0.80	0.79	702

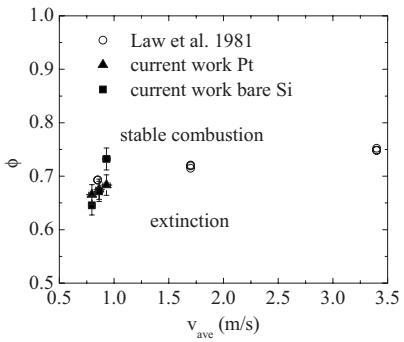

Fig. 8 Comparison between the C_3H_8 extinction limits as a function of the nozzle exit velocity measured in the present study and the results of Law et al. [9]

4.2 Catalytic Reactivity for Fuel/Air Mixtures Impinging on Heated Pt. In the subsequent set of experiments, a fresh fuel/air mixture stream at ambient conditions was impinged onto a nonreactive and catalytic surface at different heating conditions in order to identify if significant surface reactions were observed. All conditions tested had a nozzle exit velocity of v_{ave}=0.92. Initially, only air is supplied onto a heated plate, and then the fuel supply is started at the prescribed equivalence ratio. Activation of surface reactions is then identified by an additional increase in the surface temperature. As expected, no additional temperature increase was observed with bare silicon surfaces, and the results with platinum surfaces are reported in Secs. 4.2.1 and 4.2.2.

4.2.1 CH_4*/Air Mixtures Impinging on Heated Pt.* First, methane/air was supplied to the heated catalytic surface. The surface temperature, T_s, was varied from 300 K to 700 K, the average nozzle exit velocity v_{ave} was 0.92 m/s for all experiments, and ϕ was varied from 0 to 3. For all conditions considered, no increase in surface temperature was observed, indicating that catalytic reactions were not activated. The observed low methane/air/platinum activity agrees with previous studies. For example, Dupont et al. [16] reported that the conversion of methane was below 5% when the surface temperature was below 750 K. Williams et al. [7] and Veser and Schmidt [6,7] further showed that heterogeneous ignition of lean methane air mixtures on a heated platinum foil occurs in the range of 820–870 K, which was computationally confirmed by Deutschmann et al. [17]. Such high surface temperatures could not be achieved with the current experimental facility.

4.2.2 C_3H_8*/Air Mixtures Impinging on Heated Pt.* Unlike the methane/air system, however, significant surface reactions were observed with the propane/air system. Table 4 presents the results for the catalytic response of the three equivalence ratios ϕ=1, 1.8, and 3.5 that were investigated for a range of initial plate temperatures. The average nozzle exit velocity v_{ave} was 0.92 m/s for all experiments. Figure 9 shows the plate temperature as a function of time for a typical experiment where ϕ=1.8 and the initial surface temperature was T_{s0}=614 K. For each experiment the plate was initially heated until a steady temperature condition was achieved (about 60 min), after which the reactant mixture was supplied through the nozzle. The surface temperature then increased gradually until it reached a second steady condition (about 120 min). When the fuel supply was stopped, the temperature decreased to recover the initial heated temperature condition, T_{s0}. The return to T_{s0} confirms that the second temperature rise in Fig. 9 results from heat release from the surface reactions of the propane/oxygen/platinum system.

Table 4 Platinum surface temperature in response to the heated initial surface temperature, T_{s0}, with the propane/air mixture impinging on the surface. The average nozzle exit velocity was 0.92 m/s.

T_{s0}	T_{sf}	ΔT_s	ϕ
725	877	152	1.00
719	857	137	1.00
665	813	147	1.00
610	769	159	1.00
552	747	194	1.80
588	746	159	1.80
614	830	216	1.80
727	905	178	1.80
608	830	222	3.50
619	825	206	3.50
721	893	172	3.50
635	837	203	3.50

The temperature increase due to catalytic reaction is a valuable metric of the catalyst performance, as it indicates the strength of the catalytic effects. We define $\Delta T_s = T_{sf} - T_{s0}$, where T_{sf} and T_{s0} are indicated in Fig. 9, as the measure of the intensity of the catalytic reactions. This quantity was measured for different T_{s0} by changing the heat input to the surface.

Figure 10 shows ΔT as a function of the initial surface temperature T_{s0} for various ϕ conditions. Within the experimental uncertainties, ΔT_s appears to remain almost constant for the range of conditions. This suggests that the catalytic reactions on the platinum surface have reached the diffusion-limited mode. In other words, the catalytic activity is sufficiently high such that the overall heat release rate is determined by the transport rate of the reactant gases to the surface, which is fixed constant here. Nevertheless, there is a tendency that ΔT_s increases as the mixture equivalence ratio increases.

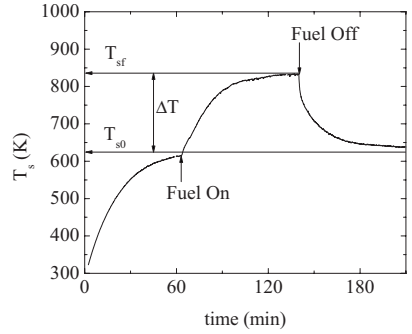

Fig. 9 Typical temperature evolution in time for unburned propane air mixture impinging on the heated stagnation surface (ϕ=1.8 and v_{ave}=0.92 m/s)

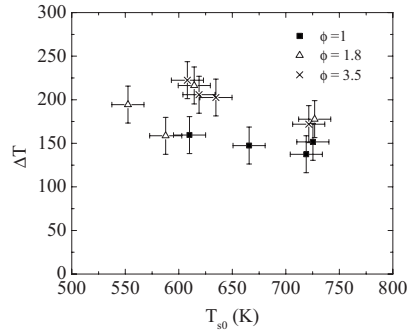

Fig. 10 Catalytic response, ΔT_s, of heated Pt surface to C_3H_8/air mixture as a function of surface heating (T_{s0}) for various equivalence ratios. The average nozzle exit velocity was 0.92 m/s.

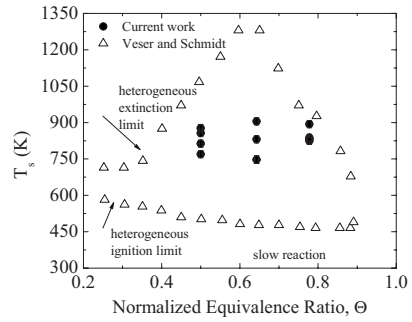

Fig. 11 Comparison between the Pt catalyst response to C_3H_8/air mixtures of the current work to Veser and Schmidt [6]

The steady state surface temperature with catalytic reaction, T_{sf}, measured in the present study is compared with the results by Veser and Schmidt [6], who investigated heterogeneous ignition and extinction characteristics of propane air mixtures on an electrically heated platinum foil. Figure 11 shows the results as a function of the normalized equivalence ratio, $\Phi = \phi/(1+\phi)$, such that the lean and rich limit is bounded between 0 and 1. The flow velocity in Veser and Schmidt [6] was 0.025 m/s, whereas in the present work the average velocity was 0.92 m/s. Note that the present experimental results show stable operating conditions in a region where Veser and Schmidt [6] found no stable operating conditions. This may be attributed to a number of factors. The present experimental setup has large heat loss associated with a large surface area and surface emissivity, unlike the case of the electrically heated foil employed by Veser and Schmidt [6]. In addition, the flow residence time is significantly lower in the present study due to the high nozzle exit velocity. The steady surface reaction temperature depends strongly on these conditions for heat and mass transport. Further studies may provide more quantitative assessment of these effects.

5 Conclusions

Experimental studies were conducted using a stagnation-point-flow combustor configuration in order to assess the feasibility of lean flammability extension by catalytic reaction. Platinum versus bare silicon surfaces were compared, while methane/air and propane/air at various mixture compositions were considered for gas-phase reactants. An additional heat supply to the catalytic surface was attempted to enhance the activity of surface chemistry. For all of the conditions considered, the lean flame extinction limits were predominantly governed by gas-phase combustion, and the presence of the catalytic surface hardly affected the extinction limits. The catalytic surface temperature at the extinction limits showed a slight, yet consistent, increase with the catalytic surface, due likely to the differences in the surface heat transfer properties. In contrast to the computational studies conducted by Li and Im [10,11], the present experimental facilities are characterized by large heat losses, resulting in catalytic surface temperatures much lower than those predicted by the modeling studies.

The extent of catalytic activity was also investigated by supplying a fuel/air mixture stream onto a heated platinum plate. For the heated surface temperature range obtained in the present study, methane/air mixtures failed to activate catalytic reaction, consistent with previous experimental findings. On the other hand, the propane/air mixtures did activate surface chemistry at a significant

level, by raising the surface temperature by a few hundred degrees. The results demonstrate that stable heterogeneous reaction conditions can be achieved with propane/air at relatively low temperatures and moderate flow rates. For the conditions under study, the magnitude of the additional surface temperature increase due to catalytic reactions was insensitive to the initial surface temperature, suggesting that the observed heterogeneous reaction was transport limited.

The present study provides useful new data on near-extinction characteristics of platinum/methane and platinum/propane reaction systems. There was clear evidence that propane can yield stronger catalytic activities. However, the benefit of catalytic reaction in achieving leaner and lower-temperature combustion in compact reactors with high surface-to-volume ratios should be carefully assessed by accounting for the fact that most such devices are likely subject to significant heat losses. Therefore, careful design and integration to ensure maximum thermal insulation are essential in acquiring the benefit of catalytic reactions. To this end, it is also of interest to investigate alternative novel catalyst materials with substantially lower activation temperatures.

Acknowledgment

This work was supported by the National Science Foundation, Grant No. CTS-0134128.

Nomenclature

A_n = nozzle exit area
$\dot{Q}$ = volumetric flow rate
T_s = surface temperature
T_{s0} = initial surface temperature
T_{sf} = final surface temperature
ΔT_s = difference in surface temperature
U_{param} = uncertainty in a given parameter
v_{ave} = average nozzle exit velocity
χ_{N_2} = nitrogen mole fraction in oxidizer
ϕ = equivalence ratio
ϕ_{min} = lean extinction limit
Φ = normalized equivalence ratio

References

[1] Boyer, R., 2006, "Annual Energy Review 2005," Energy Information Administration, Technical Report No. DOE/EIA-0384.
[2] Law, C. K., and Sivashinsky, G. I., 1982, "Catalytic Extension of Extinction Limits of Stretched Premixed Flames," Combust. Sci. Technol., **29**(3), pp. 277–286.
[3] Pfefferle, L. D., and Pfefferle, W. C., 1987, "Catalysis in Combustion," Catal. Rev. - Sci. Eng., **29**(2–3), pp. 219–267.
[4] McDaniel, A. H., Lutz, A. E., Allendorf, M. D., and Rice, S. F., 2002, "Effects of Methane and Ethane on the Heterogeneous Production of Water From Hydrogen and Oxygen Over Platinum in Stagnation Flow," J. Catal., **208**(1), pp. 21–29.
[5] Ljungstrom, S., Kasemo, B., Rosen, A., Wahnstrom, T., and Fridell, E., 1989, "An Experimental Study of the Kinetics of OH and H_2O Formation on Pt in the H_2+O_2 Reaction ," Surf. Sci., **216**(1–2), pp. 63–92.
[6] Veser, G., and Schmidt, L. D., 1996, "Ignition and Extinction in the Catalytic Oxidation of Hydrocarbons Over Platinum," AIChE J., **42**, pp. 1077–1087.
[7] Williams, W., Stenzel, M., Song, X., and Schmidt, L., 1991, "Bifurcation Behavior in Homogeneous-Heterogeneous Combustion: I. Experimental Results Over Platinum," Combust. Flame, **84**(3–4), pp. 277–291.
[8] Dupont, V., Zhang, S. H., and Williams, A., 2000, "Catalytic and Inhibitory Effects of Pt Surfaces on the Oxidation of $CH_4/O_2/N_2$ Mixtures," Int. J. Energy Res., **24**(14), pp. 1291–1309.
[9] Law, C. K., Ishizuka, S., and Mizomoto, M., 1981, "Lean-Limit Extinction of Propane/Air Mixtures in the Stagnation-Point Flow," Symposium (International) on Combustion, pp. 1791–1798.
[10] Li, J., and Im, H. G., 2006, "Extinction Characteristics of Catalyst-Assisted Combustion in a Stagnation-Point Flow Reactor," Combust. Flame, **145**(1-2), pp. 390–400.
[11] Li, J., and Im, H. G., 2007, "Effects of Dilution on the Extinction Characteristics of Strained Lean Premixed Flames Assisted by Catalytic Reaction," Proc. Combust. Inst., **31**, pp. 1189–1195.
[12] Croarkin, M. C., Guthrie, W. F., Burns, G. W., Kaeser, M., and Strouse, G. F., 1993, "Temperature-Electromotive Force Reference Functions and Tables for the Letter-Designated Thermocouple Types Based on the ITS-90," National Institute of Standards and Technology Monograph 175.
[13] Goard, R., 1966, "Application of Hemispherical Surface Pyrometers to the Measurement of the Emissivity of Platinum (A Low-Emissivity Material)," J. Sci. Instrum., **43**(4), pp. 256–258.
[14] Timans, P., 1993, "Emissivity of Silicon at Elevated Temperatures," J. Appl. Phys., **74**(10), pp. 6353–64.
[15] Incropera, F. P., Dewitt, D. P., Bergman, T. L., and Lavine, A. S., 2006, *Fundamentals of Heat and Mass Transfer*, 6th ed., Wiley, New York.
[16] Dupont, V., Zhang, S. H., and Williams, A., 2001, "Experiments and Simulations of Methane Oxidation on a Platinum Surface," Chem. Eng. Sci., **56**, pp. 2659–2670.
[17] Deutschmann, O., Behrendt, F., and Warnatz, J., 1994, "Modelling and Simulation of Heterogeneous Oxidation of Methane on a Platinum Foil," Catal. Today, **21**(2–3), pp. 461–470.

Appendix B

An experimental investigation of propane oxidation on a platinum catalyst stagnation surface

J. T. Wiswall, M. S. Wooldridge, and H. G. Im

Proceedings of the 6th U.S. National Combustion Meeting

An experimental investigation of propane oxidation on a platinum catalyst stagnation surface

J. T. Wiswall*, M. S. Wooldridge, and H. G. Im
Department of Mechanical Engineering
The University of Michigan
Ann Arbor, MI 48109

Abstract
A stagnation-point flow reactor was used to study the catalytic activity of platinum and premixed propane/air reactants at atmospheric pressure. The stagnation surface temperature was controlled to maintain constant temperatures and the catalytic activity of the Pt to C_3H_8, O_2, CO, CO_2 and NO was evaluated for catalyst stagnation surface temperatures ranging from 300°C to 800°C. Three fuel-air equivalence-ratio conditions were studied (ϕ = 0.67, 1.0 and 1.5). The heat released by surface reaction was quantified using the heater power required to stabilize the stagnation plane at the prescribed temperature. The results indicate an abrupt increase in heat release and fuel conversion occurs with increasing surface temperature. The heterogeneous ignition temperature based on these data is between 325-350 °C.

Introduction
Catalysts are playing an increasingly larger role in fuel utilization as we seek higher efficiency, more environmentally sustainable solutions to stationary and mobile power generation for a global society. Concerns regarding greenhouse gas emissions have expanded catalyst devices to include oxidation of tail-gases, such as methane from coal mines, pipelines, and oil and gas refineries [1]. Moreover, the traditional role of catalysts in exhaust-gas after-treatment will also increase dramatically in the near future with the emphasis on high-efficiency gasoline and diesel engines which require significant advances in lean NOx catalysis and particulate trap technologies. Catalysts are well known as critical components in conventional exhaust gas after-treatment systems, like automotive three-way catalysts. However, the burden on after-treatment systems has become more and more challenging, with less waste heat available to thermally activate the catalysts and with the shift in the composition of the exhaust gases caused by lean combustion.

Another important future for catalysts is in catalytic combustion systems. Modern applications use low temperature combustion, which is motivated by the combined goals of increasing thermodynamic efficiencies, while simultaneously reducing combustor and engine-out emissions. However, the combustion process becomes more limited by chemical reaction as temperatures are decreased, and homogeneous reaction alone cannot sustain stable device operation at desired lean conditions. Catalysts can provide the means to achieve stable lean combustion and maintain high fuel conversion rates. At the macro-scale, catalysts are being revisited for integration directly into the I.C. engine combustion chamber [2]. At the small scale, catalyst applications are expanding to microcombustors to improve stability, control and conversion efficiency at low temperatures [3,4].

These examples illustrate the importance and need for improved performance of catalytic reactors for a wide variety of practical applications. This work focuses on improving our quantitative understanding of the effects of platinum on propane oxidation. The technical approach leverages the unique properties of a stagnation-point flow reactor (SFR) to facilitate studies of the surface reaction chemistry. Stagnation-point flow reactors with a catalytic surface have become a preferred geometry for the investigation of the fundamental mechanisms important to catalyst systems for several reasons. One key feature is that SFRs can be used to study both flameless systems and systems where a stable gas-phase flame is present. As a consequence, catalyst effects on fuel oxidation and emissions can be considered systematically.

There have been numerous studies of propane/air combustion and oxidation in the presence of a platinum catalyst, primarily using packed bed reactors. However, relatively few investigators have studied propane/Pt catalyst systems using SFRs [5]. Veser and Schmidt [5] focused on determining the homogenous and heterogeneous ignition temperatures using a SFR and platinum foil. In our previous experiments [6], the catalytic activity of platinum for oxidation and combustion of methane and propane was evaluated in terms of the lean extinction limits (combustion) and the heat release at the catalyst surface (oxidation). The objective of this work is to quantify the platinum activity for oxidation of propane/air mixtures for controlled stagnation surface temperatures.

* Corresponding author: jwiswall@umich.edu
Proceedings of the 6th U.S. National Combustion Meeting

Experimental Approach

Following our earlier work [6], more detailed studies of flameless propane oxidation were conducted, where the catalytic activity was systematically characterized as a function of isothermal catalyst conditions using exhaust gas speciation. **Figure 1** shows a photograph of the UM SFR experimental facility. For these experiments, a propane/air mixture was impinged on the stagnation surface where a platinum catalyst was mounted. The flow direction is from the bottom of **Fig. 1** to the top. A transparent (borosilicate) cylindrical enclosure is shown in the figure. Alternatively, an aluminum wall could be used. The stagnation plane is located two nozzle diameters away from the nozzle exit, and exhaust gases are sampled after they passed over the catalyst surface. A pyrolytic graphite heater (Momentive Ceramics Inc.) mounted in a stainless steel enclosure purged with nitrogen is used to heat the catalyst. The temperature of the stagnation plane is maintained at a constant value using an electric heater and PID temperature controller. The temperature at the stagnation plane was measured using a k-type thermocouple probe (Omega Engineering Inc.) placed in a groove machined into the stainless steel mounting surface. For a worst case scenario the temperature of the stagnation plane was calculated to be within 15^{o}C from the thermocouple location. The uncertainty in the thermocouple measurement is ±2.5^{o}C up to 333^{o}C and 0.0075×T for temperatures above 333^{o}C.

A cross-sectional schematic of the UM SFR is shown in **Figure 2**. The premixed fuel/air reactants flow from a tube into a mixing chamber which is filled with glass beads. The mixing chamber ensures complete mixing of the propane and air. An alumina monolith with 600 cells per square inch (Corning Inc.) is placed within the mixing chamber immediately downstream from the glass beads with the purpose of creating a uniform velocity profile. After the monolith, the mixture flows through a nozzle with a 18.26:1 area contraction ratio (exit diameter = 10 mm i.d.) and impinges on the heated stagnation plane. The nozzle exit plane is located 26.2 mm from the stagnation surface (separation distance/nozzle diameter = L/D = 2.62). The flow profile produced using this configuration is quite uniform, as indicated by the photograph presented in **Fig. 3**, where a propane/air flame has been stabilized in the stagnation flow. The luminous region of the flame demonstrates that the flow field impinging on the stagnation plane is uniform across the nozzle exit.

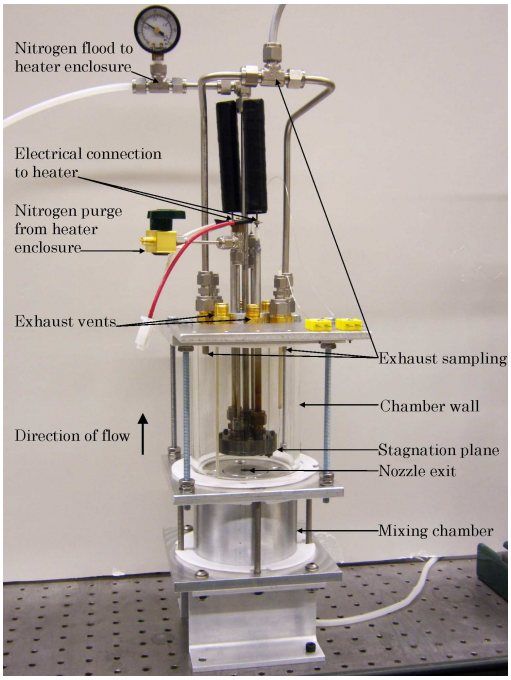

Figure 1 Photograph of The University of Michigan stagnation flow reactor (SFR) facility.

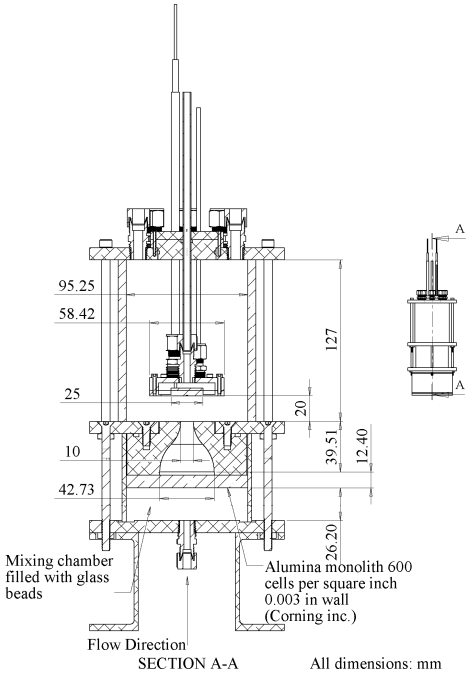

Figure 2 Cross sectional view of the UM SFR showing key dimensions.

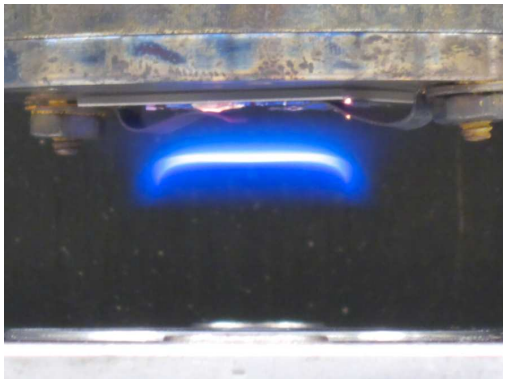

Figure 3 Photograph showing an ignited stagnation flow flame of propane and air at atmospheric pressure ($V_{nozzle\ exit}$ = 1.3 m/s, ϕ = 0.82). The visible emission from the laminar flame demonstrates the uniformity of the velocity profile that develops from the nozzle exit. The curved metal pieces in the image are the mounting clips for the catalyst.

The platinum catalyst used in these studies was deposited by physical vapor deposition (PVD) on a quartz wafer 2.54 cm × 2.54 cm (square) × 1 mm thick. In order to form a stable bond of the platinum to the quartz, a bonding layer of titanium (10 nm in thickness) was first deposited on the bare quartz. A 100 nm thick layer of platinum was then coated on the titanium layer. The wafer was mounted on the heated stainless steel surface by stainless steel clips. The catalyst was then used without any other pretreatment or conditioning.

High purity C_3H_8 (Cryogenics, 99.9%), mixed with synthetic air (O_2 20.9-21.6% and N_2) was used for all experiments. The reactant flow rates were controlled and measured using a mixing manifold and calibrated flow meters (rotameters manufactured by Omega Engineering Inc.). Each flow meter was corrected for ambient variations in temperature and atmospheric pressure. The air flow meter was calibrated using an electronic mass flow meter (TSI Inc.), and had an uncertainty of ±2% of the volumetric flow rate. The propane flow meter was calibrated using a bubble flow meter. The uncertainty of the propane flow meter was determined by calibrating the flow meter 5 times and using double the standard deviation of the 5 calibrations as the uncertainty to give a 95% confidence level in the reading. The propane had an uncertainty of ±3.5% of the volumetric flow rate. The corresponding uncertainties in ϕ and v were $\pm 0.035 \times \phi$ and $\pm 0.022 \times v$.

Three equivalence ratios, ϕ = 0.67, 1, 1.5, at an average nozzle exit velocity, v = 1.2 m/s, were studied in the experiments. The choice of v and ϕ uniquely defined the flow rate of the propane and air. The controlled catalyst surface temperature was set at 14 prescribed temperature increments in the range 100-800°C for a particular flow condition.

The exhaust gases were sampled from the exhaust vents at the top of the catalyst chamber. The species O_2, CO_2, CO, unburned hydrocarbons, and NO volume fractions were measured in the exhaust using non-dispersive infrared gas sensing equipment (Horiba Inc.). The CO_2 sensor had an interference effect from C_3H_8, and the presented results are corrected for this effect. The results are reported using the calibration of the gas analyzer. They do not include enrichment or dilution effects due to the location of the gas sampling in the SFR or due to non-isokinetic sampling. The unburned hydrocarbons are reported as the C_3H_8 equivalent in the exhaust. The sample gas was cooled to room temperature before entering the gas analyzer. A water separator was attached to the gas sampling system to remove any condensed water as the exhaust was cooled to room temperature; however, the dew point of the exhaust was below room temperature in all the experiments discussed in this work.

Using the PID controller, the system equilibrated to the set-point temperature within ~15 minutes. Exhaust gas species were sampled at a flow rate of 5000 mL/min for approximately 5 minutes after the system had reached steady state for each prescribed catalyst temperature. The volumetric flow rate of the reactants entering the chamber was 5600 mL/min

Results and Discussion

In order to establish a clear understanding of the effects of the platinum catalyst, baseline data were acquired using a bare quartz wafer at the stagnation plane. There was no detectable change in any of the species measurements using the bare quartz wafer over the range of temperatures considered, 100-800°C. Further, CO_2, CO, and NO were all below their detectability limit when using the blank quartz wafer. Hysteresis effects were considered by conducting series of experiments increasing the stagnation surface temperature and repeating the set by decreasing the stagnation surface temperature, with no detectible change in the results.

Results of the exhaust gas analysis for O_2, CO_2 and C_3H_8 for the Pt catalyst studies are presented as a function of stagnation surface temperature in **Figs. 4-6**. The error bars presented in the figures represent the uncertainty in the measurements due to the uncertainty of the gas analyzer ($\pm 0.015 \chi O_2$ for O_2, $\pm 0.025\ \chi CO_2$ for CO_2, $\pm 0.05\ \chi C_3H_8$ equivalent for unburned hydrocarbons and ±0.03 % by volume for CO). The reading of the gas sensing unit tended to increase over time within the uncertainty of the measurements for O_2 and unburned hydrocarbons. This is visible in **Figs 4** and **6**. The Pt/C_3H_8/air results show an abrupt transition in exhaust composition and electrical power required to sustain the surface temperature starting at about 300°C. The high sensitivity of the composition to the surface temperature

indicates that the surface reactions are activated and the process is rate-controlled. This behavior, however, does not continue indefinitely and the composition level levels off at approximately 500 °C and above. This implies that the surface reactions are saturated, and it is likely that the conversion rate is controlled by the transport of the reactants under these conditions. For all experiments, the NO in the exhaust was below 25 ppmv, which was the minimum amount detectable by the gas sensing unit.

Figure 7 shows the CO volume fraction in the exhaust gases for the Pt/C_3H_8/air experiments. An appreciable amount of CO was present in the exhaust only for the fuel rich case of ϕ=1.5 and only for conditions where the stagnation surface temperature was above 450°C. The presence of CO starts at higher temperatures than the shift in exhaust gas composition for C_3H_8, CO_2 and O_2 does. Note that no CO was present for the experiments using a bare quartz wafer for any conditions. Thus, the presence of CO is attributed to Pt surface activity.

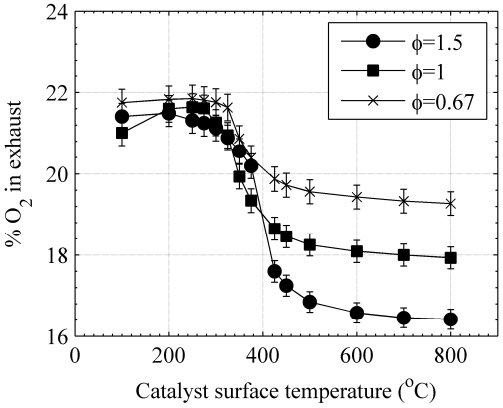

Figure 4 Platinum O_2 activity for propane/air mixtures at v=1.2 m/s.

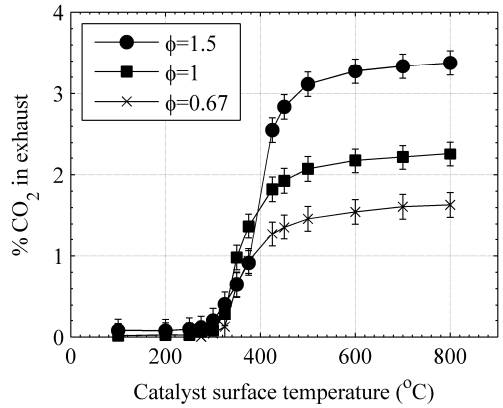

Figure 5 Platinum CO_2 activity for propane/air mixtures at v=1.2 m/s.

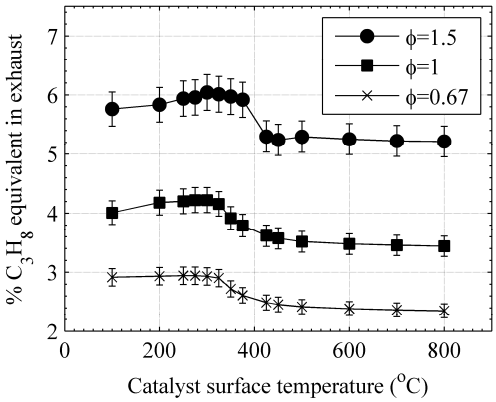

Figure 6 Platinum C_3H_8 activity for propane/air mixtures at v=1.2 m/s.

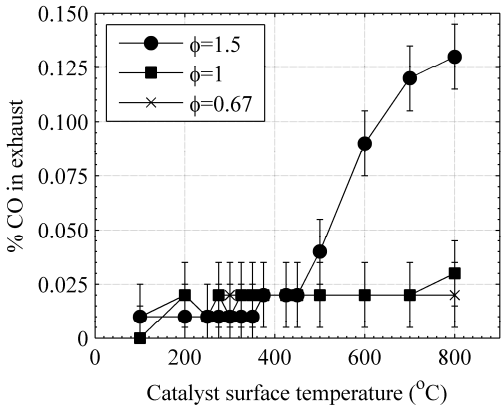

Figure 7 Platinum CO activity for propane/air mixtures at v=1.2 m/s.

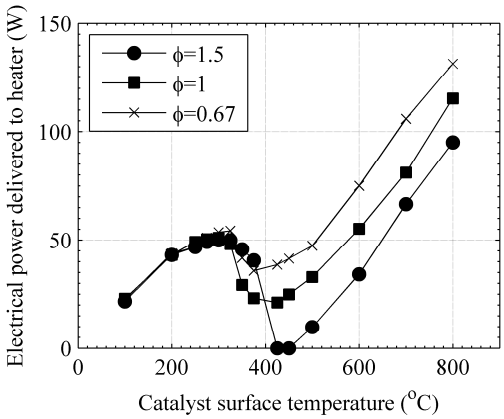

Figure 8 Power delivered to heater for Pt/C_3H_8/air experiments at v=1.2 m/s..

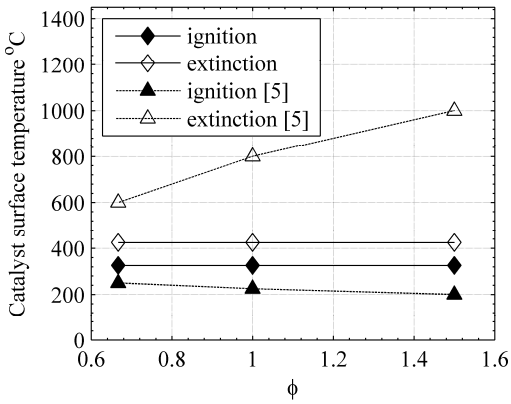

Figure 9 Comparison of the results of the current study of the Pt/C_3H_8/air system and the heterogeneous ignition and extinction data of Veser and Schmidt [5].

The power delivered to the heater to maintain the stagnation plane temperature for each experimental condition is shown in **Fig. 8**. The heater power increased with increasing stagnation plane temperature until ~350°C, consistent with the point where the C_3H_8, CO_2, and O_2 exhaust gas composition shifted markedly. After this point, the required heater power decreased significantly, with larger shifts in power associated with more fuel rich conditions. In particular, for $\phi = 1.5$, the heater power could be reduced to 0, and the catalytic reaction was sufficient to maintain the stagnation plane at high temperatures. This self-sustaining condition occurred for two temperatures of 425°C and 450°C at $\phi = 1.5$, and indicates the conditions of maximum heat release of the experimental conditions studied.

In the study by Veser and Schmidt [5], the authors reported the heterogeneous ignition temperatures of propane/air mixtures impinged on a heated platinum foil. Their experiments are analogous to supplying a constant heating power to the stagnation plane rather than using a temperature controller to maintain a constant surface temperature. Thus, the results of the current work can be compared with the Veser and Schmidt data by considering the local minimum power (425-450 °C, see **Fig. 8**) the point of catalytic extinction (where a decrease in heating power causes an extinction in the catalytic reaction) and the local maximum power (300-350 °C, see **Fig. 8**) the point of catalytic ignition (where an increase in heater power causes catalytic light off). The self-sustaining heat release conditions correspond to the auto thermal conditions observed in the Veser and Schmidt study. Note that this condition is highly dependent on the heat transfer properties of the catalyst stagnation surface.

A comparison of the current work and the ignition and extinction limits measured by Veser and Schmidt [5] is presented **Fig. 9** as a function of the equivalence ratio, ϕ. The ignition point of propane on the platinum foil is slightly lower than that indicated by the local maximum in power measured in the current work. The extinction branch measured by Veser and Schmidt is at a much higher temperature than the local minimum in the current work. The differences are likely due to differences in the in the heat transfer parameters between the foil system and the current work, which include approximately a factor of 5 higher flow velocities.

Conclusions

A stagnation-point flow reactor (SFR) facility has been developed and C_3H_8/Pt catalytic reaction characteristics were investigated by quantitative measurements of surface temperature and exhaust gas composition. The species profiles over a range of surface temperature indicate that heterogeneous ignition on the Pt occurs at approximately 350°C, and the surface becomes active towards production of CO at fuel rich conditions where the stagnation surface temperature above 450°C. The system characteristics data provide a critical temperature range in which the conversion rate is controlled by reaction rates. At higher temperatures, the conversion rate becomes insensitive to the surface temperature, suggesting that the process is transport-limited. Comparison of ignition and extinction surface temperature against previous work showed varying degrees of agreement, and the discrepancies are primarily attributed to the differences in heat losses.

References

1. Salomons, S., Hayes, R. E., Poirier, M., and Sapoundjiev, H., (2004) "Modelling a reverse flow reactor for the catalytic combustion of fugitive methane emissions," *Computers and Chem. Eng.*, **28**:1599-1610.

2. Zeng, W., and Xie, M., (2008), "A novel approach to reduce hydrocarbon emissions from the HCCI engine," *Chem. Eng. J.* **139**:380-389.

3. Okamasa, T., Gwang-Goo, L., Suzuki, Y., Kasagi, N., and Matsuda, S., (2006) "Development of a micro catalytic combustor using high-precision ceramic tape casting," *J. Micromechanics and Microengineering*, **16**:S198-205

4. Men, Y., Kolb, G., Zapf, R., Pennemann, H., Hessel, V., (2009) "Total combustion of propane in a catalytic microchannel combustor," *Chem. Eng. Res. Des.* **87**:91-96.

5. Veser, G., and Schmidt, L. D., 1996. "Ignition and extinction in the catalytic oxidation of hydrocarbons over platinum". *AIChE Journal*, **42**:1077–1087.

6. Wiswall, J., Wooldridge, M. S., Im, H. G., "An experimental investigation of the effects of platinum on methane and propane/air mixtures in a stagnation flow reactor", submitted to the *ASME Journal of Heat Transfer*, November 2008, accepted for publication, March 2009.

Appendix C

Uncertainty calculations

Programs to numerically calculate uncertainty are included in the following sections.

All programs are written for MATLAB 7.3.0.

C.1 Reactant uncertainty

```
clear all
clc

%mixing propane, air
% dC3H8 + e (O2 +  3.76 N2) for stoich
Phi = linspace(0.05,0.95,10);  % normalized equivalence ratio range
phi = Phi./(1-Phi);            % equivalence ratio range
d = 1;
e = 5*4.76.*phi;

for i = 1 : length (e)
    C3H8 = (d + ((d*0.035)).*randn(1e6,1));     % propane flow statistical variance
    C3H8p = C3H8.*(.995 + (0.005/2).*randn(1e6,1)); % propane flow statistical variance
    Air = e(i)+((e(i)*0.020)).*randn(1e6,1);    % air flow statistical variance
    O2 = Air.*(0.21 + (0.005/2).*randn(1e6,1)); % oxygen flow statistical variance

    phi = (1/5).*(O2)./(C3H8p);     % equivalence ratio statistical variance
    Phi = phi./(1+phi);             % normalized equivalence statistical variance
    V = C3H8 + Air;                 % volumetric flow statistical variance

    m_phi(i) = mean(phi);           % mean equivalence ratio
  U_phi(i) = 2*std(phi)/m_phi(i); % fractional equivalence ratio uncertainty

    m_Phi(i) = mean(Phi);           % mean normalized equivalence ratio
    U_Phi(i) = 2*std(Phi)/m_Phi(i); % fractional normalized equivalence ratio uncertainty

    m_V(i) = mean(V);               % mean velocity
  U_V(i) = 2*std(V)/m_V(i);       % fractional volumetric flow rate uncertainty
end
```

C.2 Heater-power uncertainty

```
clear all
clc

v = linspace(0.01,31,10);                  % voltage range (V)
t = linspace(400,1200,10);                 % temperature range (K)
c = linspace(0.01,6.3,10);                 % current range (A)

for i = 1:length(v)
    for j = 1:length(c)
        V = v(i) +v(i).*0.002.*randn(1e6,1);   %statistical voltage variation
        I = c(j) + c(j).*0.0005.*randn(1e6,1); %statistical current variation
        mR = mean(V./I);                %mean resistance
        uR = 2.*std(V./I);              %absolute resistance uncertainty
        UR = 2.*std(V./I)./mR;          %fractional resistance uncertainty
    end
end

for i = 1:length(v)
    for j = 1 : length(t)
        T = t(j) +((t(j).*0.022)/2).*randn(1e6,1); %statistical temperature variation
        V = v(i) +((v(i).*0.002)).*randn(1e6,1);   %statistical voltage variation
        R = -3.0363e-7.*T.^2-5.6228e-5.*T+5.3829 + ...
            (-3.0363e-7.*T.^2-5.6228e-5.*T+5.3829).*UR.*randn(1e6,1)+ ...
           ((0.27).*randn(1e6,1));   %statistical resistance variation
        P = V.^2./R;                 %statistical power variation
        mP(i,j) = mean(P);           %mean power
        uP(i,j) = 2.*std(P);         %absolute power uncertainty
        UP(i,j) = uP(i,j)/mP(i,j);   %fractional power uncertainty
    end
end
```

Appendix D

Technical drawings

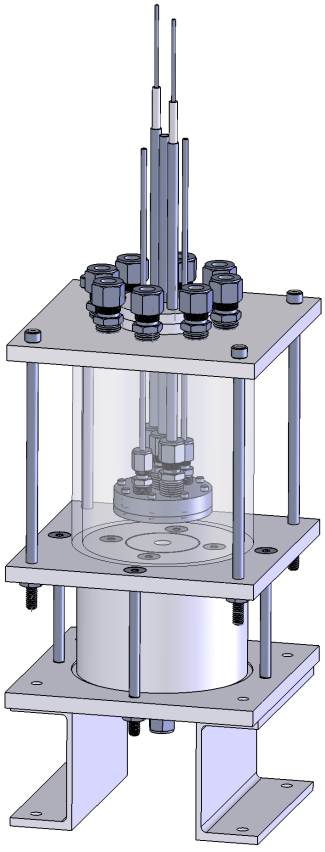

Figure D.1 The stagnation-flow reactor

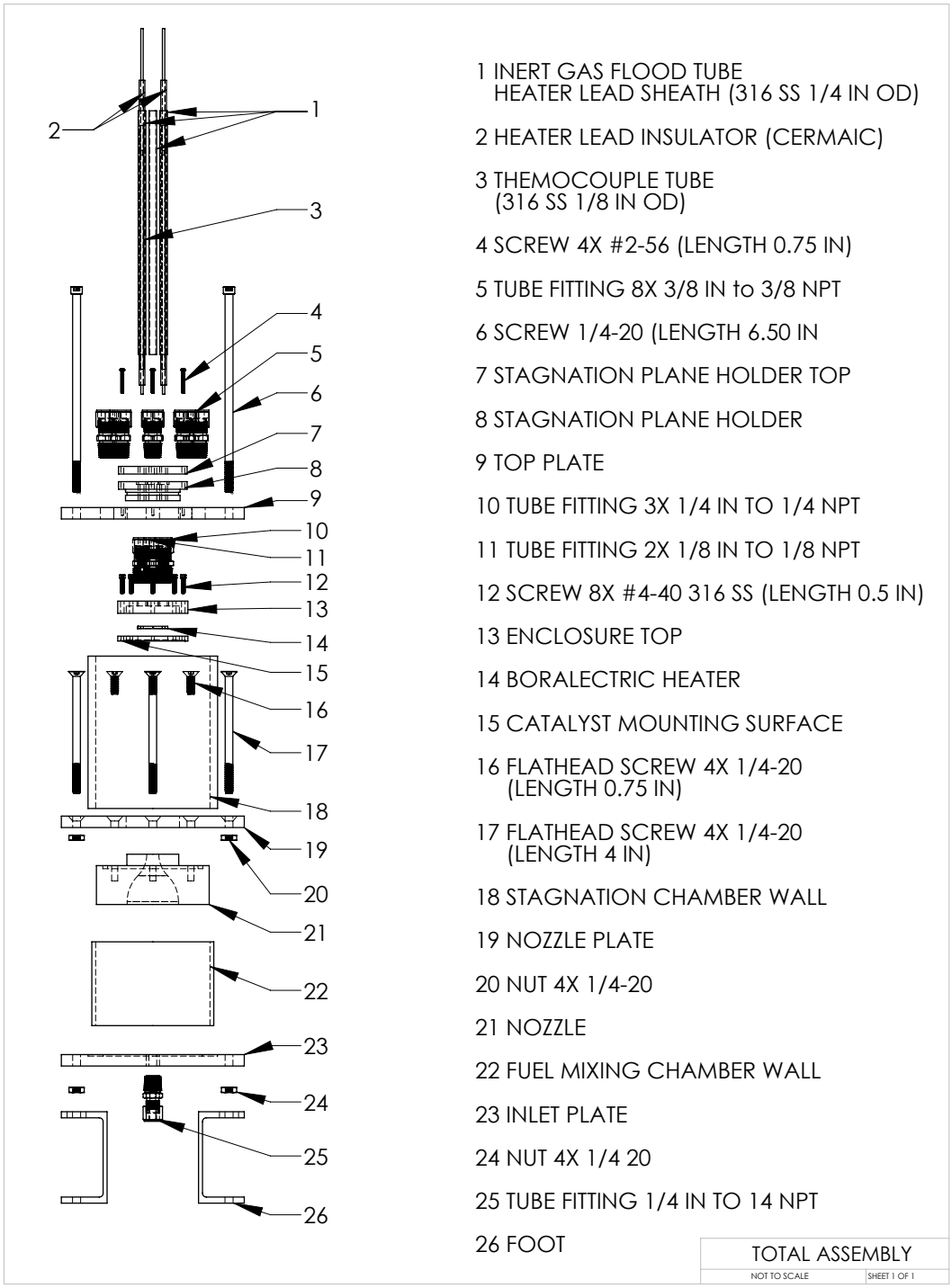

Figure D.2 Exploded view of the stagnation-flow reactor

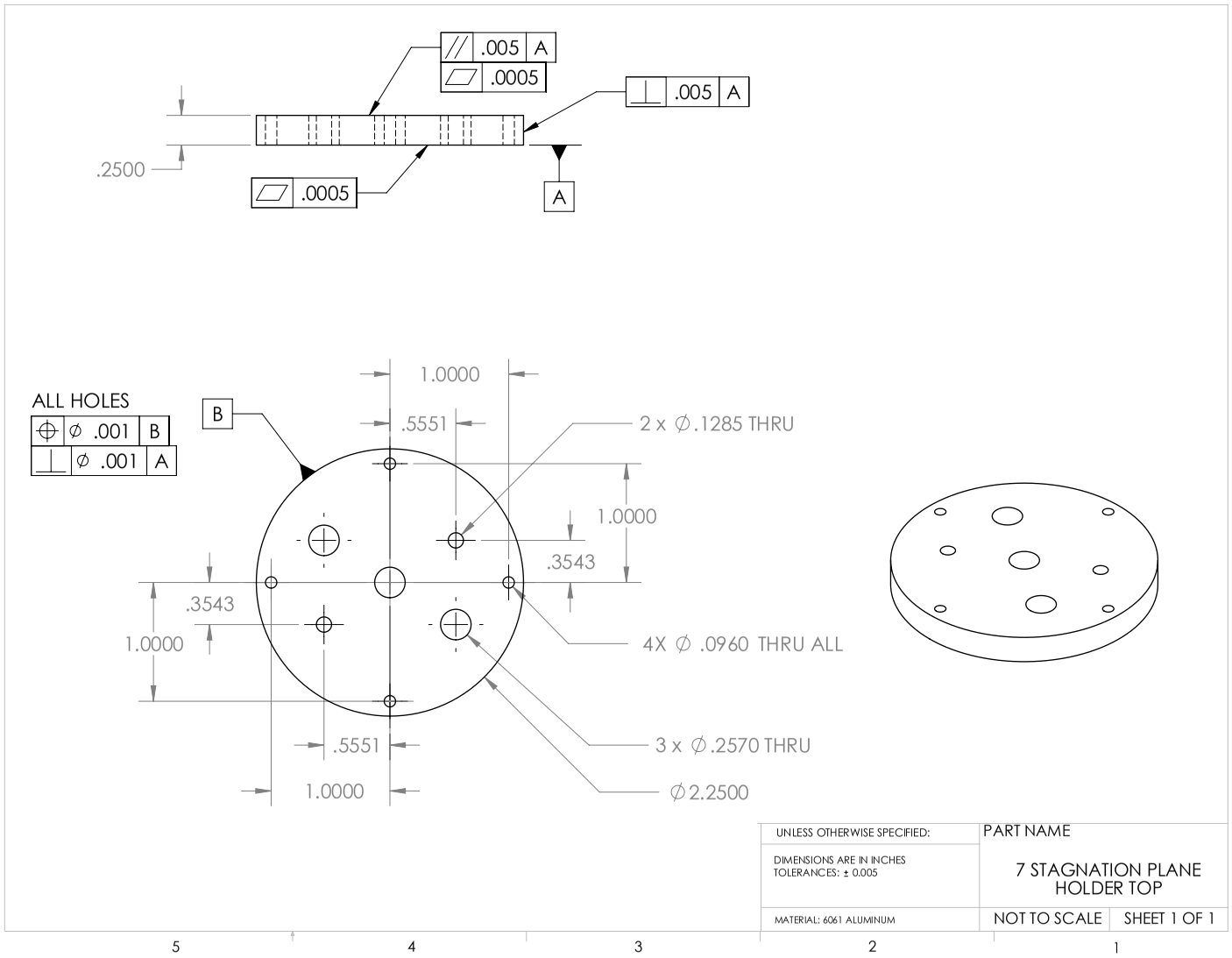
.005 A
.0005
.005 A
.2500
.0005
A
ALL HOLES
⌖ ∅ .001 B
⊥ ∅ .001 A
B
1.0000
.5551
2 x ∅.1285 THRU
1.0000
.3543
.3543
1.0000
4X ∅ .0960 THRU ALL
3 x ∅.2570 THRU
.5551
1.0000
∅2.2500
UNLESS OTHERWISE SPECIFIED:
DIMENSIONS ARE IN INCHES
TOLERANCES: ± 0.005
MATERIAL: 6061 ALUMINUM
PART NAME
7 STAGNATION PLANE HOLDER TOP
NOT TO SCALE
SHEET 1 OF 1
5
4
3
2
1

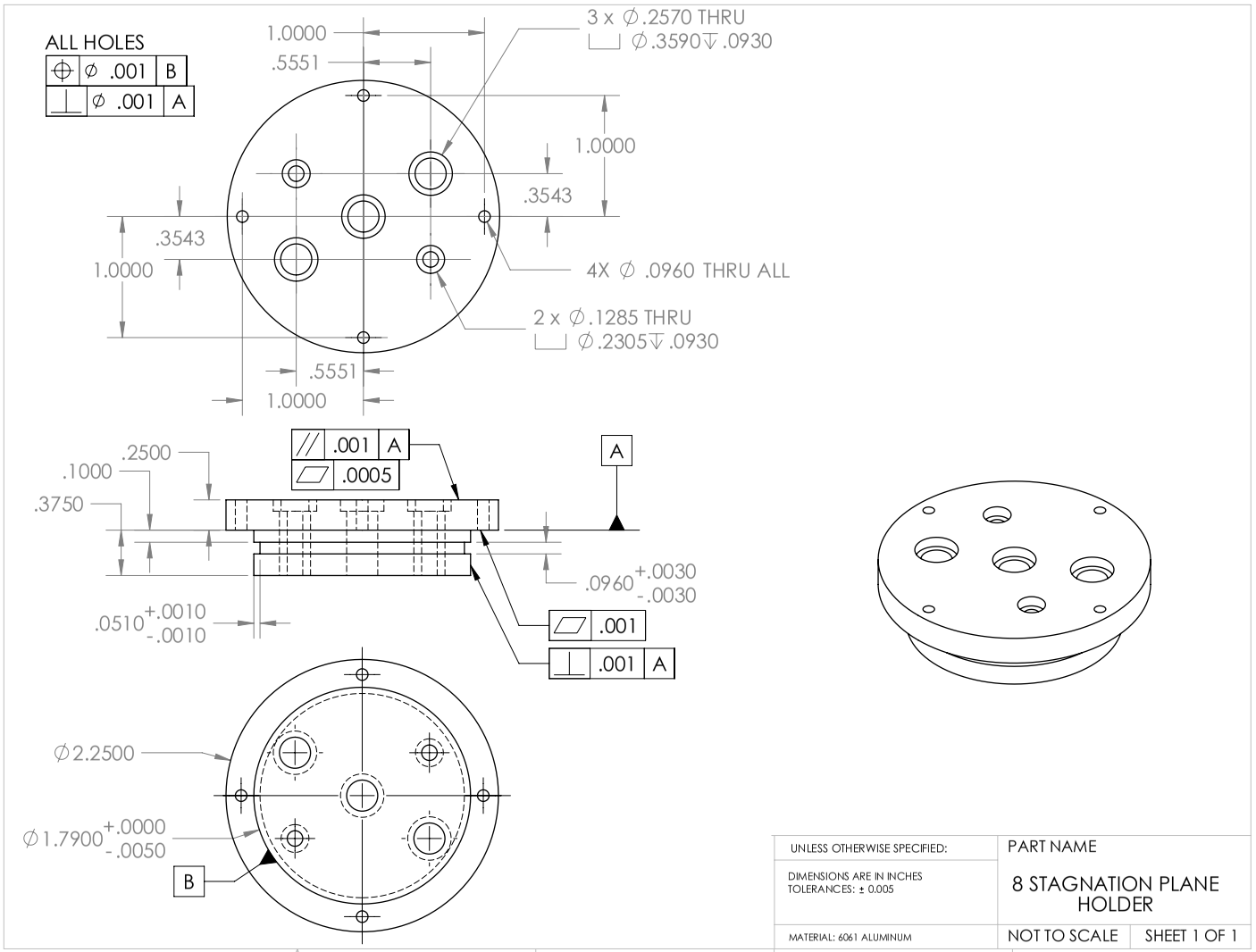
ALL HOLES
⌖ ∅ .001 B
⊥ ∅ .001 A
1.0000
.5551
3 x ∅.2570 THRU
⌴ ∅.3590↧.0930
1.0000
.3543
.3543
1.0000
4X ∅ .0960 THRU ALL
2 x ∅.1285 THRU
⌴ ∅.2305↧.0930
.5551
1.0000
// .001 A
▱ .0005
A
.2500
.1000
.3750
.0960 +.0030 -.0030
.0510 +.0010 -.0010
▱ .001
⊥ .001 A
∅2.2500
∅1.7900 +.0000 -.0050
B
UNLESS OTHERWISE SPECIFIED:
DIMENSIONS ARE IN INCHES
TOLERANCES: ± 0.005
MATERIAL: 6061 ALUMINUM
PART NAME
8 STAGNATION PLANE HOLDER
NOT TO SCALE
SHEET 1 OF 1
5
4
3
2
1

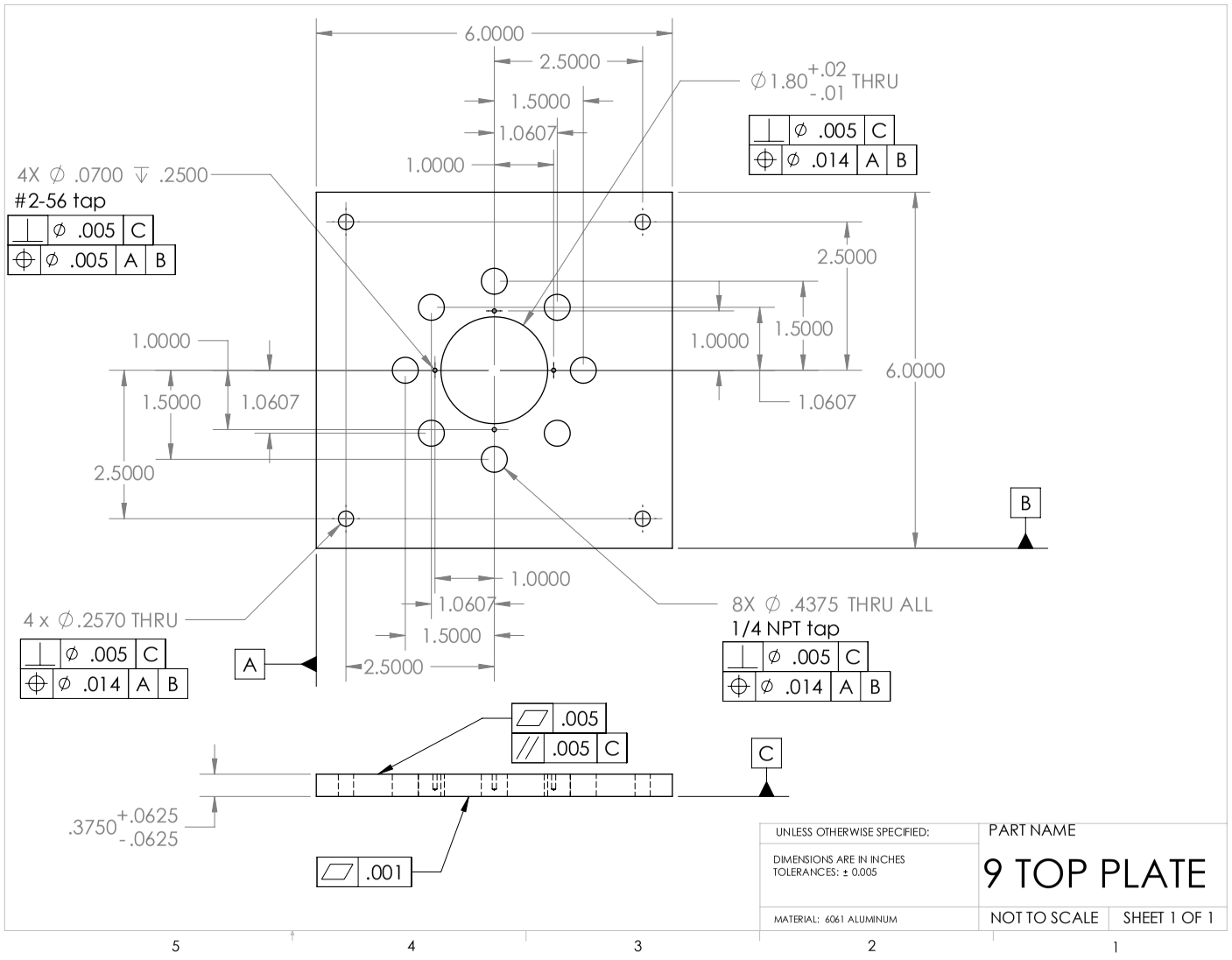
6.0000
2.5000
1.5000
1.0607
1.0000
Ø1.80 +.02 -.01 THRU
⊥ Ø .005 C
⌖ Ø .014 A B
4X Ø .0700 ↧ .2500
#2-56 tap
⊥ Ø .005 C
⌖ Ø .005 A B
2.5000
1.0000
1.5000
1.0000
1.5000
1.0607
6.0000
1.0607
2.5000
B
1.0000
1.0607
1.5000
2.5000
4 x Ø.2570 THRU
⊥ Ø .005 C
⌖ Ø .014 A B
A
8X Ø .4375 THRU ALL
1/4 NPT tap
⊥ Ø .005 C
⌖ Ø .014 A B
▱ .005
// .005 C
C
.3750 +.0625 -.0625
▱ .001
UNLESS OTHERWISE SPECIFIED:
DIMENSIONS ARE IN INCHES
TOLERANCES: ± 0.005
PART NAME
9 TOP PLATE
MATERIAL: 6061 ALUMINUM
NOT TO SCALE
SHEET 1 OF 1
5
4
3
2
1

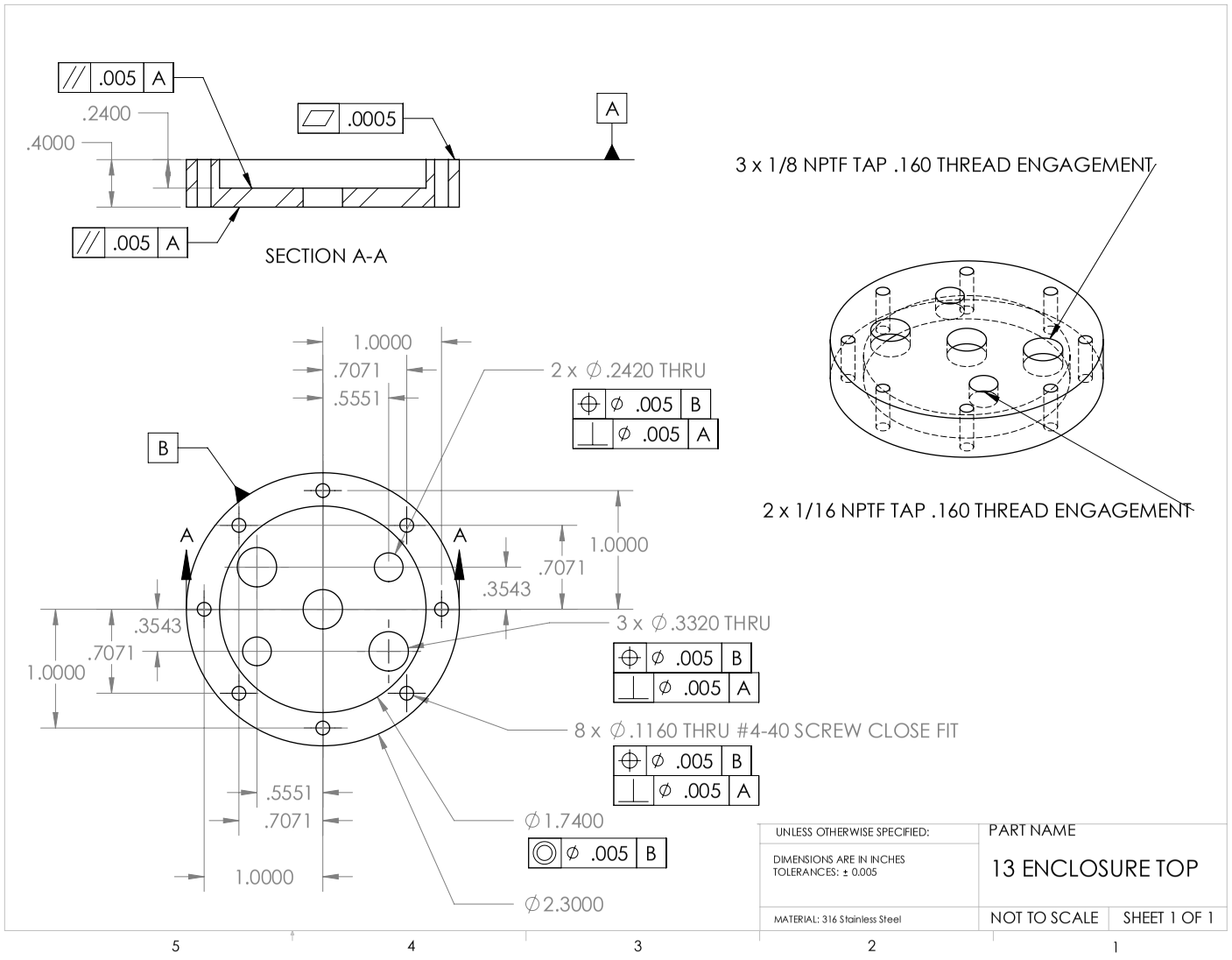
// .005 A
.2400
.4000
.0005
A
// .005 A
SECTION A-A
3 x 1/8 NPTF TAP .160 THREAD ENGAGEMENT
2 x 1/16 NPTF TAP .160 THREAD ENGAGEMENT
1.0000
.7071
.5551
2 x ∅.2420 THRU
⌖ ∅ .005 B
⊥ ∅ .005 A
B
A
A
1.0000
.7071
.3543
.3543
.7071
1.0000
3 x ∅.3320 THRU
⌖ ∅ .005 B
⊥ ∅ .005 A
8 x ∅.1160 THRU #4-40 SCREW CLOSE FIT
⌖ ∅ .005 B
⊥ ∅ .005 A
.5551
.7071
1.0000
∅1.7400
◎ ∅ .005 B
∅2.3000
UNLESS OTHERWISE SPECIFIED:
DIMENSIONS ARE IN INCHES
TOLERANCES: ± 0.005
PART NAME
13 ENCLOSURE TOP
MATERIAL: 316 Stainless Steel
NOT TO SCALE
SHEET 1 OF 1
5
4
3
2
1

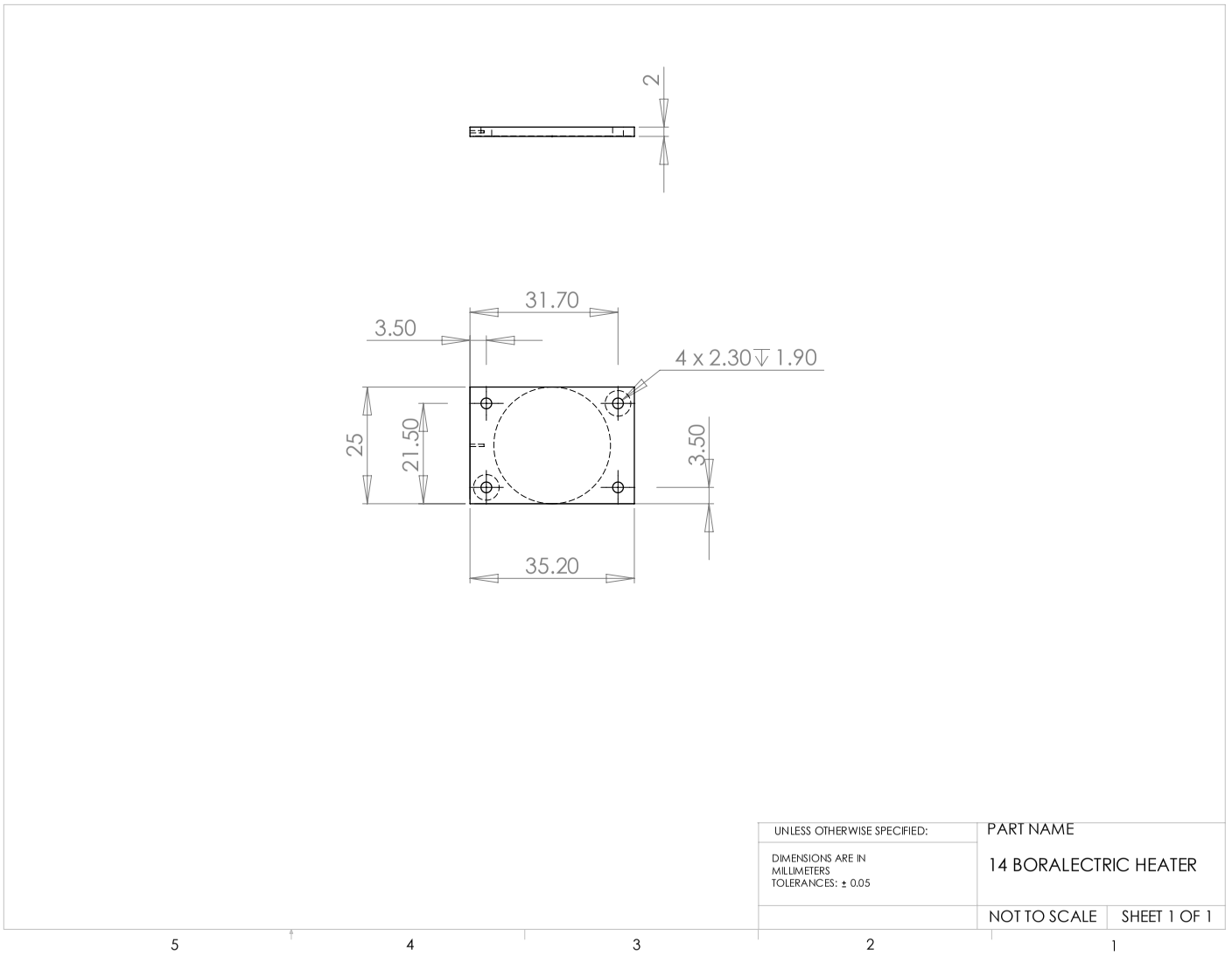

UNLESS OTHERWISE SPECIFIED:	PART NAME
DIMENSIONS ARE IN MILLIMETERS TOLERANCES: ± 0.05	14 BORALECTRIC HEATER
	NOT TO SCALE / SHEET 1 OF 1

5 4 3 2 1

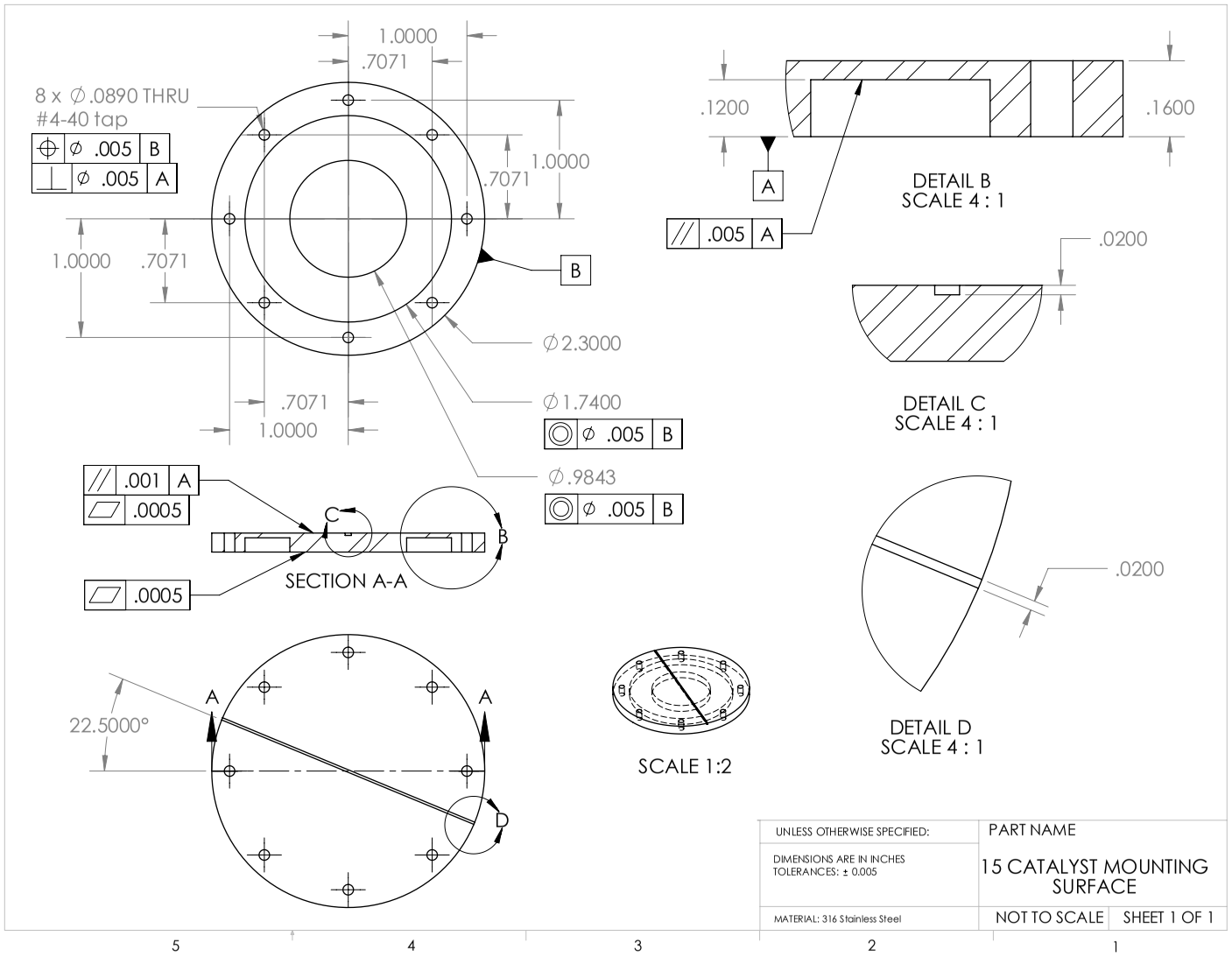
1.0000
.7071
8 x ∅.0890 THRU
#4-40 tap
⌖ ∅ .005 B
⊥ ∅ .005 A
1.0000
.7071
1.0000
.7071
B
∅2.3000
.7071
1.0000
∅1.7400
◎ ∅ .005 B
∅.9843
◎ ∅ .005 B
// .001 A
▱ .0005
C
B
SECTION A-A
▱ .0005
22.5000°
A
A
D
SCALE 1:2
.1200
.1600
A
// .005 A
DETAIL B
SCALE 4 : 1
.0200
DETAIL C
SCALE 4 : 1
.0200
DETAIL D
SCALE 4 : 1
UNLESS OTHERWISE SPECIFIED:
DIMENSIONS ARE IN INCHES
TOLERANCES: ± 0.005
MATERIAL: 316 Stainless Steel
PART NAME
15 CATALYST MOUNTING SURFACE
NOT TO SCALE
SHEET 1 OF 1
5
4
3
2
1

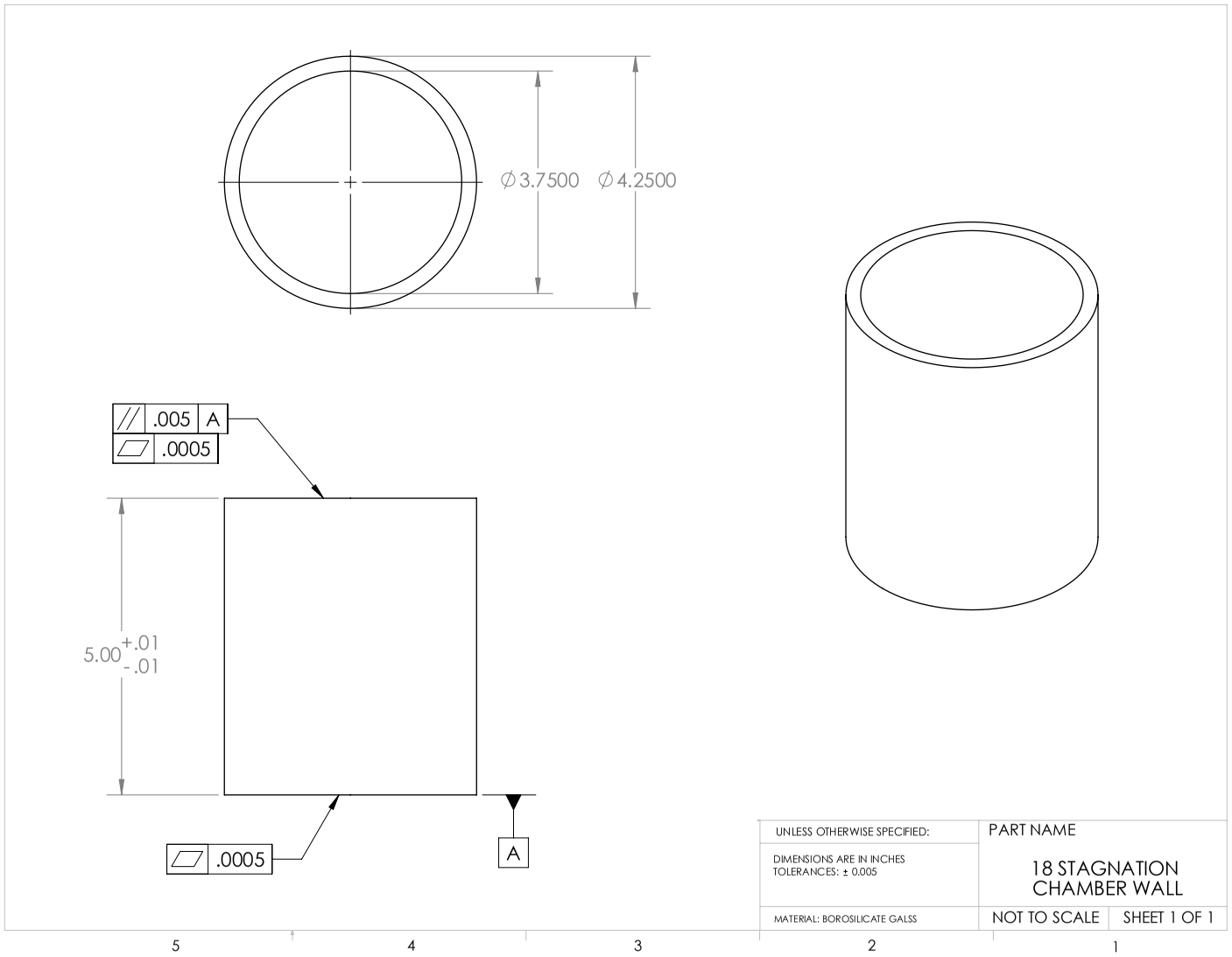
∅3.7500
∅4.2500
.005 A
.0005
5.00 +.01 -.01
.0005
A
UNLESS OTHERWISE SPECIFIED:
DIMENSIONS ARE IN INCHES
TOLERANCES: ± 0.005
MATERIAL: BOROSILICATE GALSS
PART NAME
18 STAGNATION CHAMBER WALL
NOT TO SCALE
SHEET 1 OF 1
5
4
3
2
1

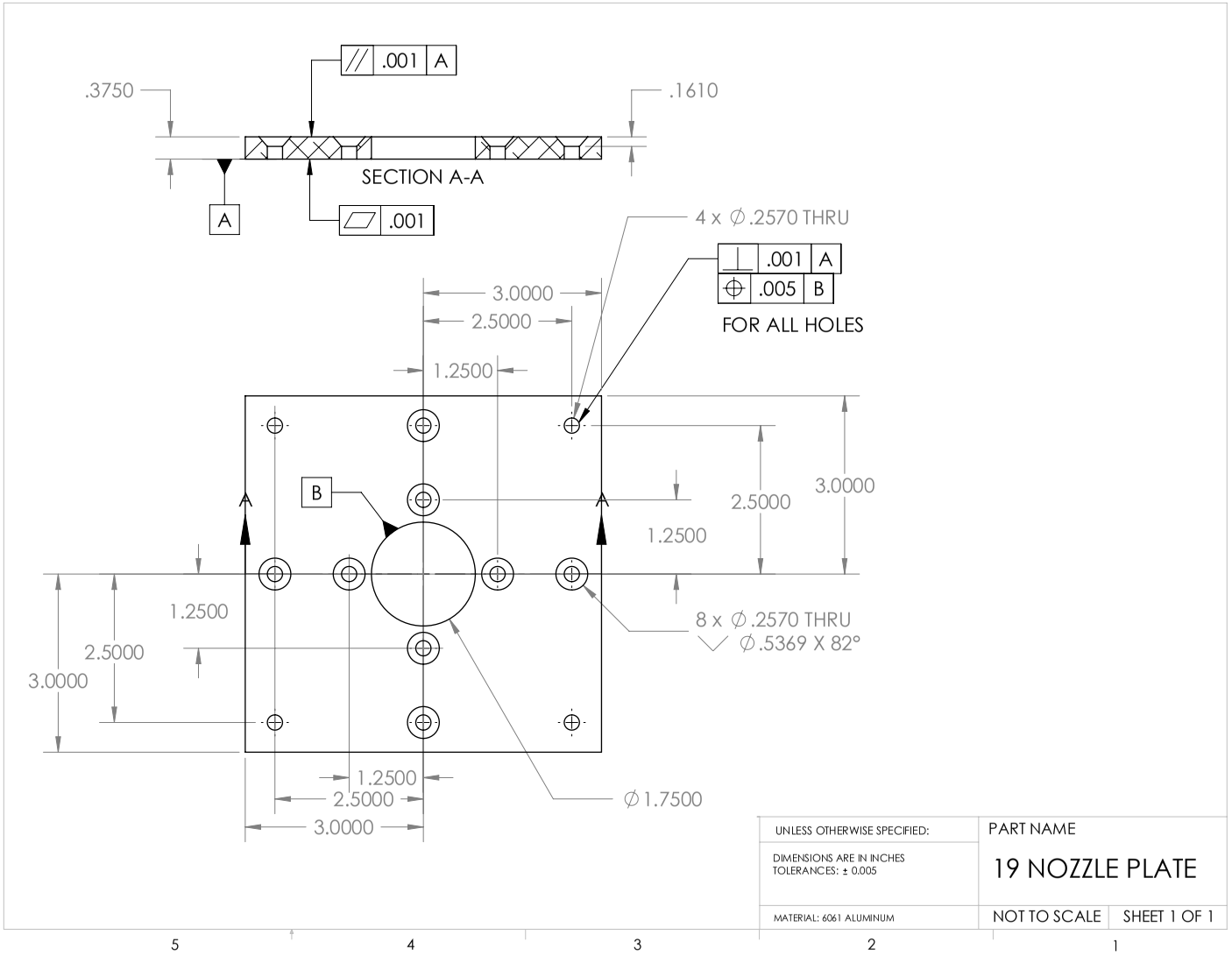
.001 A
.3750
.1610
SECTION A-A
A
.001
4 x ∅.2570 THRU
.001 A
.005 B
FOR ALL HOLES
3.0000
2.5000
1.2500
B
A
A
2.5000
3.0000
1.2500
1.2500
2.5000
3.0000
8 x ∅.2570 THRU
∅.5369 X 82°
1.2500
2.5000
3.0000
∅1.7500
UNLESS OTHERWISE SPECIFIED:
DIMENSIONS ARE IN INCHES
TOLERANCES: ± 0.005
MATERIAL: 6061 ALUMINUM
PART NAME
19 NOZZLE PLATE
NOT TO SCALE
SHEET 1 OF 1
5
4
3
2
1

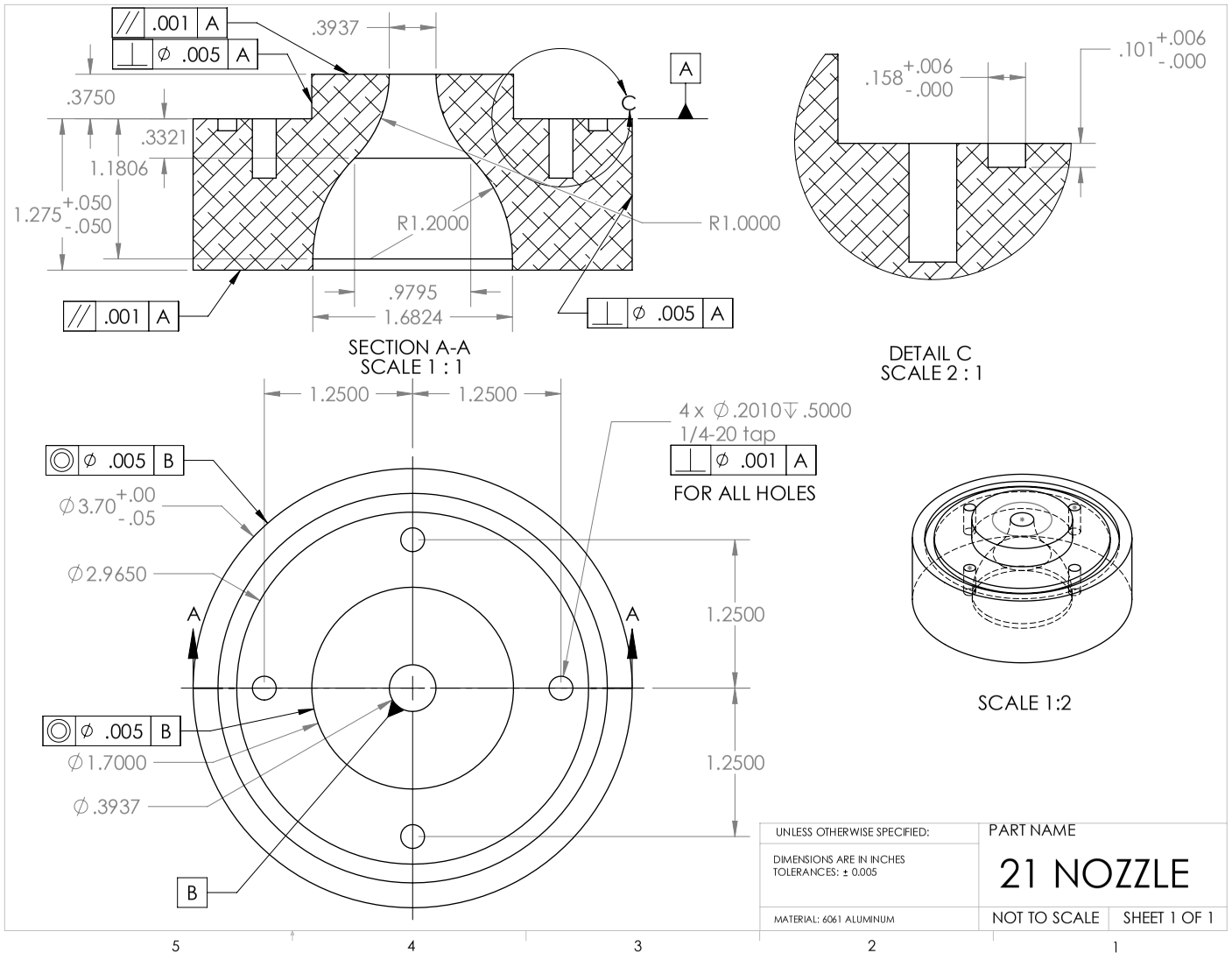
// .001 A
⌖ .005 A
.3937
A
.3750
.3321
1.1806
1.275 +.050 -.050
R1.2000
R1.0000
.9795
1.6824
// .001 A
⌖ .005 A
SECTION A-A
SCALE 1 : 1
.158 +.006 -.000
.101 +.006 -.000
DETAIL C
SCALE 2 : 1
1.2500
1.2500
4 x ∅.2010↧.5000
1/4-20 tap
⌖ .001 A
FOR ALL HOLES
◎ .005 B
∅3.70 +.00 -.05
∅2.9650
A
A
1.2500
1.2500
◎ .005 B
∅1.7000
∅.3937
B
SCALE 1:2
UNLESS OTHERWISE SPECIFIED:
DIMENSIONS ARE IN INCHES
TOLERANCES: ± 0.005
MATERIAL: 6061 ALUMINUM
PART NAME
21 NOZZLE
NOT TO SCALE
SHEET 1 OF 1
5
4
3
2
1

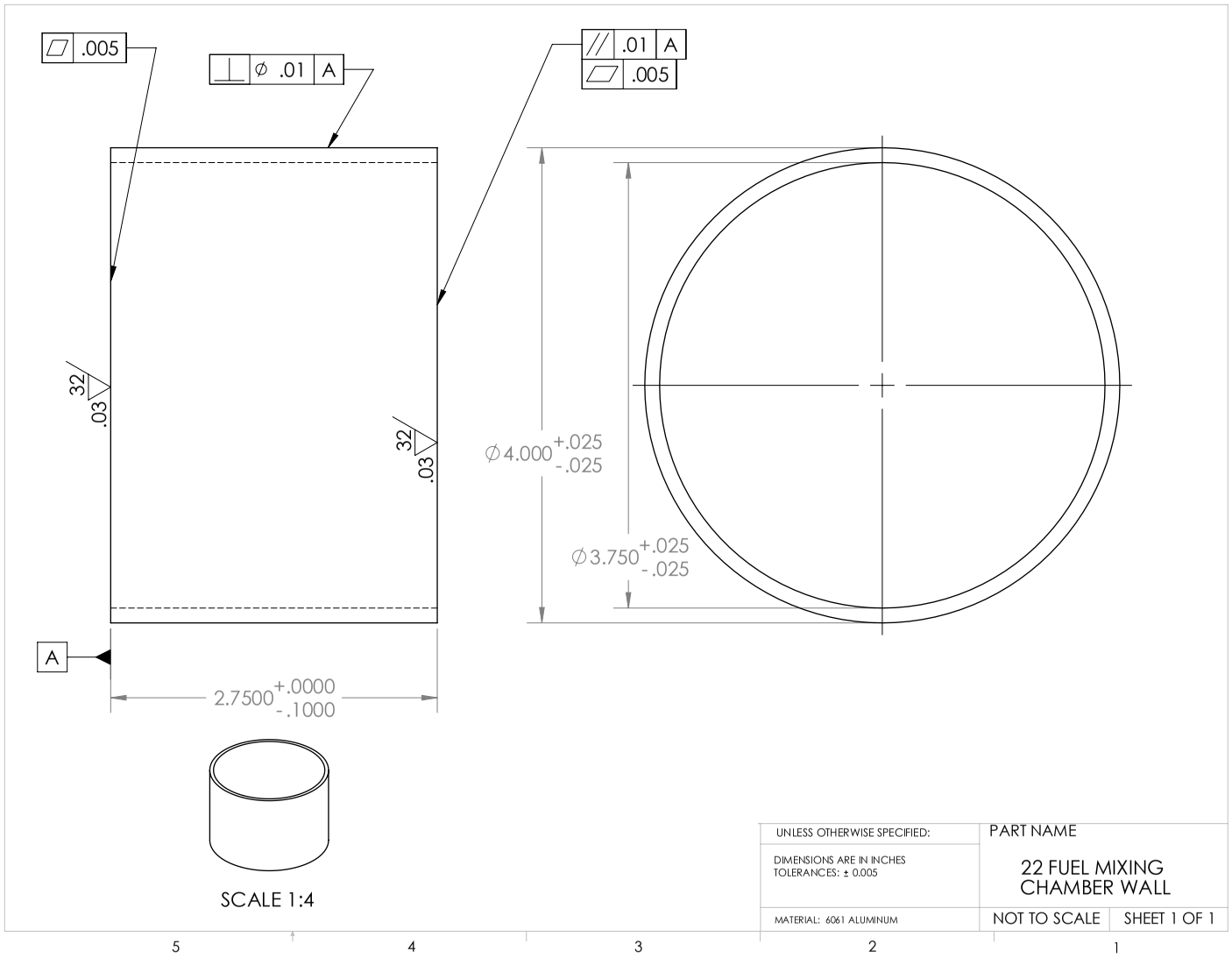
.005
⌀ .01 A
// .01 A
.005
32
.03
32
.03
⌀4.000 +.025 -.025
⌀3.750 +.025 -.025
A
2.7500 +.0000 -.1000
SCALE 1:4
UNLESS OTHERWISE SPECIFIED:
DIMENSIONS ARE IN INCHES
TOLERANCES: ± 0.005
MATERIAL: 6061 ALUMINUM
PART NAME
22 FUEL MIXING CHAMBER WALL
NOT TO SCALE
SHEET 1 OF 1
5
4
3
2
1

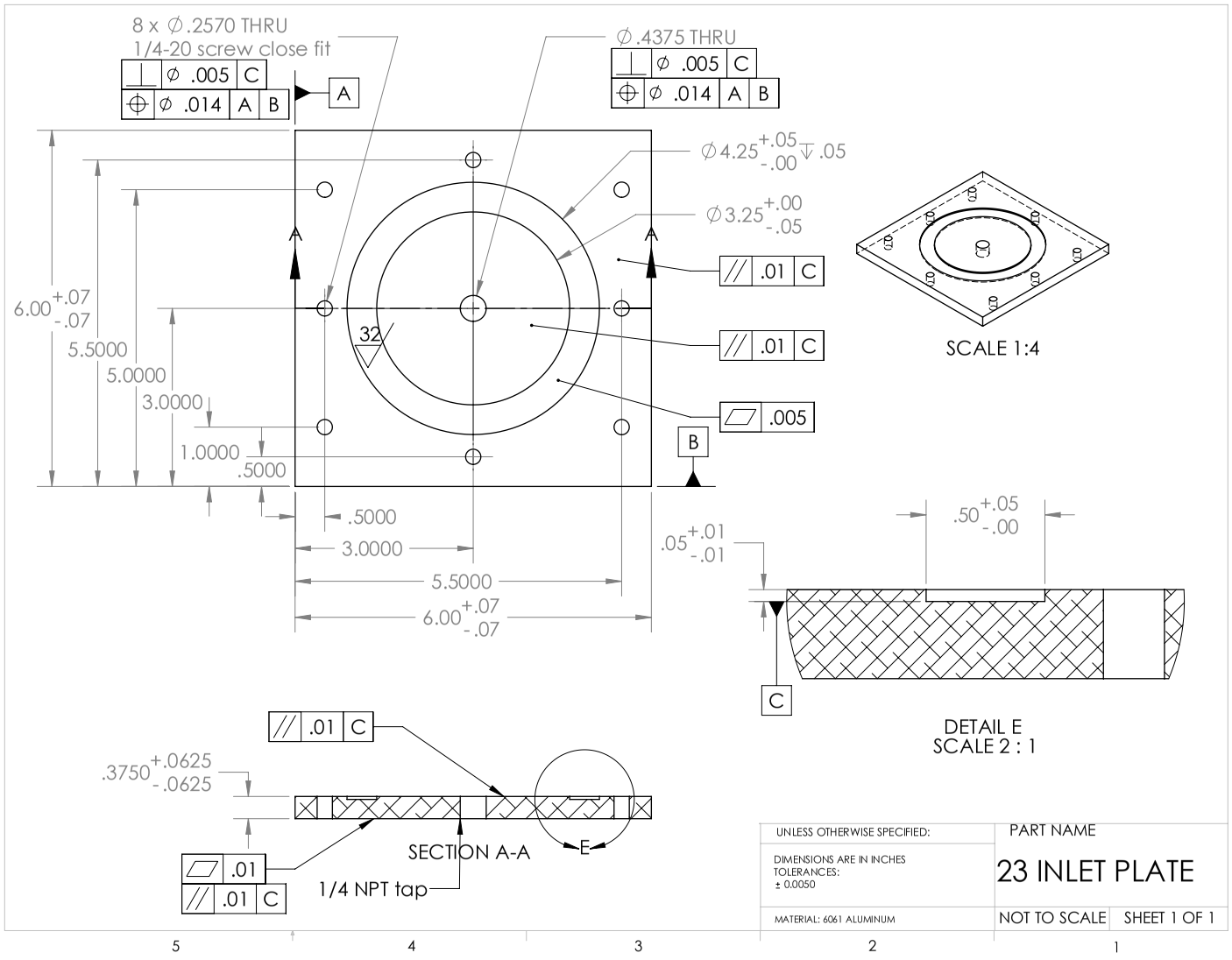
8 x ∅.2570 THRU
1/4-20 screw close fit
⊥ ∅ .005 C
⊕ ∅ .014 A B
A
∅.4375 THRU
⊥ ∅ .005 C
⊕ ∅ .014 A B
∅4.25 +.05 -.00 ↧ .05
∅3.25 +.00 -.05
// .01 C
// .01 C
.005
B
32
6.00 +.07 -.07
5.5000
5.0000
3.0000
1.0000
.5000
.5000
3.0000
5.5000
6.00 +.07 -.07
SCALE 1:4
.50 +.05 -.00
.05 +.01 -.01
C
DETAIL E
SCALE 2 : 1
// .01 C
.3750 +.0625 -.0625
SECTION A-A
E
⏥ .01
// .01 C
1/4 NPT tap
UNLESS OTHERWISE SPECIFIED:
DIMENSIONS ARE IN INCHES
TOLERANCES:
± 0.0050
MATERIAL: 6061 ALUMINUM
PART NAME
23 INLET PLATE
NOT TO SCALE
SHEET 1 OF 1
5
4
3
2
1

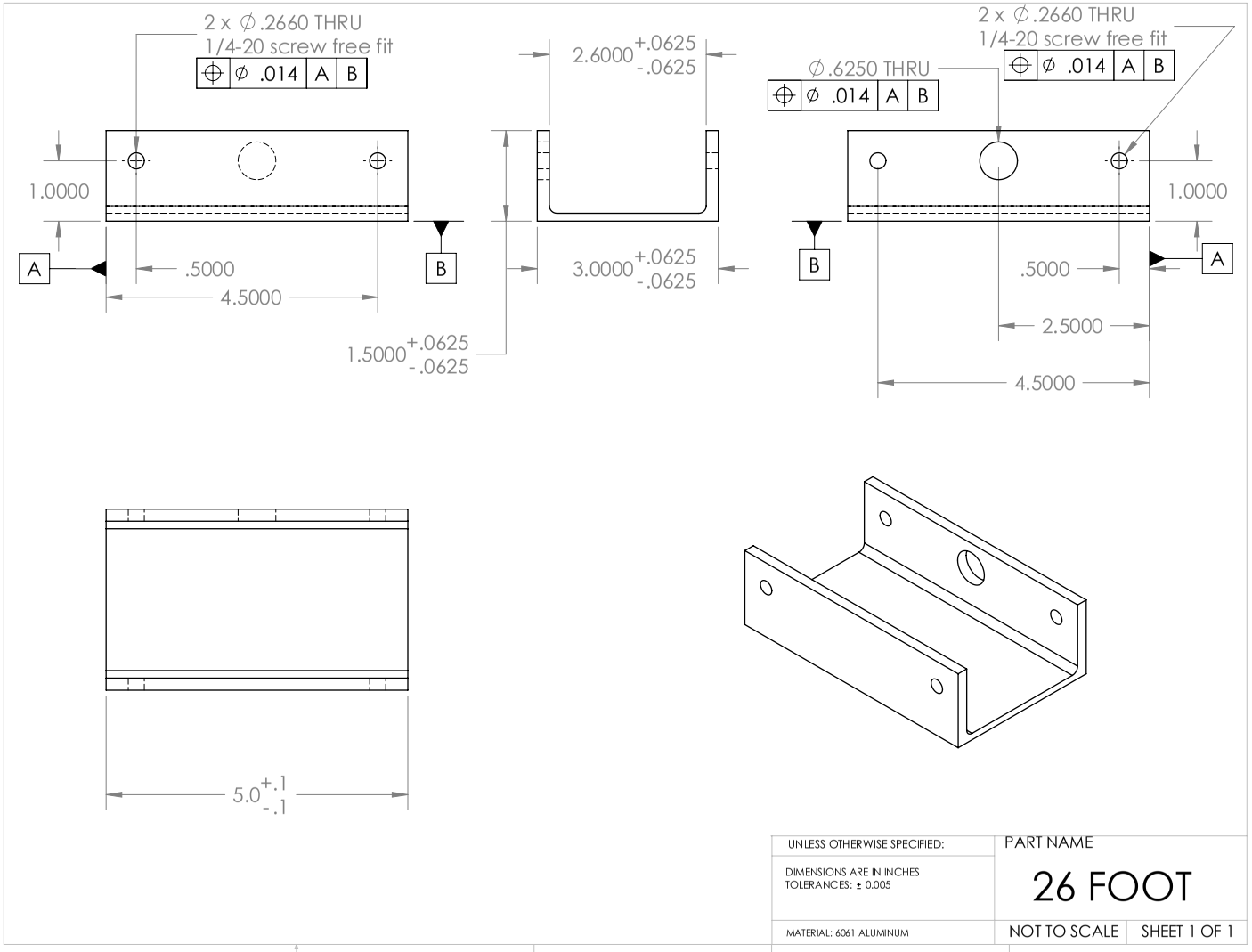
2 x ∅.2660 THRU
1/4-20 screw free fit
⌖ ∅ .014 A B
1.0000
A
.5000
4.5000
B
2.6000 +.0625 -.0625
3.0000 +.0625 -.0625
1.5000 +.0625 -.0625
∅.6250 THRU
⌖ ∅ .014 A B
2 x ∅.2660 THRU
1/4-20 screw free fit
⌖ ∅ .014 A B
1.0000
B
A
.5000
2.5000
4.5000
5.0 +.1 -.1
UNLESS OTHERWISE SPECIFIED:
DIMENSIONS ARE IN INCHES
TOLERANCES: ± 0.005
MATERIAL: 6061 ALUMINUM
PART NAME
26 FOOT
NOT TO SCALE
SHEET 1 OF 1
5
4
3
2
1

Appendix E

Defense presentation

Catalysis of Propane Oxidation and Premixed Propane-Air Flames

James T. Wiswall

Doctoral Committee:
Professor Hong G. Im Co-Chair
Professor Margaret S. Wooldrige Co-Chair
Professor Arvind Atreya
Professor Matthias Ihme

24 August 2009

Outline:

combustion LABORATORY

Introduction: objective and hypothesis

Objective: Broaden our fundamental understanding of heterogeneous catalysis to address the challenges associated with combustion

- Pollutant formation: NO_x, SO_x, CO, VOCs, PM
- High CO_2 emissions
- Low thermodynamic efficiencies

Hypothesis: Catalysis can extend the useful operating conditions for hydrocarbon oxidation and combustion, improve device efficiencies, and reduce pollutant emissions.

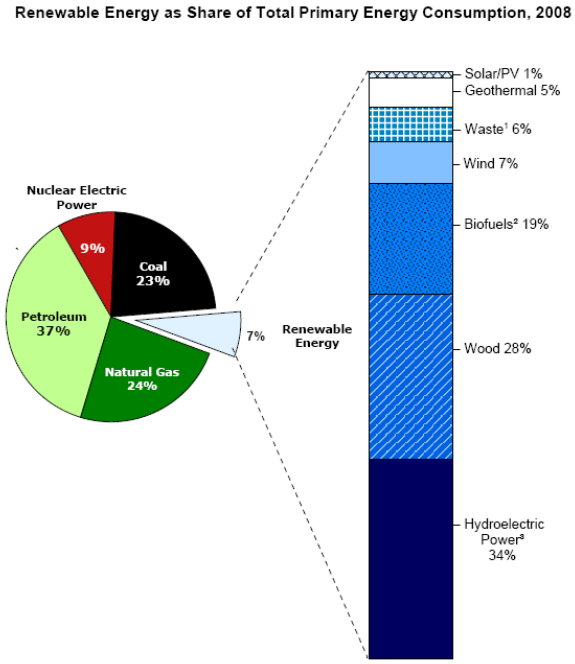

Energy Information Administration / Annual Energy Review 2008

combustion LABORATORY

Scientific background and experimental approach

combustion LABORATORY

Scientific background: catalytic reaction theory

Decomposition

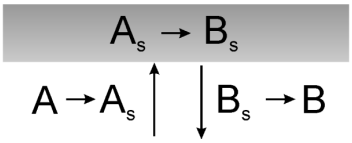

Langmuir-Hinshelwood mechanism

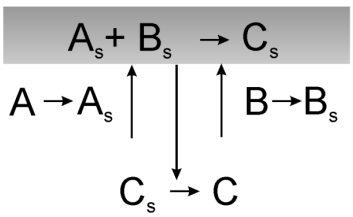

Eley-Rideal mechanism

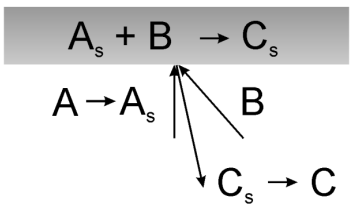

Scientific background: catalytic reaction theory

The reaction rate can be limited by the surface kinetics and/or by reactant transport to the catalyst

Example: Surface kinetics, decomposition mechanism

1. $A + S \rightarrow A_s$
2. $A_s \rightarrow B_s$
3. $B_s \rightarrow B + S$

Global: $A \rightarrow B$

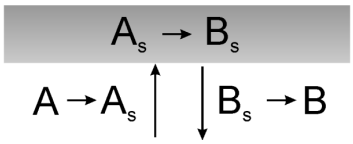

Surface-kinetics limited if 1, 2, and/or 3 are slow

- Highly dependent on catalyst temperature and microscopic surface area

Transport limited if 1, 2, and 3 are fast, causing a local depletion of A

- Highly dependent on fluid transport characteristics and geometric surface area

Experimental approach: stagnation-flow reactor

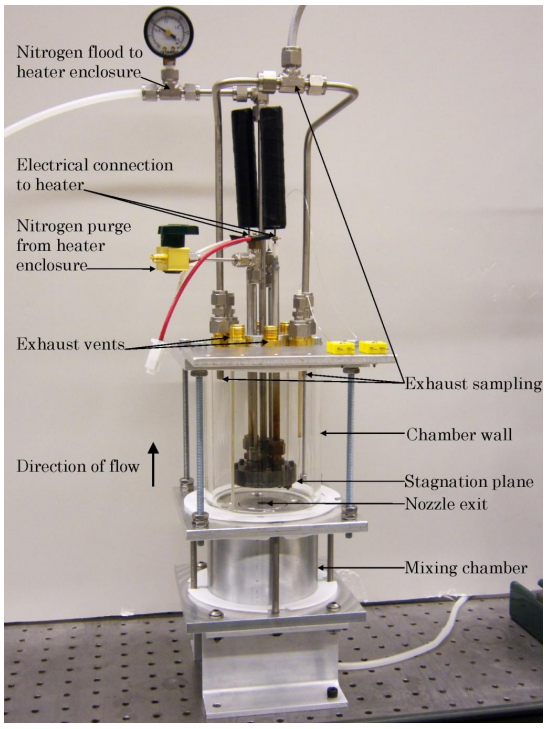

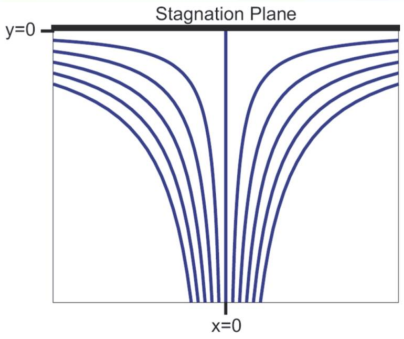

- One-dimensional species concentration, temperature, and velocity profiles
- Independent control of characteristic time scales for heterogeneous reaction and flow
- Capable to study both flame-catalyst interaction and reactant-catalyst interaction with a temperature controlled catalyst

Experimental approach: reactant flow

Image: v_{ave}= 1.3 m/s, ϕ = 0.82

The visible emission from the laminar flame demonstrates the uniformity of the velocity profile that develops from the nozzle exit

ϕ and v_{ave} calculated from volumetric flow rates

$$\phi_{C_3H_8} = \left(\frac{\dot{Q}_{C_3H_8}}{\dot{Q}_{air}}\right) \times \left(\frac{n_{air}}{n_{C_3H_8}}\right)_{stoich}$$

$$v_{ave} = \frac{\dot{Q}_{C_3H_8} + \dot{Q}_{air}}{A_n}$$

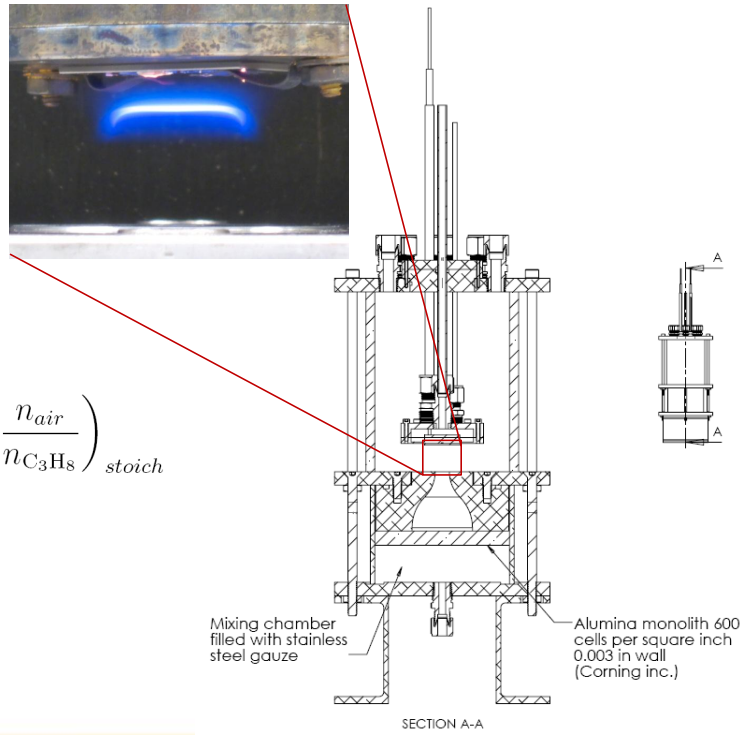

Experimental approach: catalyst manufacture and mounting

Catalyst form is 25.4 mm x 25.4 mm x less than 2 mm thick.
Catalyst is mounted to heater using clips

- Quartz substrate 25.4 mm x 25.4 mm x 1 mm thick

Pt: PVD coated quartz substrate,10 nm Ti bonding layer, 100 nm Pt as catalyst. 99.99% purity for both Ti and Pt

Pd: foil 25.4 mm x 25.4 mm x 0.025 mm thick, 99.9% purity

90%SnO_2-10%Pt: powders mixed by mass (99.9% purity). A paste of the mixed powders and methanol is dried on a quartz wafer

SnO_2: drop evaporation on quartz substrate using a 15% SnO_2 colloidal dispersion in water

combustion LABORATORY

Catalysis of propane oxidation: Pt results

combustion LABORATORY

Catalysis of propane oxidation: Pt results

Procedure:

- Incrementally increase T_s for a particular ϕ and v_{ave}
- 3 fuel air mixtures: ϕ=1.5, 1.0, and 0.67
- v_{ave} = 1.2 m/s
- Record CO_2, CO, C_3H_8, O_2, and P
- Catalysts: Pt, Pd, SnO_2, 90%SnO_2-10%Pt, and quartz

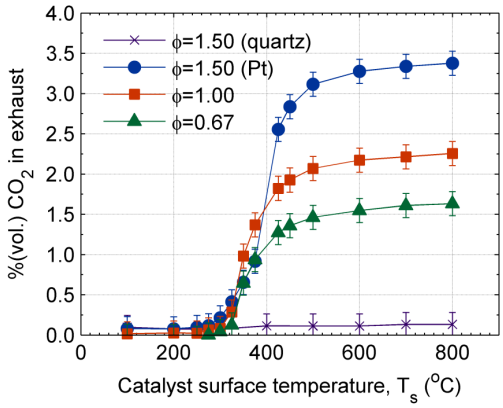

Catalysis of propane oxidation: Pt results

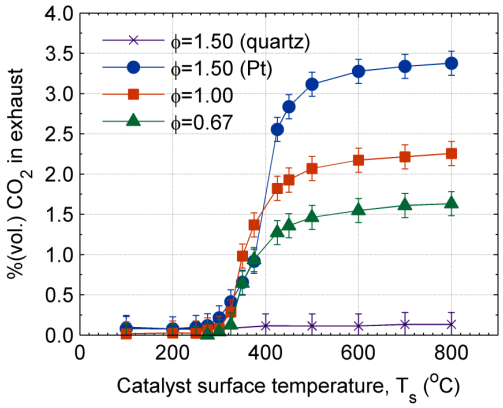

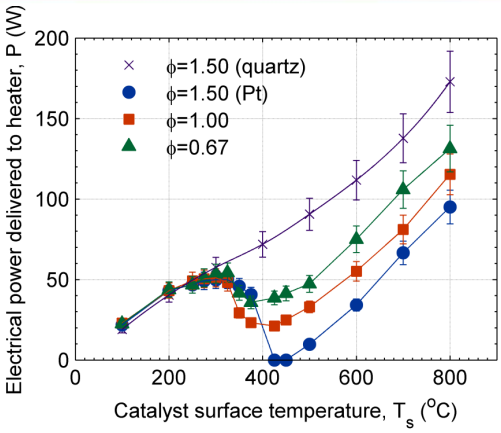

- A lower heater power corresponds to a larger CO_2 volume fraction in the exhaust
- CO_2 exhaust fraction abruptly increases and stabilizes at high temperature
- Largest CO_2 exhaust fraction occurs for the fuel-rich case
- Fuel mass consumed is largest in the fuel-rich case

Catalysis of propane oxidation: Pt results

Quartz exhibits non-reactive behavior

The support structure of the experiment is non-reactive

The reactivity is due to the presence of the catalyst materials.

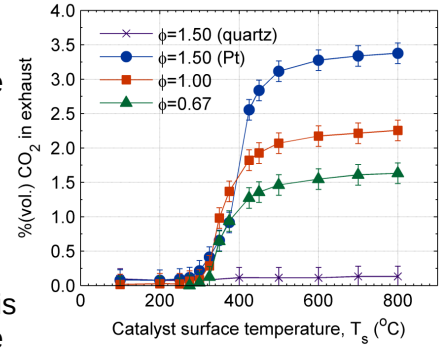

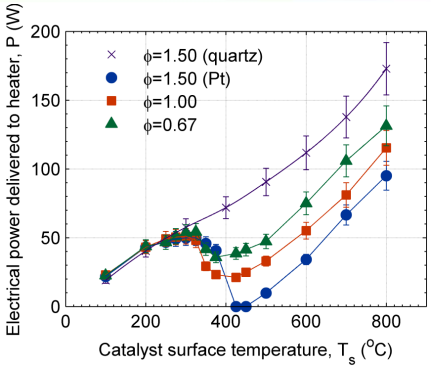

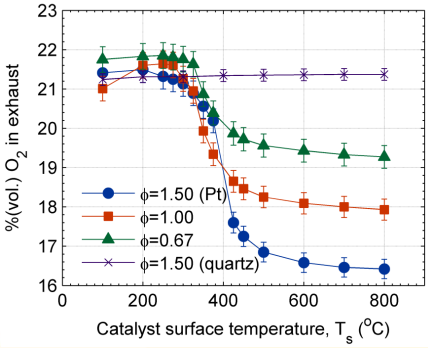

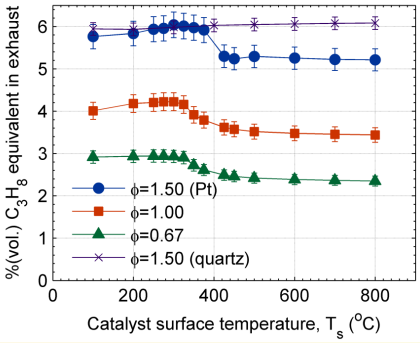

Catalysis of propane oxidation: Pt results

4 critical temperatures: $T_{P\ max}$, $T_{P\ min}$, T_{sa}, and $T_{i\ CO2}$

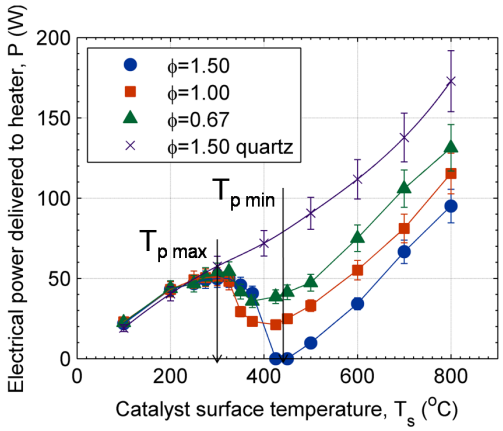

Temperature where local maximum in power occurs, $T_{P\ max}$

Temperature where local minimum in power occurs, $T_{P\ min}$

Catalysis of propane oxidation: Pt results

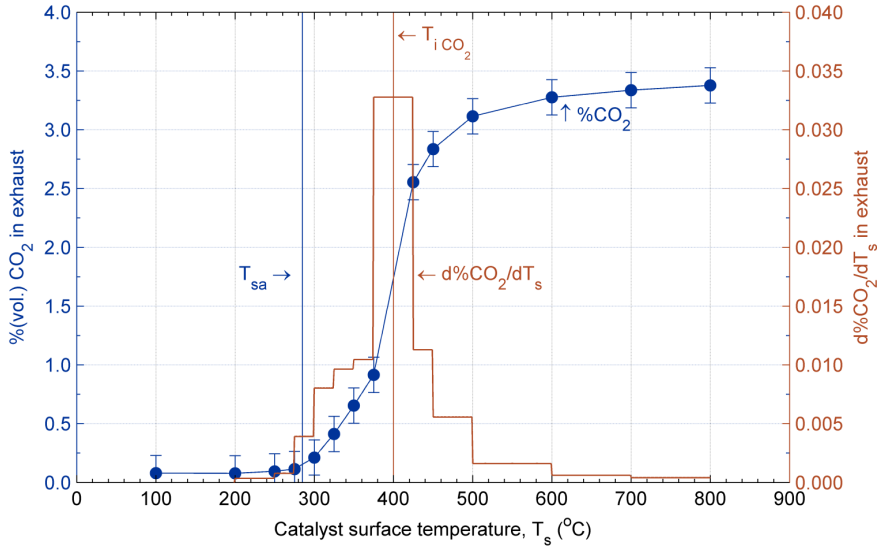

Temperature where CO_2 is first detectable (catalyst activation temperature, T_{sa})

Temperature where local maximum in the derivative of CO_2 with respect to catalyst temperature occurs, $T_{i\ CO2}$

Catalysis of propane oxidation: Pt results

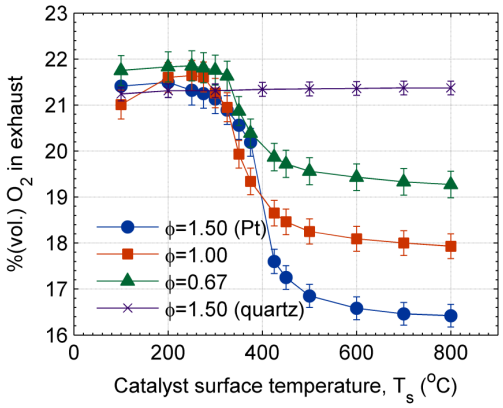

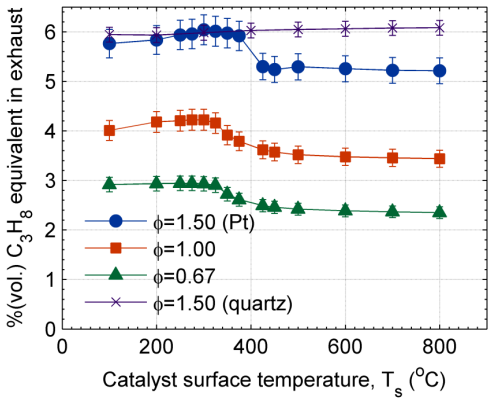

The CO_2-inflection temperature shows the transition point from surface-kinetics to diffusion limited reaction

- Rapid decrease in C_3H_8 and O_2 volume fraction corresponding to decrease in P and increase in CO_2
- CO_2 stabilizes for high temperature
- The C_3H_8 and O_2 volume fraction stabilize at non-zero values (Pt results shown in the figures)

Catalysis of propane oxidation: Pt results

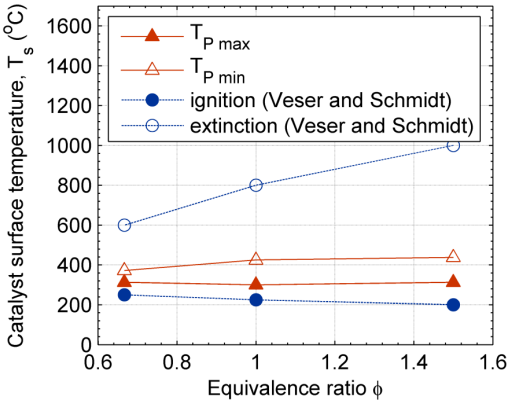

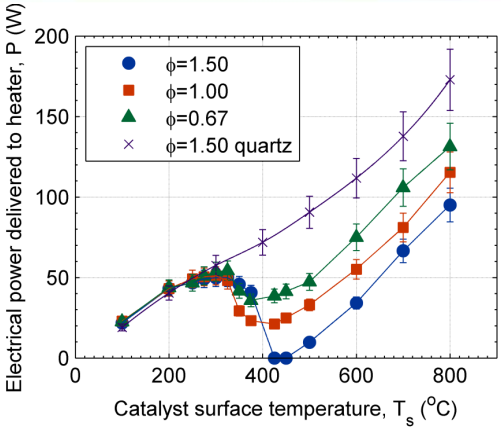

The results can be compared to a study by Veser and Schmidt using a stagnation-flow reactor

- $T_{P\ max}$ corresponds to the catalytic ignition temperature
- $T_{P\ min}$ corresponds to the catalytic extinction temperature

G. Veser and L. D. Schmidt. Ignition and extinction in the catalytic oxidation of hydrocarbons over platinum. *AIChE Journal*, 42:1077–1087, 1996.

Catalysis of propane oxidation: Pt results

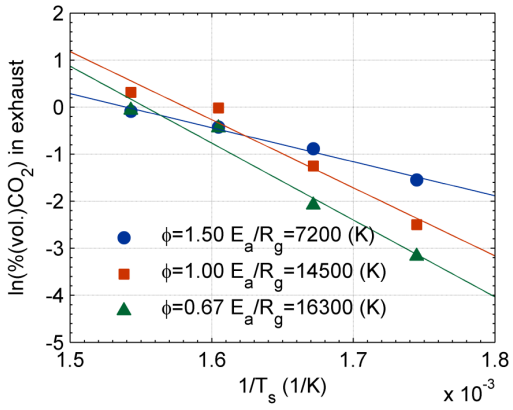

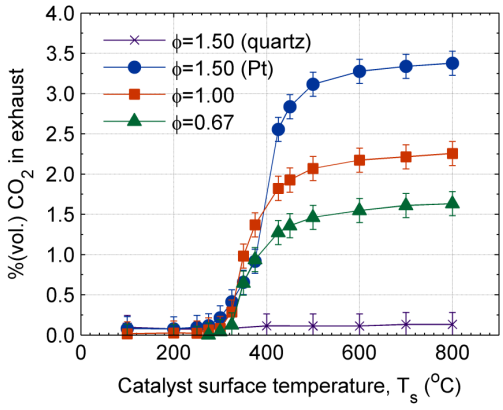

The CO_2 volume fraction follows Arrhenius behavior in the surface kinetics limited regime

$$\chi CO_2 = A_0 e^{-\frac{E_a}{R_g T_s}}$$

The Pt has a decreasing activation energy for increasing ϕ

Catalysis of propane oxidation: Pt results

CO is first produced at temperatures where CO_2 production is diffusion limited

- CO production follows separate reaction pathways from CO_2
- Minimum temperature where CO is detectable, T_{CO}

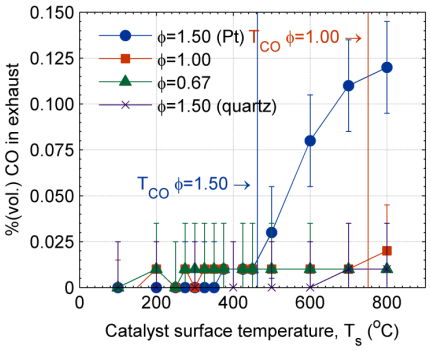

CO not produced for fuel lean case

CO not produced using quartz

- CO is catalytically produced; CO is not produced due to heated reactant stream decomposition

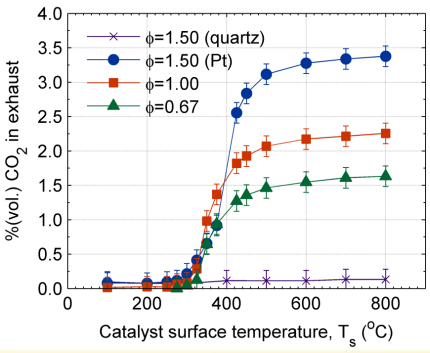

combustion LABORATORY

Catalysis of propane oxidation: comparison of catalyst performance

combustion LABORATORY

Catalysis of propane oxidation: material comparison

- Pd and 90%SnO_2-10%Pt show similar behavior to Pt
- SnO_2 shows minimal CO_2 production
- 90%SnO_2-10%Pt shows activity at a lower temperature than Pt
- Pd and Pt show higher diffusion limited CO_2 production than 90%SnO_2-10%Pt
- Pd and Pt stabilize at the same CO_2 fraction in the exhaust
- For Pt, Pd, and 90%SnO_2-10%Pt the temperature can be maintained without input heat at $T_{P\ min}$

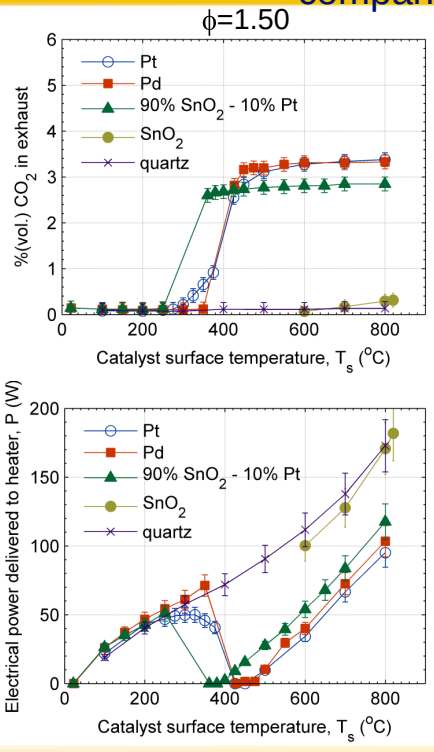

combustion LABORATORY

Catalysis of propane oxidation: material comparison

- Diffusion limited CO_2 fraction increases for increasing ϕ
- Local minimum power decreases for increasing ϕ
- Pd and 90%SnO_2-10%Pt show decreasing temperature for initial catalytic activity for increasing ϕ
- SnO_2 shows minimal catalytic activity

ϕ=1.50

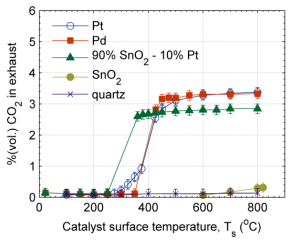

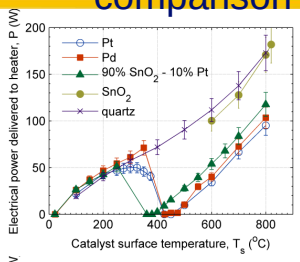

ϕ=1.00

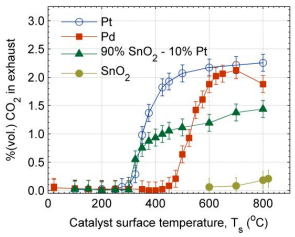

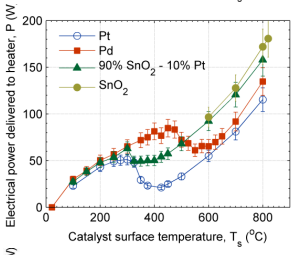

ϕ=0.67

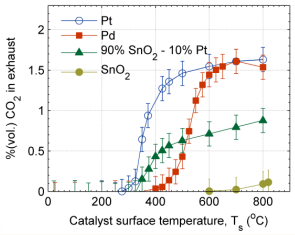

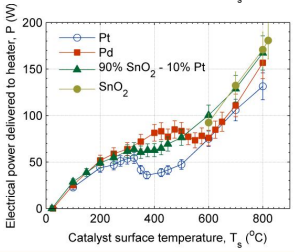

combustion LABORATORY

Catalysis of propane oxidation: material comparison

- Pd and 90%SnO_2-10%Pt show decreasing critical temperatures for increasing ϕ
- Pt shows relatively constant critical temperatures for increasing ϕ
- 90%SnO_2-10%Pt shows activity at the lowest temperature of the experiments (ϕ=1.50)

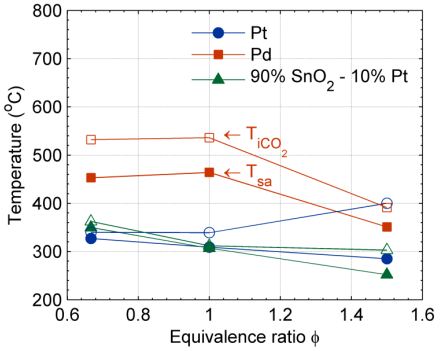

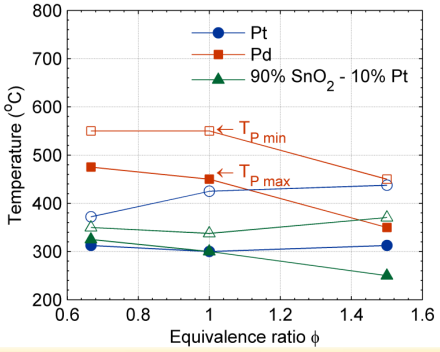

Catalysis of propane oxidation: material comparison

Compare the results for the 3 fuel-air mixtures using the fraction of carbon converted to CO_2

$$\chi_c CO_2 = \frac{\chi CO_2}{\chi CO_2 + 3\chi C_3H_8 + \chi CO}$$

Assuming the same number of moles in the products as in the reactants, the fraction of carbon converted to CO_2 equals the fraction of the carbon in the fuel oxidized to CO_2

The diffusion limited fraction of carbon converted to CO_2 is constant for Pt and Pd over the range of ϕ studied.

The 90%SnO_2-10%Pt catalyst has an increasing fraction of carbon converted to CO_2 for increasing ϕ.

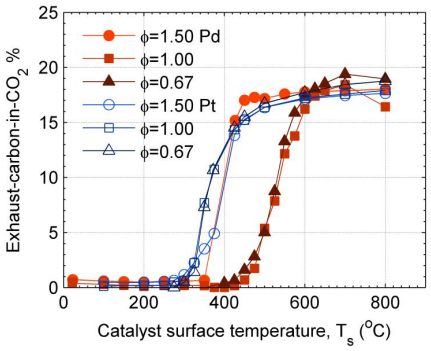

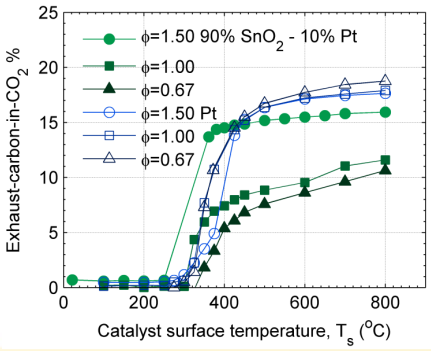

Catalysis of propane oxidation: material comparison

Pd produces the most CO and at the lowest temperature of the materials tested

90%SnO_2-10%Pt produces detectable levels of CO, but at much lower levels than Pt and Pd, and without a large increase

CO is undetectable for SnO_2 and quartz

ϕ=1.50

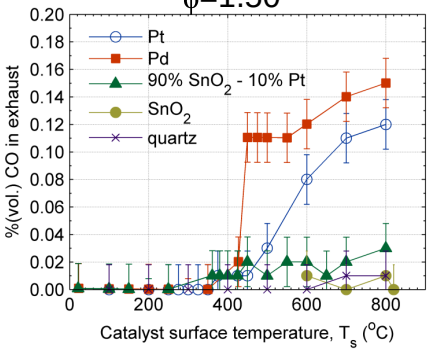

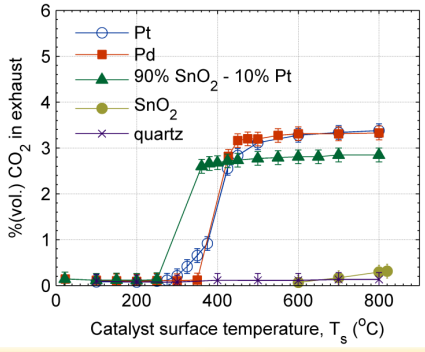

combustion LABORATORY

Catalytic influence on premixed propane-air flames: results

combustion LABORATORY

Catalysis of premixed propane-air flames: flame structure

Five different flame structures are observed

1. Cool core envelope (a)
2. Cone (b)
3. Envelope (c)
4. Disk (e)
5. Ring (f)

The flame structures spontaneously change as ϕ increases or decreases

Study catalytic influence on lean-extinction limits

Zhang and Bray observed similar structures

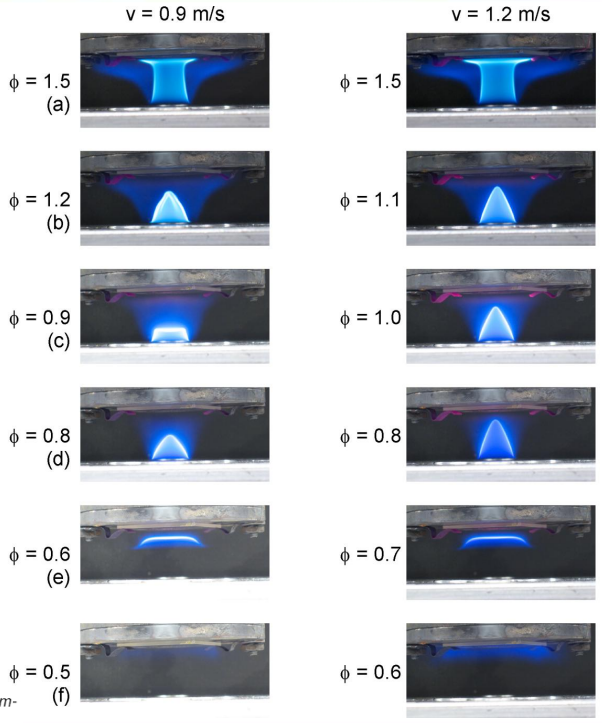

Y. Zhang and K.N.C. Bray. Characterization of impinging jet flames. *Combustion and Flame*, 116(4):671 – 674, 1999.

Catalysis of premixed propane-air flames: lean-extinction limit

Previous research suggests there can be a catalytic influence on the lean extinction limit of premixed flames

Li and Im: numerically investigated the lean-extinction limit of premixed methane-oxygen-nitrogen disk flames in a stagnation flow.

- The lean-extinction limit can be catalytically extended provided the characteristic time scales of the surface reactions are faster than the gas-phase reactions
- Surface reactions increase their relative strength for high surface temperature, reactant dilution, highly catalytically active reactants

Previous experimental results indicate the lean-extinction limit of methane-air flames are insensitive to the surface material

Investigate the catalytic influence on the lean-extinction limit of propane air flames due to the increased catalytic activity of propane.

J. Li and H. G. Im. Extinction characteristics of catalyst-assisted combustion in a stagnation-point flow reactor. *Combustion and Flame*, 145(1):390–400, 04 2006.

Catalysis of premixed propane-air flames: flame images

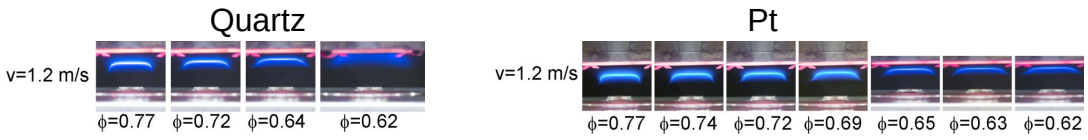

Procedure

Ignite reactant flow at lean ϕ within disk flame structure regime

Incrementally reduce ϕ while keeping v_{ave} constant until flame extinction occurs

Record a flame image and the power to the heater for each increment in ϕ.

- Image determines the flame structure and the distance between the disk flame and the stagnation plane, x_{sep}

Control stagnation-plane temperature 900 ^{o}C

v_{ave} range: 0.6 m/s – 1.6 m/s in 0.1 cm/s increments

Catalysis of premixed propane-air flames

The disk flame is insensitive to the stagnation plane material

- Lean extinction limit is insensitive to Pt
- Heater power is insensitive to Pt
- Flame location is insensitive to Pt

Pt inhibited the ring flame structure

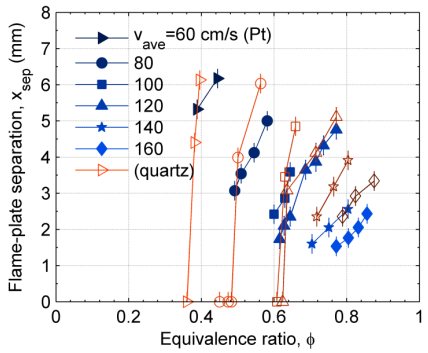

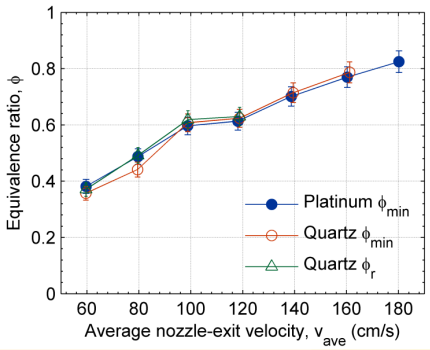

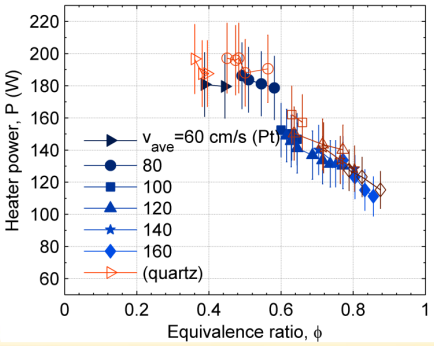

combustion LABORATORY

Conclusions and suggestions for future research

Conclusions: stagnation-flow reactor

The stagnation flow reactor provides a platform to investigate the fundamental behavior of catalytic fuel oxidation with and without an ignited flame, and the hypothesis:

- Catalysis can extend the useful operating conditions for hydrocarbon oxidation and combustion, improve device efficiencies, and reduce pollutant emissions.

- Developed from previous experimental results to have gas sampling, controlled heater temperature and a uniform flow velocity at the nozzle exit
- Gas sampling and heater power quantify the catalytic fuel oxidation
- The extinction limits and flame structure transitions quantify the catalytic influence on premixed flames
- Catalyst temperature control allows investigation of the intertwined effects of gas-phase transport, catalyst heat transfer, and surface reaction rates
- Capable to investigate both reactant and flame catalysis

Conclusions: catalytic propane oxidation, catalyst comparison

Mixing SnO_2 with Pt has a synergistic effect; catalytic oxidation activity begins at a lower temperature than for either pure component

In the diffusion limited regime, a larger fuel fraction is oxidized for both Pt and Pd than for the 90%SnO_2-10%Pt catalyst

The mass of fuel oxidized increases well into the fuel rich regime.

- Pt and Pd oxidize the same fraction of fuel for all fuel air mixtures
- 90%SnO_2-10%Pt has an increasing fuel oxidation fraction for increasing ϕ
- The activation energy of the platinum catalyst decreases for increasing ϕ

From the active catalysts, Pd produced the most CO and at the lowest temperature

CO is produced by the catalyst, not by the interaction of the heated surface with the gas-phase reactants

Conclusions: catalytic influence on flames

The disk flame is insensitive to the stagnation plane material

- The lean extinction limit is insensitive to Pt
- The heater power is insensitive to Pt
- The flame location is insensitive to Pt

Five different flame structures are observed depending on the flow rate and reactant mixture

The presence of platinum inhibited the formation of the ring flame structure

Suggestions for future research

The results suggest several directions for future research

- Development of lean NOx catalysts can decrease the pollutants emitted from high-efficiency diesel engines
- Catalyst ageing and poisoning is an important area to study for industrial implementation of catalysts
- Further study of fuel oxidation can aid the development of fuel pretreatment to aid low temperature combustor stability
- Research of fuel decomposition can show methods to process waste biomass into more easily useable fuels such as ethanol
- Development of heterogeneous reaction mechanisms can provide insight into the development of low cost catalyst materials

combustion LABORATORY

Acknowledgements

Apparatus construction

- ME machine shop staff
- Glass cutting: Harald Eberhart
- Lurie Nanofabrication Facility staff

Colleagues

- Current and former office mates, numerical studies with Jingjing Li

Family and friends

Committee: Arvind Atreya, Matthias Ihme, Hong Im, and Margaret Wooldridge

Bibliography

[1] R. Boyer. Annual energy review 2005. Technical Report DOE/EIA-0384(2005), Energy Information Administration, July 2006.

[2] C. T. Campbell, G. Ertl, H. Kuipers, and J. Segner. A molecular beam study of the adsorption and desorption of oxygen from a Pt(111) surface. *Surface Science*, 107(1):220 – 36, 1981.

[3] O. Deutschmann, F. Behrendt, and J. Warnatz. Modelling and simulation of heterogeneous oxidation of methane on a platinum foil. *Catalysis Today*, 21(2-3):461 – 470, 1994.

[4] O. Deutschmann, F. Behrendt, and J. Warnatz. Formal treatment of catalytic combustion and catalytic conversion of methane. *Catalysis Today*, 46(2-3):155 – 163, 1998.

[5] O. Deutschmann, L. I. Maier, U. Riedel, A. H. Stroemman, and R. W. Dibble. Hydrogen assisted catalytic combustion of methane on platinum. *Catalysis Today*, 59(1):141–150, 2000.

[6] O. Deutschmann and L. D. Schmidt. Two-dimensional modeling of partial oxidation of methane on rhodium in a short contact time reactor. *Symposium (International) on Combustion*, 2:2283 – 2291, 1998.

[7] V. Dupont, S. H. Zhang, and A. Williams. Catalytic and inhibitory effects of Pt surfaces on the oxidation of $CH_4/O_2/N_2$ mixtures. *International Journal of Energy Research*, 24(1):1291–1309, 2000.

[8] V. Dupont, S. H. Zhang, and A. Williams. Experiments and simulations of methane oxidation on a platinum surface. *Chemical Engineering Science*, 56:2659–2670, 2001.

[9] E. C. Fernandes and R. E. Leandro. Modeling and experimental validation of unsteady impinging flames. *Combustion and Flame*, 146(4):674 – 686, 2006.

[10] N. E. Fernandes, Y. K. Park, and D. G. Vlachos. Autothermal behavior of platinum catalyzed hydrogen oxidation: Experiments and modeling. *Combustion and Flame*, 118(1):164–178, 1999.

[11] E. Fridell, A.-P. Elg, A. Rosen, and B. Kasemo. A laser-induced fluorescence study of oh desorption from Pt(111) during oxidation of hydrogen in O_2 and decomposition of water. *Journal of Chemical Physics*, 102(14):5827 – 35, 1995/04/08.

[12] E. Fridell, B. Hellsing, B. Kasemo, S. Ljungstrom, A. Rosen, and T. Wahnstrom. Determination of the activation energy for OH desorption in the catalytic H_2 + O_2 reaction on Pt. *Vacuum*, 41(1-3 Pt1):732 – 733, 1990.

[13] E. Fridell, B. Hellsing, B. Kasemo, S. Ljungstrom, A. Rosen, and T. Wahnstrom. Hydroxyl desorption from platinum in the catalytic formation and decomposition of water. *Journal of Vacuum Science amp; Technology A (Vacuum, Surfaces, and Films)*, 9(4):2322 – 5, 1991.

[14] H. Ikeda, J. Sato, and F. A. Williams. Surface kinetics for catalytic combustion of hydrogen-air mixtures on platinum at atmospheric pressure in stagnation flows. *Surface Science*, 326(1-2):11–26, March 10 1995.

[15] S. Ishizuka, K. Miyasaka, and C. K. Law. Effects of heat loss, preferential diffusion, and flame stretch on flame-front instability and extinction of propane/air mixtures. *Combustion and Flame*, 45(3):293 – 308, 1982.

[16] R.J. Kee, F.M. Rupley, E. Meeks, and J.A. Miller. CHEMKIN-III: A FORTRAN chemical kinetics package for the analysis of gas-phase chemical and plasma kinetics. *Sandia National Laboratories Report SAND96-8216*, 1996.

[17] I. Langmuir. (1) chemical reactions on surfaces. (2) mechanism of the catalytic action of platinum in the reactions $2CO+O_2 = 2CO_2$ and $2H_2+O_2 = 2H_2O$. *Transactions of the Faraday Society*, 17:607 – 675, May 1922.

[18] I. Langmuir. Chemical reactions on surfaces. *Transactions of the Faraday Society*, 17:607 – 620, May 1922.

[19] C. K. Law, S. Ishizuka, and M. Mizomoto. Lean-limit extinction of propane/air mixtures in the stagnation-point flow. *Symposium (International) on Combustion*, pages 1791 – 1798, 1981.

[20] C. K. Law and G. I. Sivashinsky. Catalytic extension of extinction limits of stretched premixed flames. *Combustion Science and Technology*, 29(3):277–286, 1982.

[21] J. Li and H. G. Im. Extinction characteristics of catalyst-assisted combustion in a stagnation-point flow reactor. *Combustion and Flame*, 145(1):390–400, 04 2006.

[22] J. Li and H. G. Im. Effects of dilution on the extinction characteristics of strained lean premixed flames assisted by catalytic reaction. *Proceedings of the Combustion Institute*, 31 I:1189 – 1195, 2007.

[23] D. R. Lide, editor. *"Properties of Solids", CRC Handbook of Chemistry and Physics, Internet Version 2007, (87th Edition)*. Taylor and Francis, Boca Raton, Fl, 2007.

[24] S. Ljungstrom, B. Kasemo, A. Rosen, T. Wahnstrom, and E. Fridell. An experimental study of the kinetics of OH and H_2O formation on Pt in the H_2+O_2 reaction. *Surface Science*, 216(1-2):63 – 92, June 1989.

[25] M. Lyubovsky, L. L. Smith, M. Castaldi, H. Karim, B. Nentwick, S. Etemad, R. LaPierre, and W. C. Pfefferle. Catalytic combustion over platinum group catalysts: Fuel-lean versus fuel-rich operation. *Catalysis Today*, 83(1-4):71 – 84, 2003.

[26] S. B. Margolis and T. J. Gardner. An asymptotic model of nonadiabatic catalytic flames in stagnation-point flow. *SIAM Journal on Applied Mathematics*, 63:1083–1103, 2003.

[27] A. H. McDaniel, A. E. Lutz, M. D. Allendorf, and S. F. Rice. Effects of methane and ethane on the heterogeneous production of water from hydrogen and oxygen over platinum in stagnation flow. *Journal of Catalysis*, 208(1):21–29, 15 May 2002.

[28] J. Mi, G. J. Nathan, and D. S. Nobes. Mixing characteristics of axisymmetric free jets from a contoured nozzle, an orifice plate and a pipe. *Transactions of the ASME Journal of Fluids Engineering.*, 123(4):878 – 83, 2001.

[29] Y. K. Park, P.-A. Bui, and D. G. Vlachos. Operation regimes in catalytic combustion: H_2/air mixtures near Pt. *AIChE Journal*, 44(9):2035 – 2043, 1998.

[30] L. D. Pfefferle and W. C. Pfefferle. Catalysis in combustion. *Catalysis Reviews - Science and Engineering*, 29(2-3):219 – 267, 1987.

[31] W. C. Pfefferle and L. D. Pfefferle. Catalytically stabilized combustion. *Progress in energy and combustion science*, 12(1):25–41, 1986.

[32] R. Prasad, L. A. Kennedy, and E. Ruckenstein. Catalytic combustion. *Catalysis reviews*, 26(1):1 – 58, 1984.

[33] D. L. Trimm. Catalytic combustion (review). *Applied Catalysis*, 7(3):249 – 282, 1983.

[34] G. Veser and L. D. Schmidt. Ignition and extinction in the catalytic oxidation of hydrocarbons over platinum. *AIChE Journal*, 42:1077–1087, 1996.

[35] D. G. Vlachos, L. D. Schmidt, and R. Aris. Ignition and extinction of flames near surfaces: combustion of CH_4 in air. *AIChE Journal*, 40(6):1005 – 1017, 1994.

[36] W. R. Williams, M. T. Stenzel, X. Song, and L. D. Schmidt. Bifurcation behavior in homogeneous-heterogeneous combustion: I. experimental results over platinum. *Combustion and Flame*, 84(3-4):277 – 291, 1991.

[37] J. T. Wiswall. Catalytic effects of platinum on methane-oxygen-nitrogen and propane-oxygen-nitrogen mixtures in a stagnation flow. Master's thesis, The University of Michigan, Ann Arbor, 2007.

[38] J. T. Wiswall, M. S. Wooldridge, and H. G. Im. An experimental study of the effects of platinum on methane/air and propane/air mixtures in a stagnation point flow reactor. *ASME Journal of Heat Transfer*, 2009.

[39] Y. Zhang and K. N. C. Bray. Characterization of impinging jet flames. *Combustion and Flame*, 116(4):671 – 674, 1999.